Spectral Barcoding of Polystyrene Microspheres using Luminescent Semiconductor Nanocrystals (Quantum Dots)

by

Shyam V. Vaidya

Spectral Barcoding of Polystyrene Microspheres using Luminescent Semiconductor Nanocrystals (Quantum Dots)

by

Shyam V. Vaidya

A Dissertation Submitted to the Graduate Faculty in Engineering in Partial Fulfillment of the Requirements for the Degree of Doctor of Philosophy

The City University of New York

2008

INFORMATION TO USERS

The quality of this reproduction is dependent upon the quality of the copy submitted. Broken or indistinct print, colored or poor quality illustrations and photographs, print bleed-through, substandard margins, and improper alignment can adversely affect reproduction.

In the unlikely event that the author did not send a complete manuscript and there are missing pages, these will be noted. Also, if unauthorized copyright material had to be removed, a note will indicate the deletion.

ProQuest LLC
789 East Eisenhower Parkway
P.O. Box 1346
Ann Arbor, MI 48106-1346

This manuscript has been read and accepted for the Graduate Faculty in Engineering in satisfaction of the dissertation requirement for the degree of Doctor of Philosophy.

Date	Prof. Alexander Couzis (Mentor) Chair of Examining Committee
Date	Prof. Gabriel Tardos Executive Officer
	Prof. Charles Maldarelli (Co-Mentor)
	Prof. M. Lane Gilchrist (Co-Mentor)
	Prof. Raymond Tu
	Prof. Maribel Vazquez

Supervisory Committee

THE CITY UNIVERSITY OF NEW YORK

Abstract

Spectral Barcoding of Polystyrene Microbeads using Luminescent Semiconductor Nanocrystals (Quantum Dots)

by

Shyam V. Vaidya

Advisors: Prof. Alexander Couzis & Prof. Charles Maldarelli

The focus of this study is the development of optically barcoded polymer beads for use in high-throughput, multiplexed screening applications such as protein microarrays or flow cytometry. Luminescent semiconductor nanoparticles (or quantum dots (QDs)) with different emission wavelengths (colors) and incorporated in different compositions in polystyrene (PS) beads are used to define an optical barcode. The incorporation is undertaken by copolymerizing the PS beads with hydrophobically capped, core-shell, CdSe/ZnS QDs, using a spraying suspension polymerization procedure. Confocal laser scanning microscopy (CLSM) and transmission electron microscopy (TEM) images of the beads indicate that the QDs are segregated into inclusions distributed throughout the bead. The segregation of the QDs inside the polymer beads is due to enthalpy and entropy-driven rejection of the QDs from polymerizing loci as the polymerization proceeds. CLSM and fluorometer measurements of the emission spectra of PS beads embedded with three color QDs in varying concentrations are reported which verify that distinguishable optical ratio-metric

barcodes derived from the spectral scans of the barcoded beads can be obtained by this technique.

A comparison of the emission profiles of the barcoded beads with that of the same QDs dispersed in styrene indicates Luminescence Energy Transfer from the lower wavelength QDs to the higher wavelength QDs, providing evidence that the QDs are situated within nanometers of each other in the inclusions. The energy transfer limits our ability to obtain and apriori define a considerable number of ratiometric barcodes for multiplexing applications. We observed that the energy transfer could be reduced by separation of the segregating QDs from one another during the polymerization process. We used cross-linking between the polymer molecules during polymerization for separation of the QDs. Use of divinyl benzene (DVB) along with styrene for bead synthesis reduced the number of QD inclusions and dispersed the QDs to separate them by a distance of more than 10 nm as observed in the TEM images of the bead interiors. A comparison of the CLSM spectral scans of the beads prepared using DVB with that of the beads without cross-linking and a CLSM reference spectral scan – obtained from the QDs dispersed in styrene – indicates a significant reduction in the energy transfer and almost complete recovery of the emissions from the QDs similar to those dispersed in styrene.

Preface

This dissertation describes an experimental methodology to obtain spectrally barcoded polystyrene (PS) microspheres (beads) for their use in high-throughput screening applications. Luminescent spectral barcodes were obtained by incorporating luminescent semiconductor nanocrystals (quantum dots, QDs) using spraying suspension polymerization. This work was divided into three major sections: incorporation of monochromatic quantum dots in PS beads, incorporation of multicolored quantum dots in various loading concentrations in PS beads, and employing cross-linking for reducing electronic interactions between the QDs in multicolored QD encoded PS beads.

In Chapter 1, besides providing the motivation behind this work, we discuss the advantages of spectral barcoding of polymer beads using quantum dots, describe various experimental procedures that were previously employed for the incorporation of hydrophobic and surface modified QDs in the polymer matrix, and the advantages of using suspension polymerization method used in this thesis to overcome few of the shortcomings of the previous methods. A research outline describing the effects of bead size and electronic interactions among the QDs on the developed ratio-metric barcode is provided.

Incorporation of monochromatic QDs into PS beads using a spraying suspension polymerization is described in Chapter 2. Physical and spectral characterization of the QDs, pre- and post-incorporation in the PS matrix, using dynamic light scattering, spectrophotometry and of the encoded PS beads using optical microscopy, spectrophotometry, and confocal laser scanning microscopy (CLSM) shows that the QDs, which are uniformly dispersed in the monomer mixture before polymerization, are pushed into inclusions during polymerization. As discussed in Chapter 1, this

segregation of the QDs is attributed to the entropic and enthalpic energy penalty that the QDs pay for their incorporation in a non-compatible polymer matrix. Also, the surface-active partitioning of the QDs near the interface between the monomer droplet and viscous aqueous phase is observed.

In Chapter 3, we describe the synthesis of multicolored QDs-encoded PS beads using spraying suspension polymerization for development of color and intensity based ratio-metric barcodes. Advantages of the ratio-metric evaluation of the barcodes by deconvolution of emission profiles of the encoded beads are also discussed in brief. The developed color and intensity based ratio-metric barcodes are independent of the bead size.

Chapter 4 is devoted to the explanation of our understanding of a phenomenon called *electronic energy transfer* observed in the form of differences in the emissions of the QDs before and after their incorporation in the encoded PS beads. The size-independent aggregation of the QDs inside the polymerizing matrix, brings the QDs within 10 nanometers of each other and at this length scale, the lower wavelength QDs electronically transfer the luminescence energy to the higher wavelength QDs, thus altering the emission profiles. We believe that this energy transfer limits our abilities to apriory script and obtain a significant number of the ratio-metric barcodes. Highly cross-linking the polymer chains during polymerization using divinyl benzene (DVB) has been shown to significantly reduce the segregation of the QDs, and eventually reducing the observed energy transfer. CLSM, transmission electron microscopy (TEM), and differential scanning calorimetry (DSC) characterizations of the polymer beads, with and without DVB, provide objective evidence of the effect of cross-linking on the energy transfer.

Another experimental methodology of reducing the energy transfer between the QDs is demonstrated in Chapter 5, which also discusses the exciting avenues for exploring dispersion of nanostructured materials in polymers.

Acknowledgements

I am highly thankful to my mentors, Prof. Alexander Couzis and Prof. Charles Maldarelli. By providing complete independence of operation in the lab, they encouraged me to take initiatives in research and at the same time with their vast knowledge of chemical engineering discipline helped in nurturing my objective thinking and creativity. I appreciate their moral support on professional and personal fronts during the trying periods of my doctoral studies. I thank Prof. Lane Gilchrist who has been ever-helpful, specifically during the critical phases of my research work. His understanding of the field and valuable inputs during the project discussions removed the sudden road-blocks to smoothly drive my research forward. I also thank Prof. Maribel Vazquez and Prof. Raymond Tu for providing valuable feedback and comments.

I would like to thank Andy, Xu and Lisa for their help with technical and administrative matters. I thank my colleagues and members of the Surface Science Group at the City College: Nikhil K, Makonnen, Vivek, Fenfen, Jonathan, Spyros, Gerson, Ashish, and Nikhil B. Without their guidance, I could not have mastered the required analytical skills. Thanks to Dr. Jorge Morales of the Electron Microscopy Center at the City College for his guidance in using TEM. I appreciate the help received from the research groups of Prof. George John, Prof. Iban Ubarretxena, and Prof. Ronnie Ghosh for help with the fluorimeter and DSC. Thanks to K D Derr of New York Structural Biology Center for help with high-resolution TEM imaging. Special thanks to all my graduate colleagues, who helped in many ways during my graduate studies and made my stay at the City College a wonderful experience.

During my stay in New York, I got an opportunity of make many friends. The list is quite long, but I would like to mention few of them – Rohit, my batchmate from

undergraduate days and a tolerant roommate; Nikhil *buddy*, an accommodating office-mate; Manoj, the *big bro*; John *praji*, Anil, Pradeep, Ashish, Rajesh and Prasad Y. Thanks to the *bachcha* party, Amar, PM, Sandeep, Vikas, Nikhil B, Shripad, Prasad K, and Swapnil for making my stay at the City College a heartening experience. Special mention goes for Nimish, Sourabh, Hemant, Atish, Aditi, and Suchi. Many thanks to my friends of Om Sai Mandir, Art of Living NYC and Asha for Education's NYCNJ chapter for bolstering the spiritual and social dimension of my life.

I dedicate this thesis to my parents, Mr. V. D. Vaidya and Mrs. Nirmala Vaidya, and my *tai*, Dr. Madhuri. It is the result of their enduring efforts, love, and support that I have been able to undertake this task and do justice to it. I thank my brother, Dr. Shirish and brother-in-law Dr. Sushil for their encouragement and stress-relieving mischiefs. Special thanks to my soon-to-be better-half, Dr. Rukhmini, for her love, affection and caring support during the lows and highs of my graduate studies.

Contents

List of Tables

List of Figures

Chapter 1

Introduction

1.1 Motivation

Biological assays form the core of diagnostics and drug discovery applications, where interactions of antibodies – proteins generated by human body in response to a foreign molecule – with antigens are studied. For discovery of new therapeutic drug molecules or *proteomics*, study of the interactions of cellular membrane proteins with potential drug candidate molecules is important. Existing procedures for this study need large quantities of the reagents and processing times. A significant research focus is being given on developing procedures for faster and cost-effecive screening of multiple analytes simultaneously. Miniaturized microarray platforms with array densities of more than 10000 for high-throughput screening of biological molecules have been envisioned by the research community.

The overall objective of this exploratory research project is to develop a new, ultra-miniaturized, microarray platform for display of cell surface membrane receptors, such as membrane proteins, antigens, and glycolipid and glycoprotein receptors. The platform is to be used for the high throughput, multiplexed screening of the binding of membrane receptors with potential binding partners or target ligands. The design of the platform is shown in Figure 1.1: The membrane receptors are sequestered in a supported unilamellar phospholipid bilayer, which is formed around a 1 μm in diameter microbead, to form a bilayer-encapsulated bead or lipobead (Figure 1.1). The lipobeads are inserted into surface functionalized wells of similar size etched in a surface in a square grid pattern with a pitch of $\approx$3 μm. The size of the array chip is envisioned to be 1 mm x 1 mm and hence the chip contains upwards of 10^5 wells for its 1 mm^2 active area. The surface is chemically functionalized: the interior of the wells is functionalized with groups to couple to complimentary groups on the lipobead to anchor the bead to the well, and the surface area surrounding the wells is functionalized with a passivating layer to make these surroundings inert to

nonspecific adsorption of proteins and lipid matter. The physical constraint of the well and the chemical constraint of the passivating background prevents the bilayer, once inserted in the well, from unraveling and delaminating from the microbead. The sequestering of the membrane receptor in its native lipid bilayer environment allows the receptor to retain its biological conformation and binding ability, and hence this platform – with the bilayer intactly formed on beads arrayed on a surface – provides a solution to the problem of displaying high density active membrane receptors for multiplexed screening.

To tag the lipobeads so that the identity of the receptor being hosted by an individual lipobead is known, the microbeads – encapsulated by the bilayer – are barcoded for identification by using an encoding scheme based on the fluorescence of hydrophobically capped semiconductor nanocrystals or quantum dots (QDs), 2–10 nm in diameter. The emission wavelength of a QD can be tuned by changing its size. QDs with different diameters and emission wavelengths (colors) are embedded in varying numbers (hundreds to tens of thousands) to form a luminescent label consisting of a set of colors (c), and, for each color, a set of intensities (i) for an encoding capacity of i^c. The use of QDs to form a luminescent barcode instead of organic fluorophores has the advantages of higher quantum yields, stability against photobleaching, and narrow and symmetrical emission spectra. In addition, a single excitation wavelength can excite multiple colors. Each receptor to be screened is assigned a unique QD barcode. A suspension of lipobeads is prepared with receptors of only one kind sequestered in the bilayers of the lipobeads, and with the bead interiors encoded with the unique label for that receptor. Suspensions of lipobeads, each suspension containing a different receptor (and tag), are pooled into a mixture, and the mixture is deposited onto the surface etched with wells. Upon deposition, lipobeads – each displaying a different receptor – bind randomly to the wells to form an array, with only one lipobead occupying an individual well owing to the

commensurate sizes of the wells and lipobeads.

Because of the luminescent optical encoding, the arrayed lipobead platform is easily adopted to fluorescence screening assays. The array is incubated with a solution containing target molecules, which are to be screened against the displayed membrane receptors. A robotic spotter need only dispense a nanoliter of target solution to cover the 1 mm x 1 mm active area and assay the displayed receptors, 10^5 in number. As QDs of different colors can be excited by one wavelength, the optical barcode can easily be read by exciting the array at one wavelength and recording, at each well location on the chip, the QD emission intensity and wavelength to decipher the optical barcode and spatially index the array. To detect a binding event, either the targets can be fluorescently labeled or a subsequent sandwich assay can be undertaken to conjugate a fluorescent label to the bound ligand. (The emission wavelength of the targets should be distinct from the emission signatures of the optical code.) Excitation of the target produces an emission fluorescence, which signifies the binding of the ligand to the membrane receptor by noting the barcode at the site of the ligand fluorescence, the receptor binding the ligand can be identified.

This research specifically focuses on optically encoding polystyrene microbeads (termed "smart" microbeads) using a procedure in which beads are encapsulated with QDs during a suspension polymerization to form an intensity/color spectral barcode. We demonstrate that this approach effectively traps the QDs throughout the particle, allowing for a quantitative loading without loss of luminosity or spectral emission signature, and thereby resulting in a reproducible and readable optical barcode. A paradigm is presented for the construction of a high capacity encoding (or barcoding) scheme based on relative intensities which insures that codes do not overlap even in the presence of changes in luminescence intensity due to variations in the bead diameter and/or electronic interactions between the QDs.

1.2 Background

A smart microbead is a micron-sized (1–100 μm), freestanding particle engineered with unique labels to allow the bead to be detected and individually identified in an environment. In the literature, several schemes have been considered for encoding beads (for a review see Finkel et al.[1]), and among the methods explored have been: (i) molecular tags [2, 3, 4] which are molecules covalently attached to the particle and read by cleaving the tag and identifying the molecule, (ii) infrared and Raman spectral labels [5, 6] which consist of molecules with distinct spectral signatures which are embedded in the beads and read by obtaining the bead spectrum, and (iii) visual bar codes read optically which include tagging particles by varying their shape [7, 8, 9], and spatially patterning their reflectivity by metal deposition [10, 11, 12, 13]. Apart from these techniques, photoluminescent spectral encoding of microbeads has emerged as a very effective strategy for particle labeling (for reviews see Finkel et al.[1] and Wang et al.[14]).

1.2.1 Photoluminescent Encoding of Polystyrene Microspheres

This encoding strategy was initially developed using micron-sized polymer latex beads, which were encoded by encapsulating organic chromophores (or luminescent lanthanide chelate complexes) that fluoresce at a particular emission wavelength upon excitation. A spectral bar code is constructed by embedding the beads with chromophores with different excitation wavelengths (colors, c) and for each color, different loading concentrations, i, to achieve varying levels of color and intensity and an encoding capacity of i^c. The label is read optically by recording the emission spectrum and deconvoluting from the spectrum the colors present, and for each color, the intensity level. The emerging importance of fluorescence encoding is due to the facility with which the code is read as a spectral emission profile, which lends itself

to many potential applications. Fluorescent microbeads have potential applications in the visualization of flow and mixing in microfluidics[15, 16], and in biological applications, such as mapping blood perfusion or particle accessibility (as a function of particle size) in tissue and organ compartments for drug delivery[17]. A major potential application is their use in the development of bead-based platforms to meet the demand for high-throughput multiplexed screening assays. The screening of the binding interactions of a large numbers of probe molecules with a particular target is an essential part of genomics for DNA hybridization detection (for gene expression profiling, sequence specific identification and single polymorphism genotyping), and proteomics for probing the interactions of proteins with binding ligands (for protein expression profiling, for clinical diagnosis through identification of disease markers and for drug discovery). Particle based screening platforms conjugate the probe molecules to the surface of the encoded microbeads, with the bead label identifying the probe molecule at the surface. Beads with different probe molecules are then mixed together and binding assays of a target with the collection of probes is undertaken, either in a homogeneous suspension format using flow cytometry for bar code reading and assaying (suspension array technology; for reviews, see [18, 19, 20, 21, 22, 23]) or a heterogeneous microarray format (see the articles by Walt et al.[24, 25, 26] and Stevens [27]), in which the beads are fixed onto a surface in a grid, and codes are read using wide field or confocal laser scanning microscopy.

1.2.2 Quantum Dots: The Luminescent Semiconductor Nanocrystals for Encoding

The organic chromophores (or luminescent lanthanide chelate complexes) which have been used to fluorescently encode microbeads to date have several disadvantages. These luminescent molecules readily photobleach and can be chemically unstable. In addition, these chromophores have different excitation wavelengths, and hence

a collection of chromophores – as in a barcode – cannot all be excited with one wavelength. A further disadvantage is the emission spectra of organic chromophores and lanthanide chelates are often broad and asymmetric, which can lead to a spectral overlap that makes it difficult to deconvolute distinct codes from the spectra. Luminescent semiconductor nanocrystals or quantum dots (QDs) are potentially more suitable as fluorescent labels to encode beads.

Quantum dots are composed of 2–10 nm sized core crystals containing thousands of atoms of II–VI, III–V, or IV–VI group semiconductor materials, such as cadmium (Cd)–selenide (Se), cadmium–telluride (Te), which are coated with another semiconductor material shell (zinc sulfide, ZnS) and long chain organic molecules to improve the optical properties of the material and to impart them hydrophobic characteristics. Figure 1.2 shows a schematic representation of a CdSe/ZnS core/shell QD capped with trioctylphosphine oxide (TOPO) and hexadecylamine (HDA). Because of smaller crystal size – even smaller than Exciton (an electron-hole pair in a semiconductor material) B*ö*hr Radius – the energy level in a QD crystal are discrete leading to a quantum confinement of the excitons (Figure 1.3). Owing to quantum confinement effects, the peak emission wavelength is tunable by the size of the core crystal as well as the composition [28], and as a result, different sized QDs can provide a source for a large number of tunable fluorescent tags (see Figure 1.4) with distinct spectral signatures which is ideal for barcoding. In addition, the emission spectrum for each QD is Gaussian, symmetric and relatively narrow (20-30 nm full width at half maximum, FWHM), and their absorption spectra exhibit peak adsorption in a common band of UV wavelengths, also ideal for barcoding. Figure 1.5 shows absorption and emission spectra of CdSe/ZnS core/shell QDs (reported by Evident Technologies, Inc. [www.evidenttech.com]), which emit in the visible range of the light spectrum. These advantages have provided the impetus for several investigations on this topic. We briefly review these here as a background for our own

study on QD barcoding of microbeads.

1.2.3 Incorporation of Quantum Dots in Polystyrene Microbeads

The incorporation of QDs in microbeads for encoding have been undertaken using three principal routes:

1. the QDs are trapped or affinity partitioned directly into a preformed bead,
2. a shell of QDs is encrusted on the surface of a bead or
3. the QDs are incorporated in the beads during the bead synthesis, either by encapsulation or chemical grafting.

Nie et al.[29, 30, 31, 32] encoded polystyrene microbeads with QDs by directly impregnating the QDs into pre-formed beads. Polystyrene beads were first dissolved in a chloroform/alcohol solution, which penetrates the network of mesopores of the beads causing the particles to swell and the pores to enlarge. The swelling solution also contained hydrophobically capped CdSe/ZnS core shell QDs, which are soluble in the infiltrating/swelling solution. The QDs diffuse through the pores of the swelled beads and adsorb onto the hydrophobic pore walls; removal of the swelling solvent contracts the pores and effectively traps the QDs. Nie et al. loaded QDs with a single color (monochromatic) and demonstrated that the photoluminescence of a single bead was linearly proportional to the number of QDs embedded. Nie et al. also loaded beads with three colors, and obtained a spectrum in which the peak emission wavelengths of the colors were identical to the values recorded dispersed in a non-aggregated form in a nonpolar solvent. Using the same impregnation procedure, Vincent et al.[33] used confocal laser scanning microscopy to obtain serial sections of the photoluminescence of beads with monochromatic QDs, and showed that the depth of impregnation into the bead increases with the chloroform content of

the swelling solution. Infiltration incorporation of monochromatic hydrophobically capped QDs in polystyrene microbeads were also undertaken by Nabiev et al.[34] and Riegler et al.[35], and for hydrophilically-capped, water soluble QDs into hydrogels by Mohwald et al.[36, 37]. Zhao et al.[38] used the infiltration method to incorporate in polystyrene beads hydrophobically capped QDs with two different colors; they demonstrated that by varying the molar ratio of the two QDs in the impregnating solution, the intensities of the two colors in the bead emission spectra can be varied.

The process of arranging QDs into a shell around the periphery of a preformed microbead was undertaken by Bawendi et al.[39] on silica beads by reacting QDs with a siloxane surface functionalization with silica seed particles in an ethanol dispersion by St*ö*ber growth (see also Hirai et al.[40] for thiol binding of QD shells). Ruhl et al.[41] obtained a QD shell by first adsorbing poly-(vinyl-pyrrolidone) (PVP) to hydrophobically capped CdSe/ZnS QDs to make them hydrophilic, then adsorbing the PVP modified QDs directly onto amino functionalized silica particles and finally using a St*ö*ber growth to coat the particles with a shell of silica and seal the QDs in the bead. The incorporation of monochromatic QDs in concentric shells around a seed particle was obtained by Rogach, Caruso and Mohwald[42, 43, 44] using a layer-by layer (LBL) assembly technique in which polyelectrolyte layers of alternate charge and polar capped QDs are sequentially deposited onto a surface, and held together by electrostatic interactions. The LBL technique was also used by Su et al.[45] to load QDs with two different colors, at different loading ratios.

The direct in situ encapsulation of QDs in microbeads during the bead polymerization has been accomplished via two routes. In the first, beads form from nuclei that are dispersed in a continuous phase. Monomer, initiator, and QDs, cap exchanged to make them dispersible in the continuous phase and functionalized to make them reactive to the polymer, are required to transport to the nuclei and become incorporated in the growing bead. Bawendi et al.[46] encapsulated

monochromatic QDs in polystyrene beads in an ethanol dispersion polymerization. Scanning transmission electron microscopy sections of the beads showed that the QDs were dispersed uniformly but the bead size had decreased and the distribution had become broadened relative to the beads formed without the QDs. In addition, non-integrated QDs were found in the dispersion. Bawendi et al. concluded that the inability to quantitatively load the beads, and the disruption of the size distribution makes this route problematic for barcoding. Monochromatic QDs have also been encapsulated in polystyrene beads during the polymerization step using the micelles of an emulsion as the nucleating centers (emulsion polymerization [47, 48]) and in silica beads in a silicate polymerization [49].

A second route is to use suspension polymerization [50], in which monomer, polymerizing initiator and QDs are first mixed together, and dispersed as microdroplets in a continuous phase in which the QDs and monomer are not soluble. Polymerization is then initiated in the droplet phase by activation of the initiator, and the QDs, owing to their insolubility in the continuous phase, remain sequestered in the droplets as the droplets evolve to a polymer bead. This route has been used for the encapsulation of QDs in polystyrene beads by OBrien et al. [51, 52] by dispersing nonpolar styrene and initiator in an aqueous phase and loading the QDs in the styrene phase. OBrien et al. used monochromatic QDs which were functionalized with vinyl groups to enable polymerization with styrene, and later showed that QDs without a polymerizable ligand can also be incorporated as long as they are dispersible in styrene. The suspension technique was also utilized to encode polystyrene nanobeads [53] with QDs by using a miniemulsion procedure [54] in which styrene monomer with hydrophobic QDs is dispersed into nanodroplets in an aqueous phase by the addition of surfactant to lower the surface energy of the droplets, and sonication to disperse the monomer to the nanodroplet size (see also Fleischhaker and Zentel [55]). Transmission electron microscopy sections of these

beads showed that the QDs were dispersed throughout the bead interior, but also indicated that there was aggregation. The aggregation was attributed to a phase separation between the QDs and the polystyrene as the polymerization proceeded. OBrien et al. [52], using the suspension technique to fabricate micron sized particles, has also noted regions within the beads where QDs concentrate, noting that they can occur at defects in the polymer matrix. Gao et al. [56] used the suspension polymerization method to form polystyrene beads encapsulating vinyl capped QDs with two different colors.

Particle solvent evaporation/casting techniques are routes to incorporating QDs into polymer microbeads, which are conceptually similar to suspension polymerization methods in the sense that the beads are formed from liquid droplet precursors [57, 58]. In these techniques, an organic solvent is used to form a solution containing dispersed, hydrophobically capped QDs and dissolved polymer, and droplets of this solution are dispersed in water. The solvent partitions from the droplets into the water during the curing process, forming polymeric particles, which entrap the QDs. Both monochromatic and multicolor encoded beads have been fabricated with this process.

1.3 Research Outline

In this research, we used the suspension polymerization method to embed QDs into microbeads. This technique is chosen because it allows the facile, quantitative loading of QDs in the beads, which is a pre-requisite for accurate encoding. Our investigation has the following three objectives.

1. to verify the applicability of suspension polymerization for the quantitative incorporation of quantum dots (QDs) in polymer beads

2. to address the effect of the bead size on the encoding and develop a coding

scheme, which is independent of the bead size

3. to examine the effect, on the spectral code, of electronic interactions among the QDs sequestered in the beads when the QDs are electronically excited by radiation.

The scope of each of these objectives is briefly described below.

1.3.1 Suspension Polymerization for Quantitative QD Incorporation in Polystyrene Beads

In the literature described above, monochromatic QDs have been successfully incorporated into polymer beads using suspension polymerization. However, these studies do not undertake a detailed examination of the distribution of the QDs in polymer matrix. Our objective is to use confocal laser scanning microscopy to examine the distribution and study its effect on the emission spectrum of the beads.

1.3.2 Effect of Bead Size on Encoding

The suspension polymerization technique does not produce the narrow size distribution characteristic of beads fabricated by techniques involving polymerization growth from nuclei (e.g. emulsion and dispersion polymerization, St*ö*ber synthesis). When the bead size is not finely tuned, intensity codes can overlap as the larger beads in a batch indexed with a smaller number of QDs can have a smaller luminescence than the smaller beads of a batch indexed with a larger number of QDs. To remove this dependence on bead size, we will demonstrate how the ratio-metric construction of a code, in which the intensity code for a particular color is formulated as a ratio of that color intensity to the total intensity, removes the dependence of the code on the bead size.

1.3.3 Effect of Electronic Interactions among QDs on Spectral Code

As we noted in Section 1.2, when a suspension polymerization is used to embed QDs in polymer beads, evidence suggests that the QDs aggregate or phase separate into micro-domains as they are rejected from the polymerizing matrix of the beads. In these micro-domains, the QDs can conceivably be pushed to within nanometers of one another. Several studies have been undertaken of the effect, on the luminescence, of electronic interactions of QDs, which are separated by nanometer scales. Particularly relevant are studies of electronic interactions in QD assemblies consisting of evaporated films [59, 60, 61, 62, 63, 64, 65, 66, 67], monolayers and multilayers of QDs formed by Langmuir-Blodgett or layer-by-layer deposition [65, 68] and QD molecules consisting of covalently conjugated or electrostatically cojoined dots [69, 70, 71]. These studies have shown that electronic interactions in the form of electronic coupling and exciton energy transfer can affect the QD absorption and emission spectra. In electronic coupling [62, 63] electronic excitations delocalize across multiple dots, leading to states described by the superpositions of electron and hole wave functions. These coherent interactions require a high degree of structural order, and have been observed as a red shift in the absorption and emission spectrum for very small inter-dot separations ($<$ 1 nm) and small QDs ($<$2 nm in diameter). These conditions allow the extension of the evanescent wave function sufficiently far outside the individual QDs. Coupling is most likely not relevant in the QD microdomains in beads, since the QDs used are usually larger than 2 nm and there is not a high degree of structural order. In exciton energy transfer [59, 60], electrons and holes are confined to individual QDs, and energy is transferred non-radiatively from an excited dot (the donor) to a ground state dot (acceptor), returning the donor to its ground state and promoting the acceptor to a higher excited state. Examinations of the luminescence emission spectra and lifetime of QDs in the close packed

assemblies mentioned above indicate a quenching of the luminescence and lifetime of the smaller dots accompanied by an enhancement of the luminescence and lifetime of the larger dots, i.e., a transfer of electronic excitation from small dots to larger dots. These measurements are consistent [59, 60, 65, 67, 68] with long range resonance transfer arising from coupling between the transition dipoles in the excited donor and ground state acceptor. This transfer is effective over inter-dot distances between 1–10 nm and requires the acceptor to have a transition resonant with the donor and a lower energy state in which to trap the excitation. Hence, as in the observations, the small dots are donors and the large dots are acceptors. Förster theory [72, 73] relates this interaction to the spectral overlap of the donor emission and acceptor adsorption, and has been used to successfully model the luminescence lifetime measurements in the solid films. Evidence for this energy transfer in the QD micro-domains of polymer beads prepared by suspension polymerization is present in the results of Gao et al. [56] who encoded (smaller) green (546 nm peak emission wavelength) and (larger) red (634 nm) QDs in polystyrene beads at different molar ratios. The emission spectra of the two-color encoded beads demonstrated that the ratio of the peak intensities of red to green QDs was always much larger than the molar ratio of these dots, indicating the possibility of electronic transfer from the green to the red QDs. This difference could also be accounted for by differences in the absorption and quantum yields of the two QDs, and reference emission spectra of non-interacting (isolated) QDs separated in a dispersing solvent and at the loading concentrations used in the encoded beads was not taken into account for these effects. Yin et al. [58] encapsulated two colors (orange, 560 nm and red, 620 nm) in microbeads using the solvent extraction technique, which can also lead to phase separation of the QDs in micro-domains as the solvent transfers out of the beads during the curing step. They did compare the luminescence emission spectrum of the QDs in the beads with the spectrum of the QDs loaded at the same concen-

tration in solution, and found electronic energy transfer from the orange to the red QDs. Hence, the transfer can change the spectrum from what would be expected if the QDs are non-aggregated in the bead and do not transfer electronic energy, and our aim is to carefully study this transfer when the QDs are encapsulated in beads using a suspension polymerization.

These objectives were addressed during the scope of this research work. By incorporating monochromatic QDs in PS beads, we demonstrate, in Chapter 2, our ability to obtain successful incorporation of the QDs inside PS beads using suspension polymerization. In Chapter 3, we describe the qualitative and quantitative incorporation of multicolored QDs into the PS beads using the suspension polymerization for development of color and intensity based ratio-metric barcodes. Chapter 4 describes the effect of electronic energy transfer on the developed ratio-metric barcodes followed by methods, which we employed for reduction of the electronic energy transfer.

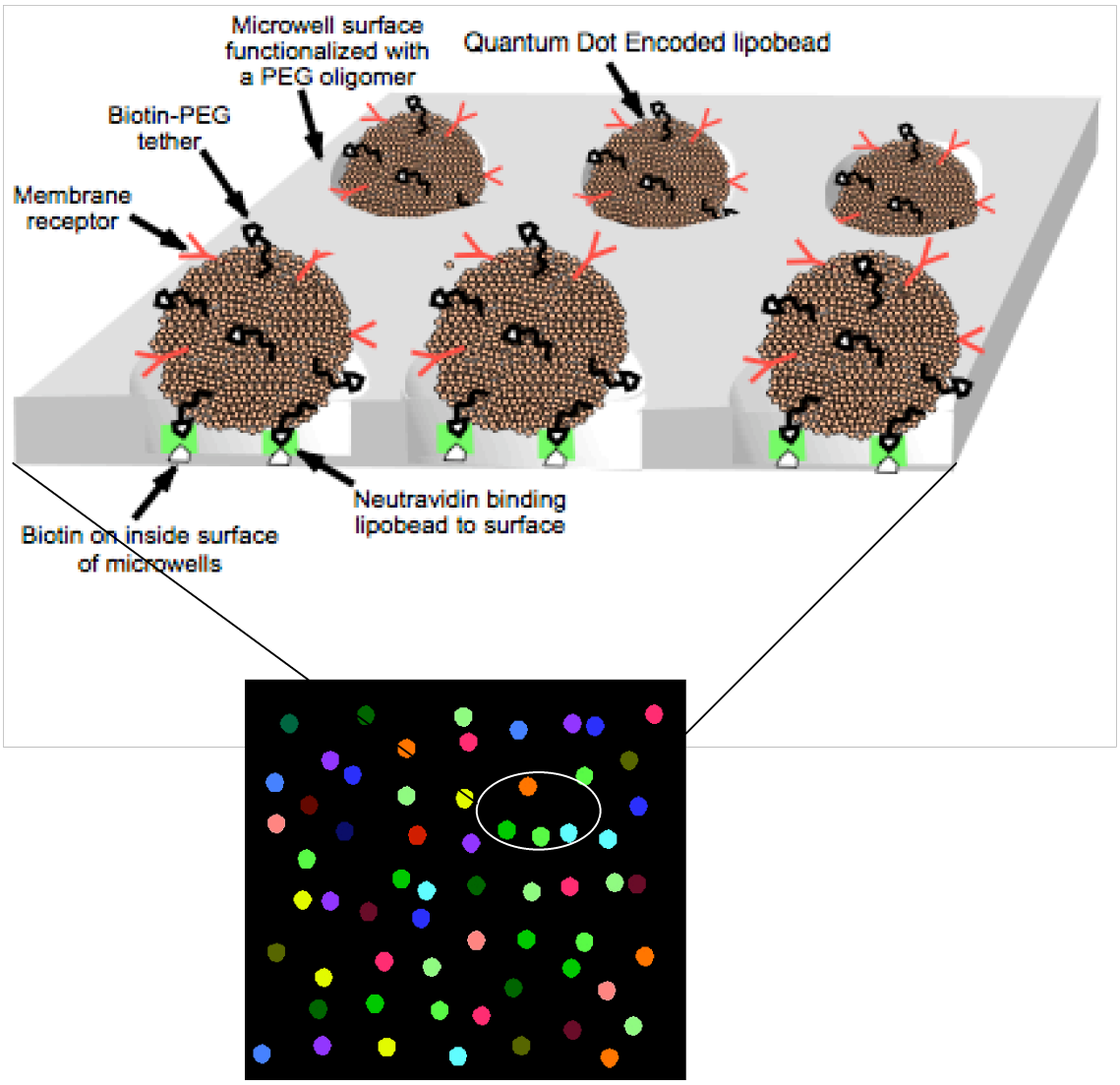

Figure 1.1: Localization of lipobeads displaying a membrane receptor in microwells. The lower image show a schematic version of the readout from a far-field microscope. The top image is a zoom-in showing the proposed microarray platform.

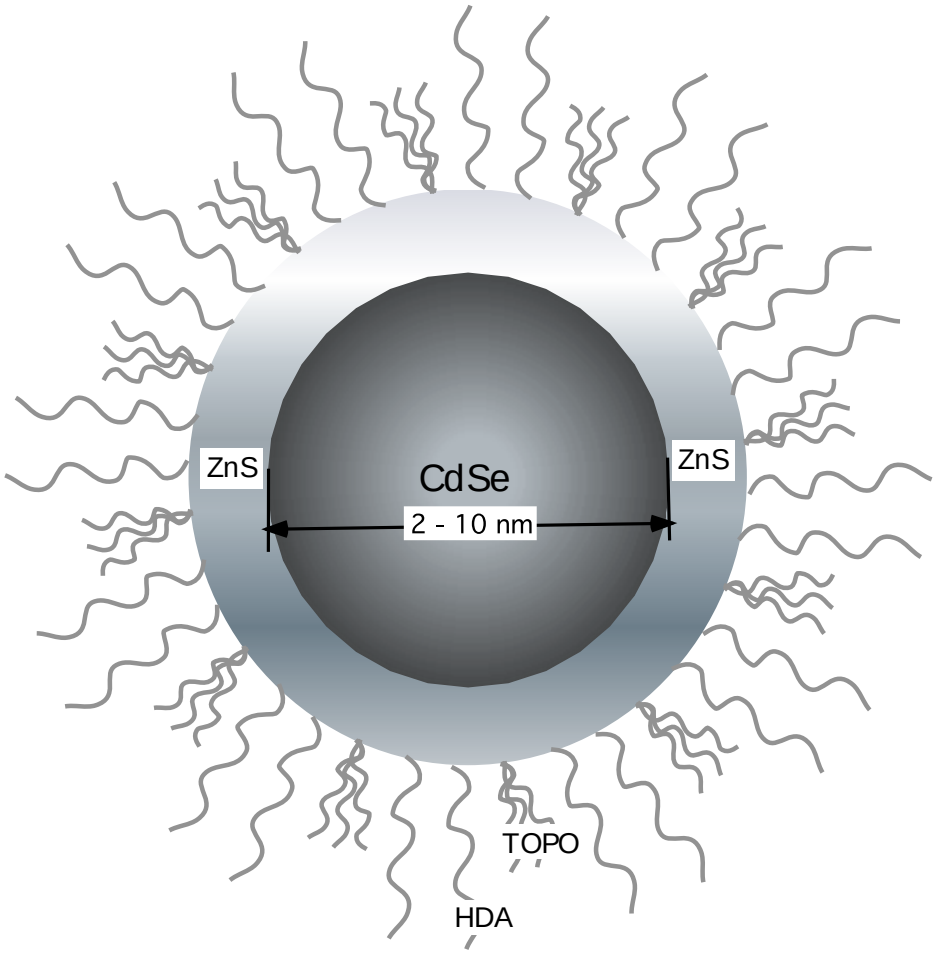

Figure 1.2: Schematic representation of Cadmium Selenide (CdSe)/Zinc Sulfide (ZnS) core/shell QD capped with long chain capping agents such as trioctylphosphine oxide (TOPO) and hexadecylamine (HDA).

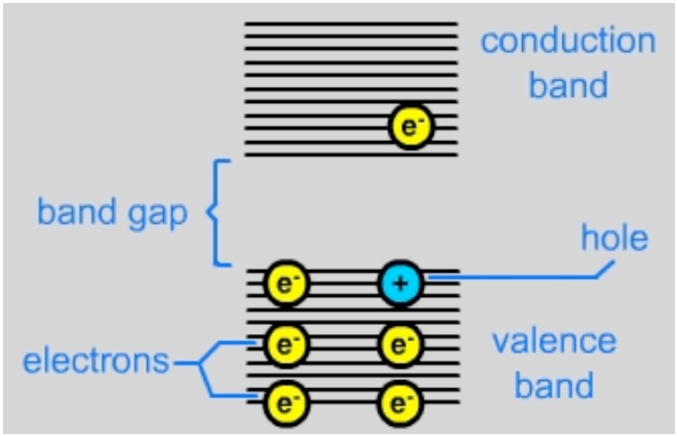

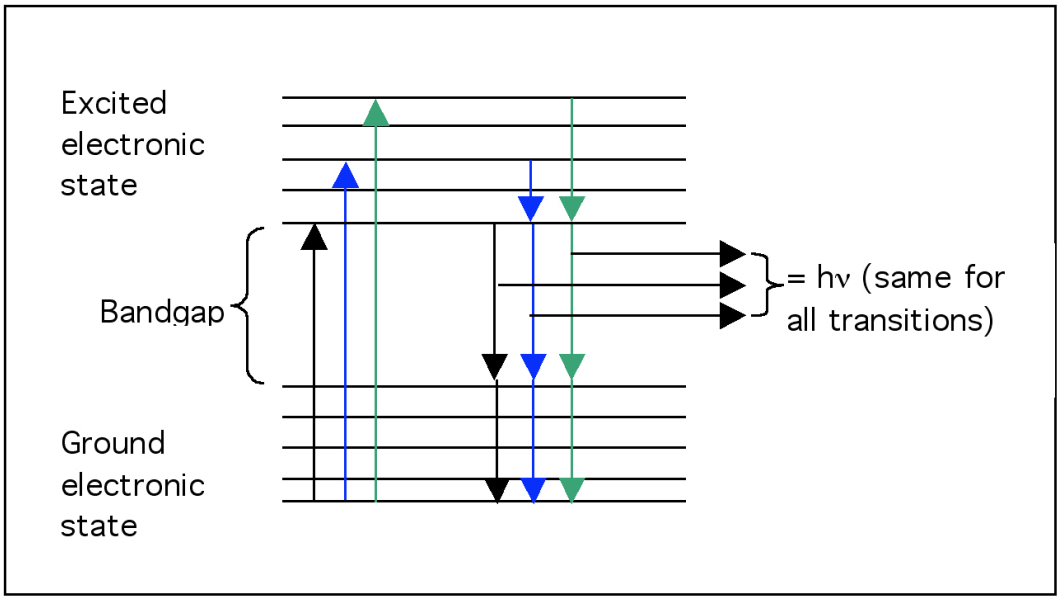

Figure 1.3: *Top schematic*: Energy levels in a semiconductor. A hole is created in the velence bond due to transition of an electron to the conduction band leading to formation of an exciton (electron-hole pair). Confinement of the excitons is dependent on size of band-gap and smaller the quantum dot crystal, larger the band-gap and hence larger the quantum confinement energy. *Bottom schematic*: Emission of photons due to the transition of electrons from the bottom of the excited electronic state i.e., conduction band to the top of the ground electronic state i.e., valence bond.

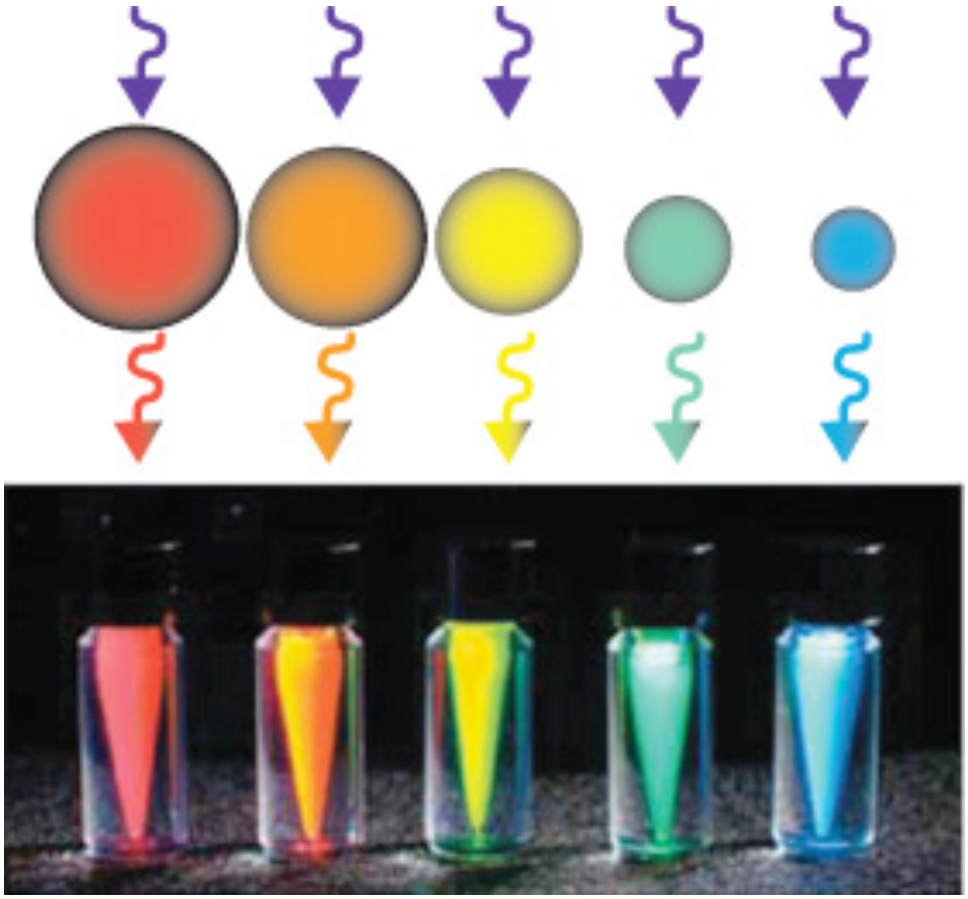

Figure 1.4: Quantum Dots: Tunable luminescent tags. Five different sized QD solutions excited with long-wavelength UV lamp. The size of the QD determines the color. *http://probes.invitrogen.com/products/-qdot/overview.html*

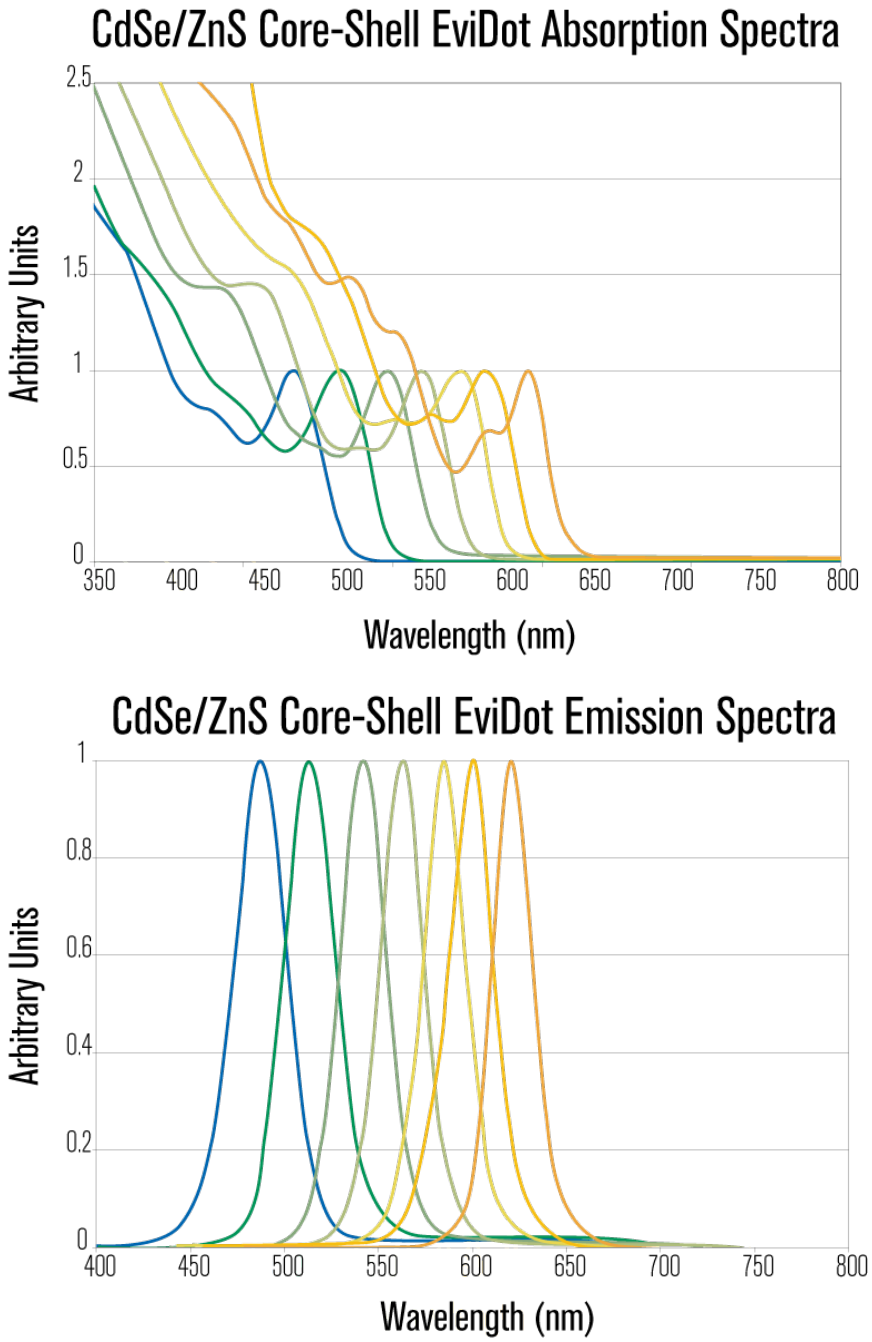

Figure 1.5: *Top*: Absorption spectra – normalized to equal absorption intensities at the first exciton wavelength – of CdSe/ZnS core/shell QDs capped with long chain amine capping agents. *Bottom*: Photoluminescence emission spectra – normalized to equal emission intensities – of CdSe/ZnS core/shell QDs with long chain amine capping agents. Absorption spectra shows that the recommended excitations for these QDs is using UV wavelengths of light and all of them could be excited using a single wavelength. *http://www.evidenttech.com/products/-evidots/evidot-specifications.html*

Chapter 2

Monochromatic Quantum Dots Encoded Polystyrene Beads

2.1 Introduction

In this chapter, we describe the employment of free-radical suspension polymerization for incorporation of hydrophobic monochromatic quantum dots (QDs) in polystyrene (PS) beads. We modified the suspension polymerization procedure (hereafter denoted *spraying suspension polymerization*) by employing a syringe pump and an ultrasonic nozzle – as shown in Figure 2.1 – to generate monomer droplets and spray it over the viscous aqueous phase maintained at the polymerization conditions. The idea behind this modification is to take advantage of free-radical polymerization kinetics for sequestering the QDs inside the polymerizing beads. Dynamic light scattering, confocal laser scanning microscopy, and fluorimetry were employed for characterization of the QDs dispersed in base solvents, monomer solutions, and embedded in polymerized beads.

2.2 Experimental Section

2.2.1 Materials

Styrene (ACS reagent grade), poly-vinyl alcohol (PVA; hydrolyzed, average molecular weight - 88,000), ethyl alcohol (ACS reagent grade), methyl acrylic acid (MAA; ACS reagent grade), and methyl methacrylate (MMA; ACS reagent grade) were purchased from Spectrum Chemicals, CA. 2,2'-Azobis-(2-methylpropionitrile) (AIBN, 98%) was obtained from Sigma Aldrich Co. CdSe/ZnS core/shell QDs, capped with trioctylphosphine oxide and hexadecylamine, dispersed in toluene were obtained from Evident Technologies, NY. Monochromatic QDs with emission maximum (as reported by the manufacturer) at 620 nm (denoted red) were used. Deionized (DI) water with resistivity equal to 18 MΩ·cm was obtained using a Millipore system. All chemicals were used as is without further purification.

2.2.2 Encapsulation of Quantum Dots into Polystyrene Microspheres

Polystyrene (PS) microspheres (beads) embedded with QDs were obtained using a spraying suspension polymerization procedure. The aqueous phase was a 2 wt% aqueous PVA solution continuously stirred with a magnetic stirrer and maintained at 80 °C. QDs suspended in toluene with emission at 620 nm emission wavelength were dispersed at room temperature into 1.25 mL of monomer mixture, containing styrene (St), AIBN (5 wt% St), and MAA (5 wt% St), abbreviated St/MAA/AIBN.

This mixture was sprayed using a Sono-Tek ultrasonic nozzle (S/N 12311, Sono-Tek Corp.) with the monomer mixture being pumped to the nozzle using a syringe pump (XL3000, Cavro). The size of the drop is determined by the vibration frequency, nozzle diameter, liquid density, air/liquid tension, pump flow rate, and piezo amplitude. For the monomer mixture, a frequency of 120 kHz and a nozzle with a diameter of 760 μm were used to produce polymerized beads of the order of tens of micrometers in diameter with an average size of $\sim$50 μm. A total of 1.25 mL of reaction mixture if pumped within 30 seconds. We assume that the polymerization reaction is initiated upon completion of the fluid delivery. After 2 hours of polymerization, the reaction mixture was cooled, and the beads were recovered using centrifugation and subsequently washed with a 40:60 mixture of ethanol and water. The beads were stored in DI water.

2.2.3 Characterization of QDs and PS Beads

Dynamic light scattering was used to characterize individual and mixture of QDs dispersed in toluene or monomer mixtures before polymerization. We used confocal laser scanning electron microscopy (CLSM) and spectrofluorimetry to characterize the luminescence of the QDs dispersed in toluene, monomer mixture or embedded in polystyrene beads obtained using suspension polymerization. CLSM shows lumi-

nescence representation of the distribution of QDs in the polymerized bead matrix. Spectral scans obtained using CLSM and the fluorimeter were used for calculation of ratio-metric barcodes.

Particle Size Analysis using Dynamic Light Scattering

The size distribution of the QDs dispersed in toluene and the monomer mixture was measured using dynamic light scattering (DLS; Zetasizer ZS90, Malvern Instruments). Particle size analysis instruments employ a process called Dynamic Light Scattering (DLS). DLS measures Brownian motion and relates this to the size of the particles. It does this by illuminating the particles with a laser and analyzing the intensity fluctuations in the scattered light.

When light hits small particles, the light scatters in all directions (Rayleigh Scattering) but at a different frequency. Small particles in a solution are constantly undergoing Brownian motion and the speed of particle motion depends upon the size of the particle, for example, smaller particles move quickly compared to larger particles. Due to their higher average velocity, smaller particles create larger shift in the scattered frequency of light than the larger particles. This difference in the frequency of the scattered light by particles of different sizes is used to determine the sizes of the particles present in the solution. This constant motion of the particles along with the scattering from them generate constructive and destructive interference patterns leading to temporal (time dependent) fluctuations in the scattering intensity. The relationship between the particle size and its speed of motion in the solution is given in the form of Stokes-Einstein equation.

Optical Microscopy

Optical imaging of the dried beads was done using a Nikon measuring microscope (20x magnification) in order to determine the bead morphology, bead diameter, and their size distribution.

Spectrofluorimetry

A spectrofluorimeter (FluoroMax-3, Horiba Jobin Yvon) was used to measure the absorption and emission spectra of QDs dispersed in either toluene or the monomer mixture or embedded in beads dispersed in DI water. The fluorimeter was set at a slit width of 1 nm for obtaining the spectra for QDs in the monomer mixture or toluene and of 2 nm for QDs embedded in beads. Emission spectra were obtained by exciting the QDs at 458 nm.

Confocal Laser Scanning Microscopy, CLSM

Main hardware parts of a confocal laser scanning microscope are: illumination laser sources, a scan head with necessary optics and electronics including the photomultiplier tube detectors, a microscope, and a computer interface. Schematic representation of the beam path for a confocal microscope has been shown in Figure 2.2. Incident light beam from the laser source is first attenuated through a narrow aperture called the source pinhole, which reduces the beam size to few microns. The beam is subsequently reflected through a dichromatic mirror, passes through the objective and illuminates a point on the focal plane on the sample. Part of fluorescence generated from this illuminated spot which travels backward through the objective can pass through the dichroic mirror and is subsequently focused onto the detector pinhole.

It is the combination of source and detector pinholes which makes laser confocal scanning much more prominent compared to traditional widefield fluorescence microscopy. In a widefield microscope incident light from a mercury or xenon light source is focused down to the sample using an objective, thus illuminating a large spot on the sample. This leads to fluorescence generation from the entire depth of the illuminated spot and results in poor resolution along the depth of the sample. In laser scanning confocal, the source pinhole attenuates the incident beam size down

to a few microns, which subsequently gets focused down to a small spot on the sample ($\approx$1 μm diameter). The sample is then scanned point-by-point with a fine illuminated spot on the sample plane and fluorescence signal is accumulated on the PMT detector through the detector pinhole. 3-D intensity variation of a focused laser beam in CLSM, called the point-spread function (PSF) is assumed to be radially and axially Gaussian [74]. This implies that there will be minimal excitation of the sample above and below the focal plane. Furthermore, any fluorescence signal generated from Out-of-Focus excitation gets further attenuated at the detector pinhole. Hence the combination of source and detector pinhole improves the vertical resolution significantly. In traditional widefield epi-fluorescence microscopy the fluorescence from the illuminated region can be viewed directly through the eyepiece or recorded onto a detector. In the case of confocal laser scanning microscope, fluorescence image is generated through point-by-point scanning of a defined region of the sample. The scan head controls the movement of the illuminated fine spot through galvanometer-based raster scanning mirror system.

Major advantages of laser confocal scanning system are as follows: the first is the improvement in the vertical resolution and contrast as discussed above. In addition, one can image multiple focal planes of a thick sample and reconstruct a three-dimensional image from it. Also, scanning confocal microscopes have the ability to excite and detect multiple fluorescent probes simultaneously. This opens the opportunity for studying the structures based on distribution of specific labeling of a complex structure. This also gives the ability to study structures based on co-localization of the fluorescent probes of interest. Another major advantage of the confocal systems is the inherent improvement in the speed of the image acquisition. This leads to the possibility of dynamic studies on the structures of interest.

Confocal laser scanning microscopy (CLSM; Leica TCS SP2 AOBS, employing an acoustic-optical beam splitter and a prism spectrophotometer detector; 63x oil

immersion objective, NA=1.4, pin hole size 1.0 Airy units) was used to spatially observe the luminescence pattern of the QDs in the beads in serial slices and obtain the emission spectra of individual beads, and of luminescing regions within the beads. Glycerol was used for refractive index matching. All confocal images were acquired using an 8-bit pixel depth false color settings. In the characterizations using CLSM, the beads were excited by a 458 nm laser line.

2.3 Results and Discussion

2.3.1 Physical and Spectral Characterization of QDs in the Monomer Dispersion

The particle size distribution of the 620 nm QDs in toluene and the photoluminescence (PL) spectrum in toluene and in the St/MAA/AIBN monomer mixture serve as a reference for the physical and spectral characterization of these QDs when they are embedded in the polymerized beads. The measured average size (Figure 2.3) of 12.3 nm is consistent with the reported measurement of $\sim$12 nm for the core (CdSe) semiconductor crystals along with the shell (ZnS) and the capping agents. The size distribution of the QD mixture in St/MAA/AIBN are identical to that in toluene, allowing us to conclude that the dispersion of the QDs in the monomer dispersion at the loading concentrations used for bead preparation does not lead to QD aggregation. This is to be expected, since St/MAA/AIBN is hydrophobic and, like toluene, therefore readily disperses the hydrophobically capped QDs. Hence, importantly the starting point for the bead synthesis are micrometer-sized droplets of monomer solution with the QDs uniformly dispersed, and any subsequent aggregation can be attributed to the polymerization process itself.

We also verified that the emission spectra of the QDs when suspended in toluene or St/MAA/AIBN are identical (Figure 2.4). This identical spectral behavior provides additional confirmation of the equivalence of toluene and St/MAA/AIBN as

dispersing solvents for the QDs. In agreement with the observations discussed by Bawendi et al. [46], prolonged exposure of the QDs to AIBN in the St/MAA/AIBN reduces the luminescence intensity of the QDs. For this reason we have carried out the polymerizations of the beads immediately after the addition of the AIBN to maintain a high luminescence intensity.

2.3.2 Monochromatic QD Incorporation in PS Beads

We studied bead embedded with 620 nm QDs at a loading concentration in St/MAA/AIBN equal to 6.12 x 10^{-7} M (moles per liter of styrene), to characterize the luminescence intensity of the QDs and their distribution in the bead. Figure 2.5 shows the optical micrograph and the particle size distribution histogram of the PS beads. On average, each bead contains 2.31 x 10^{7} QDs, as estimated by dividing the known total number of QDs dispersed in the St/MAA/AIBN spray by the number of beads formed. The total number of beads formed is estimated from the total volume of the monomer mixture divided by the volume of a bead with a diameter of (50 μm) approximately at the center of the particle size distribution of beads.

Figure 2.6(a) shows a CLSM luminescence image of one bead, $\sim$45 μm in diameter, loaded with 620 nm QDs, excited by a 458 nm laser line and with their luminescence collected using a detection window from 570 to 660 nm. This z-section image emcompases a $\sim$400 nm thick planar section (given the operating parameter of CLSM), parallel to the coverslip and near the equator of the bead as shown in the inset schematic. Figure 2.6(b) is a superimposition of the luminescence and the interference contrast transmission images of the bead.

The luminescence image provides visual clues that the QDs encapsulated during free-radical suspension polymerization collect in domains, which are distributed throughout the bead. This was also observed in the confocal images of the luminescence of beads embedded with QDs using suspension polymerization as obtained

by O'Brien et al[51, 52] and Vincent et al[33]. The free-radical polymerization reaction of styrene is thermally initiated by AIBN, which, like the QDs, is initially dissolved in the monomer droplet. The time scale for the equilibrium of the temperature within the beads with the surrounding aqueous phase is of the order of several milliseconds (estimated as d^2/κ, where d is the diameter of the bead and κ is the thermal diffusivity of the liquid styrene (about 10^{-3} cm^2/s)). This scale is much shorter than any time scale associated with the kinetics of the free-radical polymerization, or of diffusion of the QD (d^2/D, where D, the diffusivity of a QD in styrene monomer, is of the order of 10^{-10} cm^2/s). Hence, the thermal activation and initiation can be thought of as uniform and instantaneous, and polymerization by free-radical addition of monomer is therefore nucleated at sites uniformly distributed throughout the bead. The consolidation of QDs in the bead into domains from their initial uniform dispersion in the monomer mixture indicates that the QDs are rejected from the polymerizing matrix and are pushed into accessible spaces, e.g., interstitial void spaces, defects, grain boundaries between polymerizing nuclei, or the surface. 3D analysis of the z-sections (i.e., parallel to the coverslip) of the luminescence images reveals that this segregation has led to an interconnected network of QDs distributed throughout the bead.

The rejection of the QDs from the polymerizing matrix of the polystyrene and their self-corralling has both enthalpic and entropic origins and is generally observed in the incorporation of nanoparticles in polymers to form a composite[75]. Enthalpically, the organic ligands capping the QDs are incompatible with the styrene polymer host matrix and this incompatibility drives phase segregation; Russell et al.[76] have observed a self-corralling of CdSe nanorods, capped with hydrophobic ligands, when the nanorods are dispersed in a solution of chloroform and polystyrene and the chloroform is allowed to evaporate. This segregation did not occur when the dissolved polymer and the ligands capping the nanorods were compatible (see also ref [77] for

bulk phase separation between hydrophobic QDs and polystyrene). Entropically, the size of the nanoparticle QDs is such that the entropic cost to the polymer of wrapping around the nanocrystal to accommodate it in the polymerizing matrix is comparatively large, and segregation and self-corralling as a depletion attraction is energetically more favorable[75]. The entropically driven depletion attraction is also evident in the encapsulation of nanoparticles in polymer melts, where glass transition drives nanoparticles into surface cracks and into pre-crazes intentionally introduced in a polymer film[78], in the latter case even when the surface of the nanoparticle is modified with ligands compatible with the polymer. The segregation observed here for the 620 nm QDs in beads is also evident in the case of the smaller QDs, i.e., those luminescing at 520 and 580 nm, indicating that, at least for capped core/shell QDs investigated in this study, the QDs segregate.

QD segregation to the bead surface represents an accessible route for the relocation of QDs, which are initially located near the surface in the monomer mixture, and are being pushed aside as the PS matrix evolves. QD relocation to the surface has also been attributed to a surface-active partitioning of QDs at the aqueous/monomer interface at the beginning of the polymerization [53]. QDs adsorbed at an interface can reduce the interfacial tension of the monomer droplet, and this provides a driving force for their adsorption from the monomer liquid sublayer to the surface. Both surface activity and segregation are reasons for surface relocation, which can explain the usual presence of a luminescent circle around the periphery of the beads in the CLSM z-sections.

Figure 2.7 shows the confocal spectral scan of the luminescence from the z-section in Figure 1a. The emission peak is centered at 617 nm, in good agreement with the emission spectrum obtained for QDs in St/ MAA/AIBN using a fluorimeter. Thus in the context of bar-coding, the encapsulation of a single color in the beads by the spraying suspension polymerization technique retains the color label placed in the

bead.

2.4 Conclusion

We examined the spraying suspension polymerization method for incorporating monochromatic (620 nm emission maximum; red color) quantum dots in the interior of polymer (polystyrene) microspheres. CLSM luminescence images showed that the QDs were pushed into inclusions in the polymerized beads. Comparison of spectral emission profile measured by CLSM demonstrated that the peak emission wavelength of the hydrophobically capped QDs remains unshifted from their value recorded from a reference consisting of a solution of the QDs dispersed in a solvent at the same loading concentrations as in the bead.

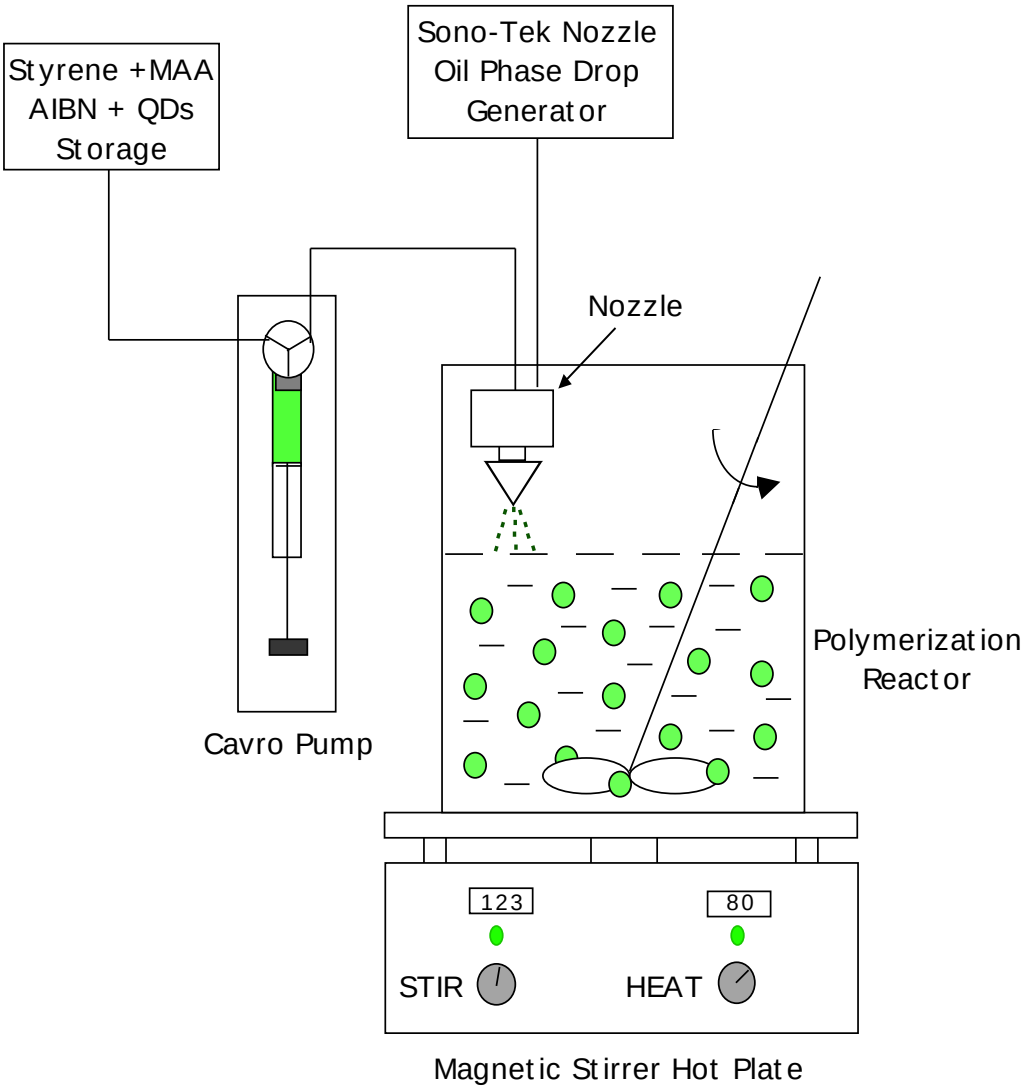

Figure 2.1: A schematic representation of the experimental set up for spraying suspension polymerization.

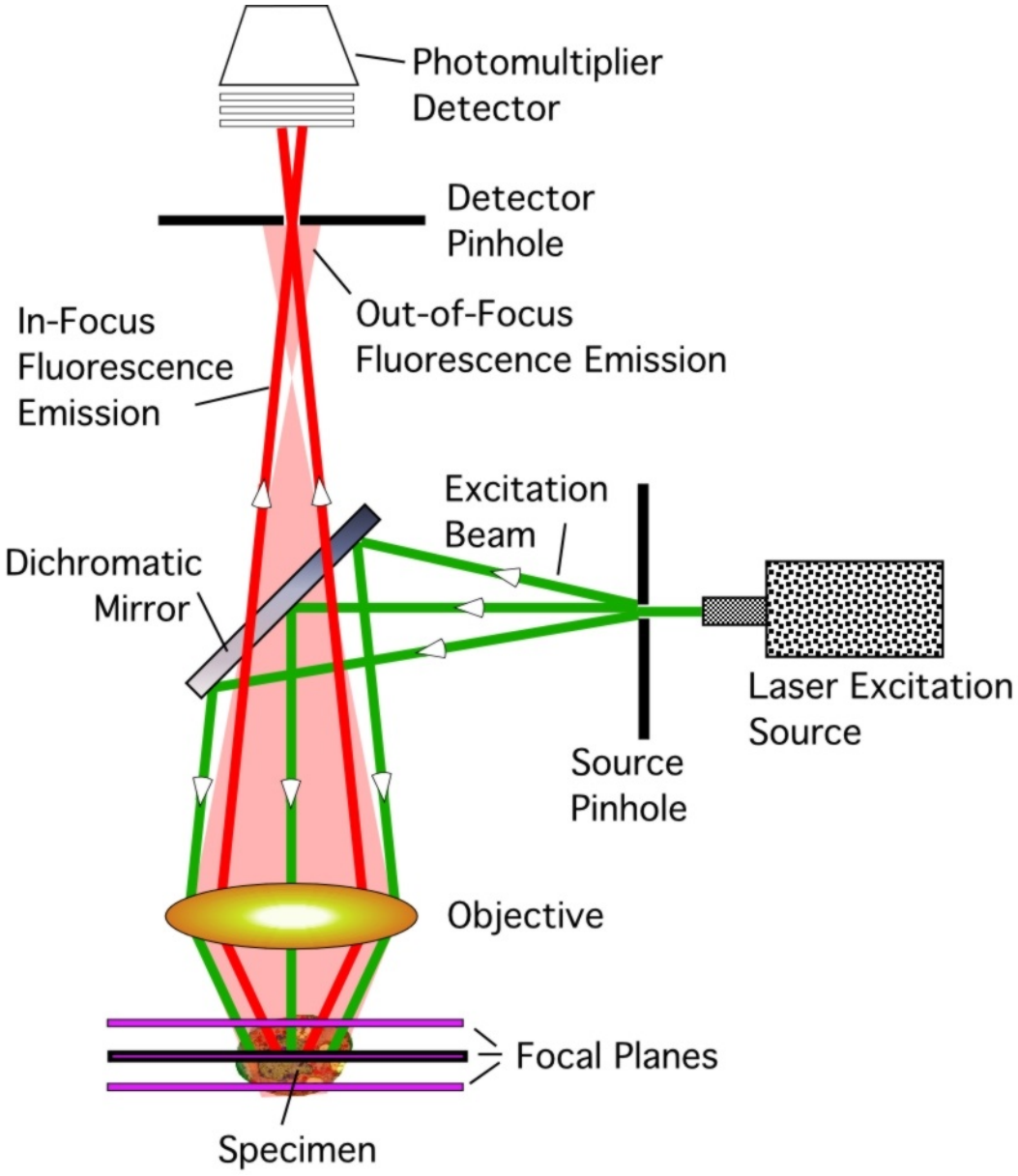

Figure 2.2: Schematic representation of the beam path in a confocal laser scanning microscope (CLSM). Excitation beam is attenuated by source pinhole, reflected by the dichroic mirror and is focused onto a small spot by the objective. Fluorescence generated from the excitation plane makes its way through the objective, dichroic mirror and detector pinhole into the photomultiplier detector. Fluorescence signal generated from the Out-of-Focus plane is rejected by the detector pinhole.

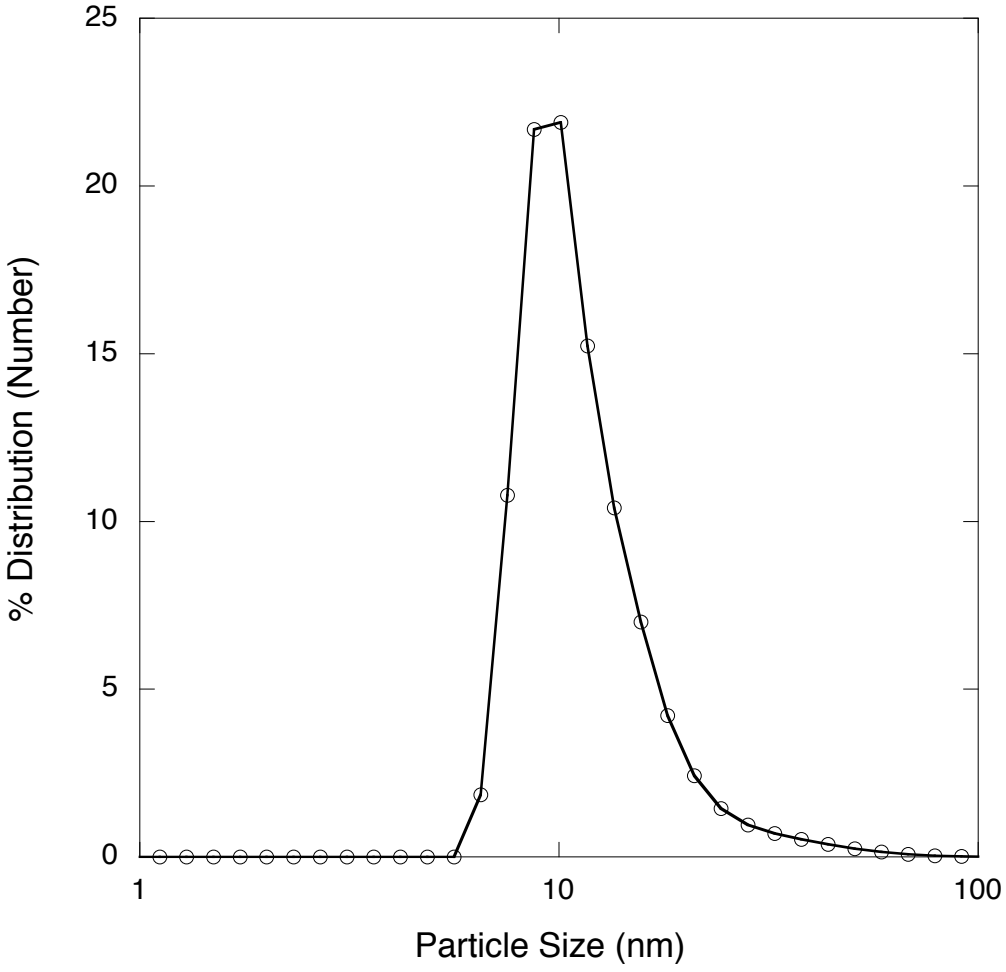

Figure 2.3: Physical characterization of the 620 nm QDs. Particle size distributions as measured by dynamic light scattering of 620 nm QDs dispersed in St/MAA/AIBN.

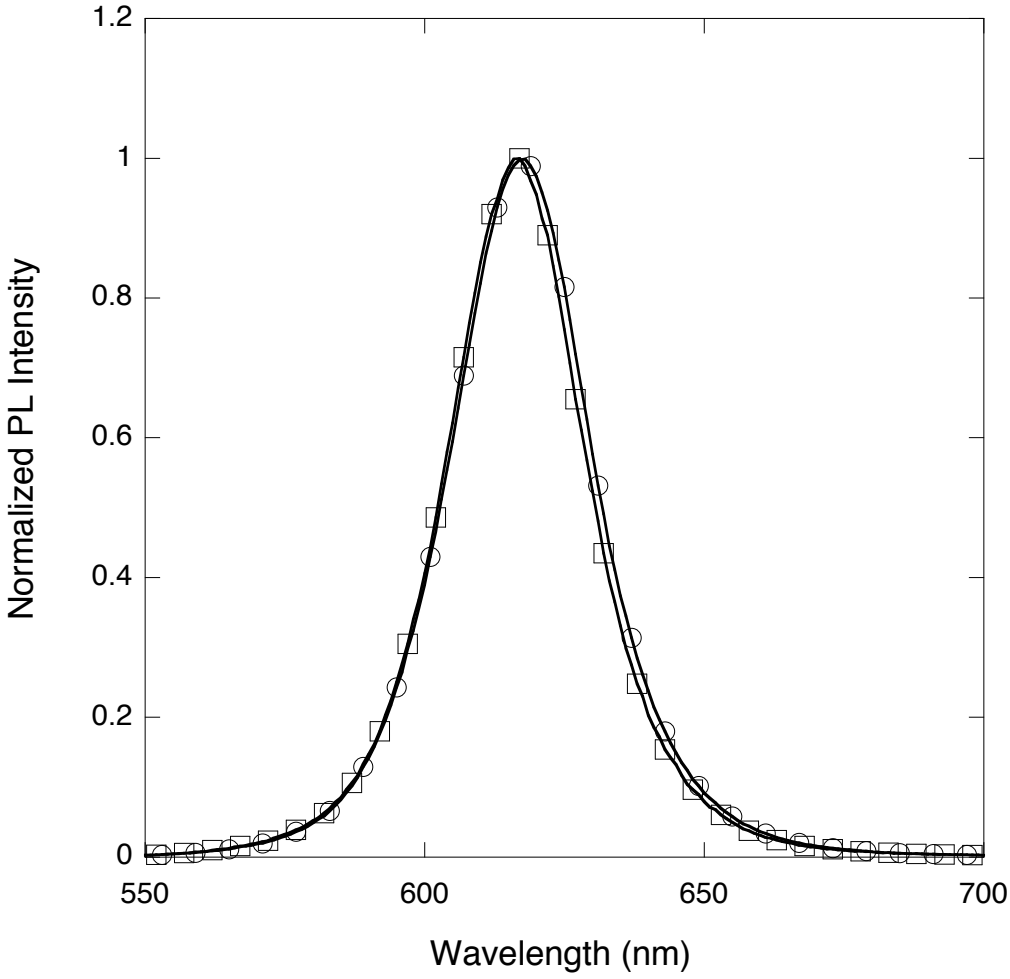

Figure 2.4: Spectral Characterization of the 620 nm QDs. Photoluminescence (PL) emission spectra of the QDs dispersed in toluene (□) and St/-MAA/AIBN (◯).

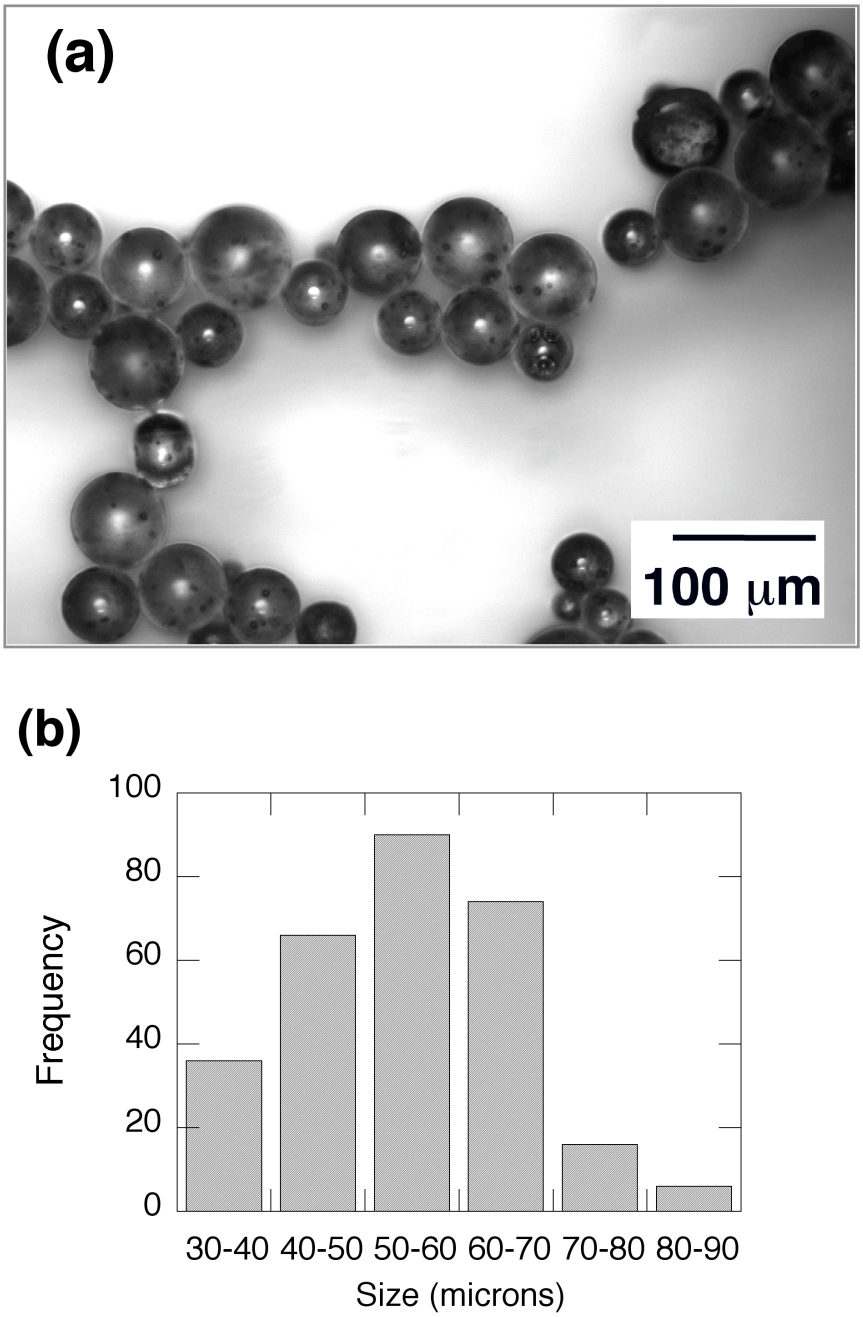

Figure 2.5: Optical characterization of the PS beads obtained using spraying suspension polymerization. (a) Optical micrograph image at 20x magnification. (b) Particle size distribution histogram. The beads are between 30-90 μm in diameter. Average diameter is $\sim$50 μm.

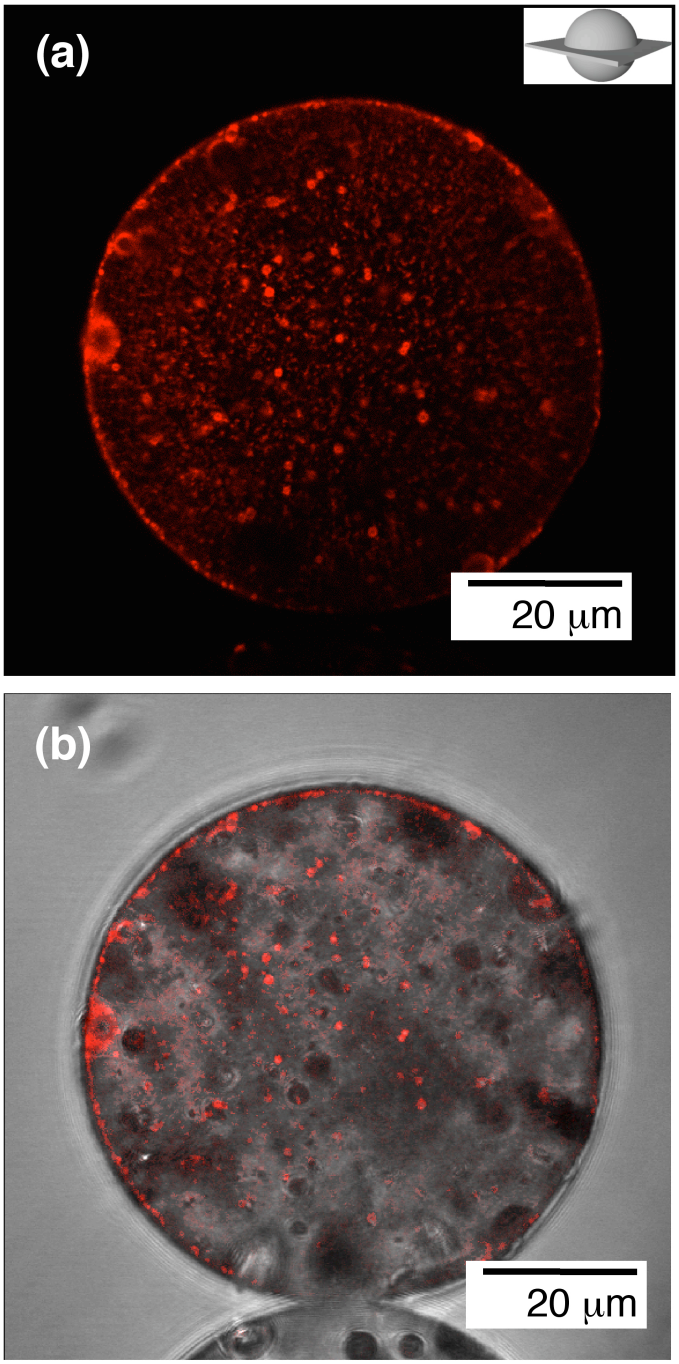

Figure 2.6: CLSM images of PS beads obtained using spraying suspension polymerization and loaded with 6.12 x 10^{-7} M (moles per liter of styrene) 620 nm emission maximum QDs. (a) CLSM luminescence image of the PS bead. Luminescence was collected in 570-660 nm window. (b) Superimposition of the luminescence image (a) and interference contrast transmission image (not shown) of the beads, indicating the appearance of luminescence from the beads.

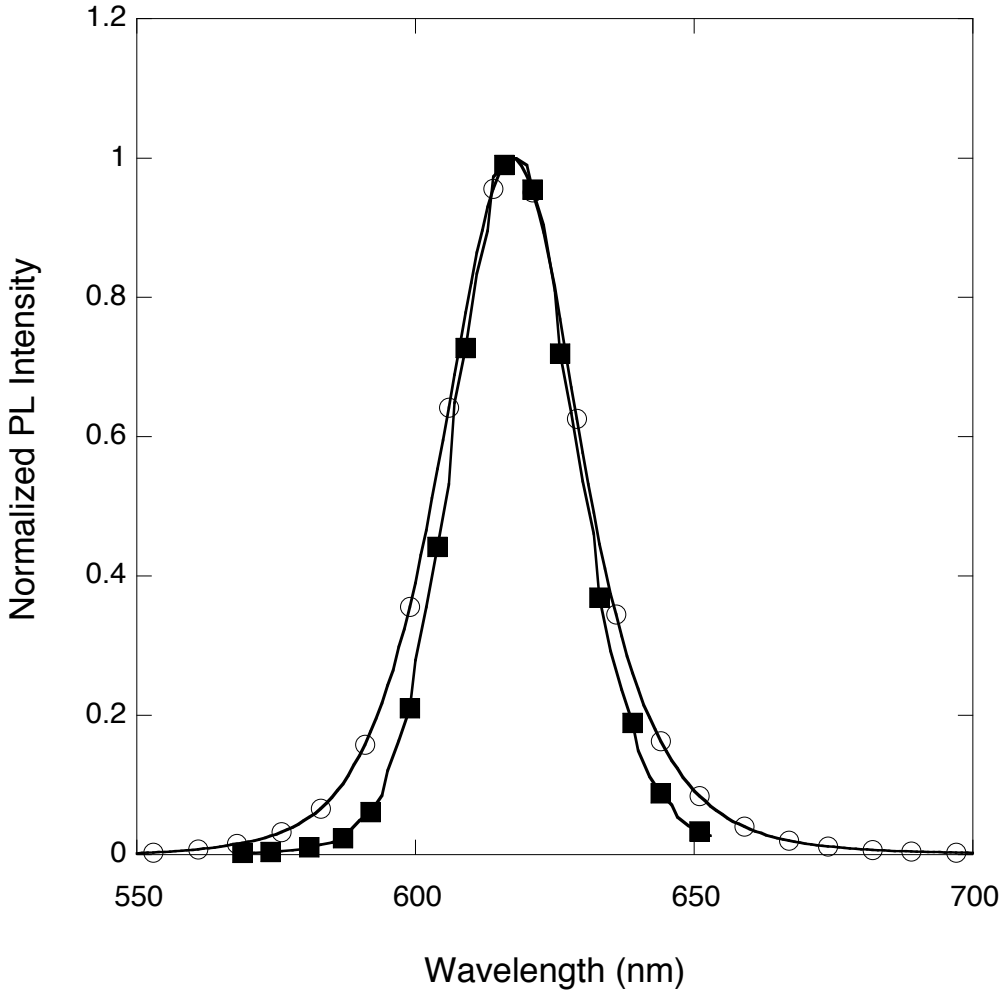

Figure 2.7: Comparison of the CLSM spectral scan (■) of the bead in Figure 2.6 with the fluorimeter emission spectrum (◯) of the 620 nm QDs dispersed in St/MAA/AIBN. The emission peak for the bead is in good agreement with that of QDs in St/MAA/AIBN.

Chapter 3

Ratio-metric Barcoding using Multicolored Quantum Dots

3.1 Introduction

In Chapter 2, we demonstrated use of spraying suspension polymerization in qualitative incorporation of the monochromatic quantum dots in polystyrene beads. We further used this approach to incorporate multicolored QDs at different loading concentrations inside PS beads. In this chapter we discuss the development of the color and intensity based ratio-metric barcodes by incorporating three colored QDs at two different loading concentrations inside PS beads and the dependence of the developed ratio-metric barcodes on the bead size.

3.2 Experimental Section

3.2.1 Materials

Styrene (ACS reagent grade), poly-vinyl alcohol (PVA; hydrolyzed, average molecular weight - 88,000), ethyl alcohol (ACS reagent grade), methyl acrylic acid (MAA; ACS reagent grade), and methyl methacrylate (MMA; ACS reagent grade) were purchased from Spectrum Chemicals, CA. 2,2'-Azobis-(2-methylpropionitrile) (AIBN, 98%) was obtained from Sigma Aldrich Co. CdSe/ZnS core/shell QDs, capped with trioctylphosphine oxide and hexadecylamine, dispersed in toluene were obtained from Evident Technologies, NY. Three different color QDs with emission maximums (as reported by the manufacturer) at 520 (denoted green), 580 (denoted orange), and 620 nm (denoted red) were used. Deionized (DI) water with resistivity equal to 18 MΩ·cm was obtained using a Millipore system. All chemicals were used as is without further purification.

3.2.2 Encapsulation of Multicolored QDs in PS Beads

Polystyrene (PS) microspheres (beads) embedded with multicolored QDs were obtained using a spraying suspension polymerization procedure (Figure 2.1). The

aqueous phase was a 2 wt% aqueous PVA solution continuously stirred with a magnetic stirrer and maintained at 80 °C. QDs suspended in toluene with different emission wavelengths (colors) and in different quantities (tens of microliters, for each color) were dispersed at room temperature into 1.25 mL of monomer mixture, St/MAA/AIBN or 1.2 mL of MMA and AIBN (5 wt% MMA), abbreviated MMA/AIBN. This mixture was sprayed using the Sono-Tek ultrasonic nozzle with the mixture being pumped to the nozzle using the Cavro syringe pump. After 2 hours of polymerization, the reaction mixture was cooled, and the beads were recovered using centrifugation and subsequently washed with a 40:60 mixture of ethanol and water. The beads were stored in DI water.

3.2.3 Characterization of the multicolored QDs dispersed in monomer and embedded in PS beads

The multicolored QD encoded beads and the QDs dispersed in monomer mixtures were characterized using the CLSM, fluorimeter, optical microscopy and DLS (as described in Chapter 2).

3.3 Results and Discussion

3.3.1 Multicolored QD Encoded Beads

Polystyrene beads with multicolored QDs were prepared by using the spraying suspension polymerization method to incorporate QDs emitting in the green (520 nm), orange (580 nm) and red (620 nm) parts of the spectrum with a relative molar ratio of 21.7:6.1:1 and a total loading concentration of 5.29 x 10^{-6} M dispersed into the St/MAA/AIBN. In Chapter 2, we discussed the identical behavior of the particle size distributions of 620 nm QDs when dispersed in toluene and in the St/MAA/AIBN monomer mixture. Here we report the particle size distributions (Figure 3.1(a)) of the green, orange, and red QDs used in multicolored bead prepa-

rations, and the measured and the reported average sizes of these QDs dispersed in toluene were in good agreement with one another. Comparison of the particle size distributions of 21.7:6.1:1 molar ratio mixtures of these QDs dispersed in toluene and in St/MAA/AIBN monomer mixture (Figure 3.1(b)) shows that the dispersion of the QDs in the monomer-QD solution at their loading concentrations used for bead preparation does not lead to QD aggregation.

Figure 3.2(a–c) are the confocal luminescence images of equatorial z-sections of three beads, approximately 50 μm in diameter, obtained by simultaneous collection of the photoluminescence in three detection windows: 480–545 nm (green), 545–590 nm (orange), and 590–660 nm (red) respectively for the 520, 580, and 620 nm QDs. Figure 3.2(d) depicts the superimposition of the above three images. The visual evidence of these figures indicates that all three colors are present in each of the QD domains in the beads. This suggests that the QDs, despite their differences in size–measured from the particle size distribution data of the individual QDs dispersed in toluene (Figure 3.1(a))–are segregated into the void spaces as they are rejected from the polymerizing polystyrene matrix. Spectral scans of the luminescence from the z-section of each of the beads in Figure 3.2 are shown in Figure 3.3, and these spectra are virtually identical from bead-to-bead. The spectra of these individual beads obtained using CLSM also show a close resemblance with the emission spectra of an ensemble of these beads (dispersed in DI water) obtained using the fluorimeter.

The self-corralling of the QDs during the polymerization – as observed in Chapter 2 for monochromatic QDs embedded PS beads – is evident from the confocal luminescence images. The effect of self-corralling on the emissions from the individual QDs have been discussed in Chapter 4.

3.3.2 Ratio-metric Color/Intensity Barcodes

The QD barcode of a bead is read by deconvoluting the emission spectra to recognize

- the color labels through the identification of the peak emission wavelengths,
- the intensity levels for each color from the magnitude of the peak.

For the QD encoded beads fabricated in this study by encapsulating the QDs in the beads in a spraying suspension polymerization, the colors corresponding to each of the peak emission wavelengths are easily identified. The reason is that the peak emission wavelengths corresponding to individual colors are not shifted when the QDs are incorporated in the beads from their locations in the spectrum of the QD dispersions in toluene (see Figure 3.4). Given the fact that the emission peaks of nanocrystals can be tuned continuously over the visible spectrum by their size, a large number of colors are available to insure a high coding capacity.

Ratio-metric Barcoding

It is more challenging to read the intensity of each color component of the barcode. The intensity is controlled by the QD loading in the bead. In the simplest approach for QD intensity barcoding, as outlined by Nie et al. [29], the intensity level of each bead is varied in a series of i levels by loading different numbers of QDs, i.e., n_1, $n_2 \ldots n_i$, and this is referred to as absolute intensity encoding. The requirement on the loading concentrations in absolute encoding is that the resultant intensities have to be distinguished from one another in a spectral scan. This unique identification of intensity levels encounters two difficulties: First, in any of the techniques for encapsulating QDs in beads (impregnation by infiltration, outer shell embedding or encapsulation by in situ polymerization), the larger the bead size (or shell) the larger the QD loading. Hence larger beads encoded with a low intensity level could in principle have the same code as smaller beads encoded with a higher level. Variations in the bead size have to be considered in devising loading levels to make sure that the intensity codes can be read uniquely. A second difficulty in intensity decoding is insuring a large enough signal to noise ratio for all the beads to be de-

coded. As noted by Eastman et al. [79] in a study using QD shell-encoded beads to develop a functioning multiplexed microarray assay, for the signal-to-noise ratio to be acceptable for all beads *read*, it is important that the total intensity level in each bead be approximately constant. In this way there are no weak emitting beads that can be affected by noise. Without regard for this, in a collection of beads in which each bead has an arbitrary intensity level (absolute intensity encoding) the detector has to be adjusted to read accurately (without saturation) the spectra of beads with each color loaded at the highest intensity levels. As a result, the beads with lower intensities for each color will have a much smaller signal to noise ratio than the beads encoded with higher color intensities, and this can lead to errors in decoding.

Eastman et al.'s solution to this problem is to load the beads with QDs in such a way that the total intensity is approximately constant. Although there are several ways to undertake the encoding with this constraint, Eastman et al. parcel the QDs in packets of intensities: They set a total luminescence intensity of the QDs to be included in a bead equal to s, and divide this number into i identically numbered "packets," with each packet having intensity equal to s/i. The number of QDs in each intensity packet is different for each color. Summing of packets of a particular color represents encoding the intensity level of that color. The QDs were distributed in each bead in these packets, and a total of i color packets are included per bead so that the total intensity per bead is s. The packets included in a bead are varied to generate different codes under the constraint of including exactly i packets; thus in some beads some packets of a particular color can be absent representing a zero intensity for that color. For example, Eastman et al. examined 12 intensity levels and 4 colors for a total of 455 combinations. To encode larger numbers (which would be of interest in the use of these beads for multiplexed assays) advantage can be taken of the large numbers of colors available for QDs; for this same 12 intensity

levels, and seven colors, 1.9 x 10^4 codes can be generated.

Embedding the beads with a constant total QD intensity has the added advantage that the encoding of intensities of individual colors can be scripted by using the ratios of color intensities in the beads rather than their absolute measure. In ratio-metric encoding, the intensity code for each color is the intensity of its peak in the spectrum divided by the total intensity of all the peaks. This type of approach makes decoding much more accurate because, as reported by Weiss et al. [80] for molecular imaging, and Nie et al. [32] for decoding QD barcodes in beads, ratio-metric measurements are superior to absolute measurements because the simultaneous measurement reduces the effect of instrumental drift or fluctuations. When the intensity part of the code is based on decoding absolute intensities with varying numbers of QDs in the bead, the ratio-metric code can be non-unique: Two beads with identical fractions but one with a higher total number of QDs than the other would have the same ratio-metric code but not the same absolute intensity code.

Ratio-metric encoding has the added advantage that it removes the dependence of the intensity code on the bead size, which as we mentioned above was one of the two essential problems associated with absolute intensity barcoding. In the context of this study in which the QDs are encapsulated using spraying suspension polymerization, because the beads develop from monomer droplets, each with the same composition of QDs (since they were sprayed from a well-mixed reservoir), whatever the size of the droplet the mole fractions of the QDs should be identical, and their relative color intensities should be equivalent.

Ratio-metric Barcoding by Color

To demonstrate how ratio-metric encoding removes the dependence of the bead size on the intensity part of the code for QDs encapsulated by spraying suspension

polymerization, we decode the beads described in Section 3.3.1, which encapsulated three QDs, green (520 nm), orange (580 nm) and red (620 nm) with a relative molar ratio of 21.7:6.1:1 and a total loading concentration of 5.29 x 10^{-6} M. The spectrum of an individual bead is obtained by taking serial z-sections luminescent images of a bead and adding them to obtain a cumulative emission spectrum. Each peak in this spectrum is modeled as a Gaussian curve, and the entire spectrum is fitted by summing the individual Gaussian peaks. Once the spectrum is fitted, the areas under the Gaussians for each color are obtained to calculate the individual color intensities, and the area under the fitted spectrum (which is the sum of the individual Gaussian areas) is computed to evaluate the total intensity. The relative intensity of each color is then obtained by dividing the individual color intensities by the total. Table 3.1 gives the results for the ratio-metric barcodes of seven beads, with different sizes as noted in the table. As is evident in the table, despite a large variation in the bead size the average code is within ≈5% of the codes for the individual beads for a variation in the bead diameter of ≈10%.

Ratio-metric Barcoding by Intensity

The generation of a large number of codes requires that several different intensity levels be distinguished per color in the encoded beads. To illustrate that our spraying suspension polymerization method can be used for synthesis of beads with distinguishable intensity levels for each color, we reduced the amount of 620 nm QDs and increased the amount of 520 nm QDs in the 21.7:6.1:1 molar ratios of the three colored QDs. For the new ratio, we incorporated the three colored QDs in a relative molar ratio of 22.0:6.1:0.33 and a total concentration of 5.23 x 10^{-6} M in PS beads. We imaged these new beads along with the beads embedded with the same three colored QDs in 21.7:6.1:1 molar (previous ratio). Figures 3.5(a) is a superimposition of the CLSM luminescence images comparing two PS beads em-

bedded with the two molar ratios of the QDs, i.e., 21.7:6.1:1 and 22.0:6.1:0.33 both at almost similar total concentrations. The beads were excited by the 458 nm laser line and the luminescence was collected in the following detection windows: 470-545 (green), 545-600 (orange), and 600-660 (red) nm. Although visually the difference in the luminescence between the two beads is not obvious, their co-additions of the spectral scans (Figure 3.5(b)) are clearly distinguishable. Table 3.2 gives the result of the ratio-metric barcodes of three beads, of different sizes (noted in the table), prepared by using 22.0:6.1:0.33 molar ratios of the three colored QDs. Again, as is evident in the table 2, despite a large variation in the bead size the average code is within $\sim$5% of the codes for the individual beads with more than a 10% variation in the bead diameter. We believe these results to be typical of the ability to distinguish two closely related codes, supporting our view that the approach has an inherently high encoding capacity. The ratio-metric codes appeared stable over several months, with only a small blue shift ($<$5 nm) in the peak intensity due to oxidation of the shell of the QDs.

As can be seen, the spectra of the equatorial z-section (Figure 3.3) and of the co-addition (Figure 3.5(b)) for Bead 1 show a lower ratio of the green intensity peak to the red peak. This can be accounted for by reabsorption; luminescence from the green QDs reaching the detector travels through the lower half of the bead where it can be reabsorbed by the red QDs. Spectra taken from lower z-sections that approach the cover slip have a shorter path length and hence a smaller reabsorption; the composite of Figure 3.5(b) reflects these shorter path length contributions. This reabsorption is also evident in Figure 3.3, which compares the CLSM equatorial spectra of a single bead with the spectra of an aqueous dispersion of beads measured in a cuvette by a fluorimeter with a 1-cm path length. The lower ratio of the green to the red reflects the greater reabsorption in the dispersion due to the larger path length of the dispersion than the equatorial section.

3.4 Conclusion

We demonstrated capability of incorporating three colored QDs (520nm (green), 580 nm (orange) and 620 (red) nm)) in PS beads using spraying suspension polymerization to obtain two distinct concentration barcode scripts. Confocal laser scanning microscopy (CLSM) luminescence images showed, multicolored scripts, the results showed that the QDs of all colors, despite their size difference, are pushed as a group into the inclusions. The spectral emission profiles for individual beads and for the two scripts as measured by the CLSM demonstrated that the peak emission wavelength of the hydrophobically capped QDs remain unshifted from their values recorded from a reference consisting of a solution of QDs individually dispersed in a solvent at the same loading concentrations as in the bead. This allows the color parts of the code to be easily recognized.

A second issue, which was addressed is the effect of the bead size on the barcode. Suspension polymerizations are problematic for producing beads in which the particle size distribution is rather broad. This can have an adverse effect on deconvoluting the intensity part of the bar code, since smaller beads encoded with a higher intensity of a particular color (a higher concentration of that colored QD) could – because of its smaller size – have a measured intensity for that color lower than that of a larger bead with a nominally lower encoded intensity for that color. We demonstrate that by reading the barcode as a ratio-metric code – i.e., constructing the code as the intensity of a particular color divided by the total intensity – removes the dependence of the code on the bead size. For each of the two scripts studied, tables of the ratio-metric barcode for beads of varying size were compiled, and the codes were shown to differ by less than 5% for a 10% or more variation in the bead size.

Table 3.1: Comparison of estimated Barcodes for the PS beads embedded with 21.7:6.1:1 molar ratio of 520, 580, and 620 nm QDs.

QDs	**Bead**								
	[No.]	1	2	3	4	5	6	7	mean
	[size(μm)]	(52)	(50.7)	(54)	(44)	(50.4)	(47)	(48.7)	
520 nm		0.156	0.142	0.164	0.156	0.148	0.148	0.152	0.152
580 nm		0.303	0.283	0.305	0.278	0.281	0.272	0.307	0.290
620 nm		0.541	0.575	0.531	0.566	0.571	0.580	0.541	0.556

Table 3.2: Comparison of estimated Barcodes for the PS beads embedded with 22.0:6.1:0.33 molar ratio of 520, 580, and 620 nm QDs.

QDs	**Bead**				
	[No.]	1	2	3	mean
	[size(μm)]	(52.56)	(67.2)	(56.19)	
520 nm		0.202	0.210	0.199	0.203
580 nm		0.516	0.489	0.501	0.502
620 nm		0.282	0.301	0.300	0.294

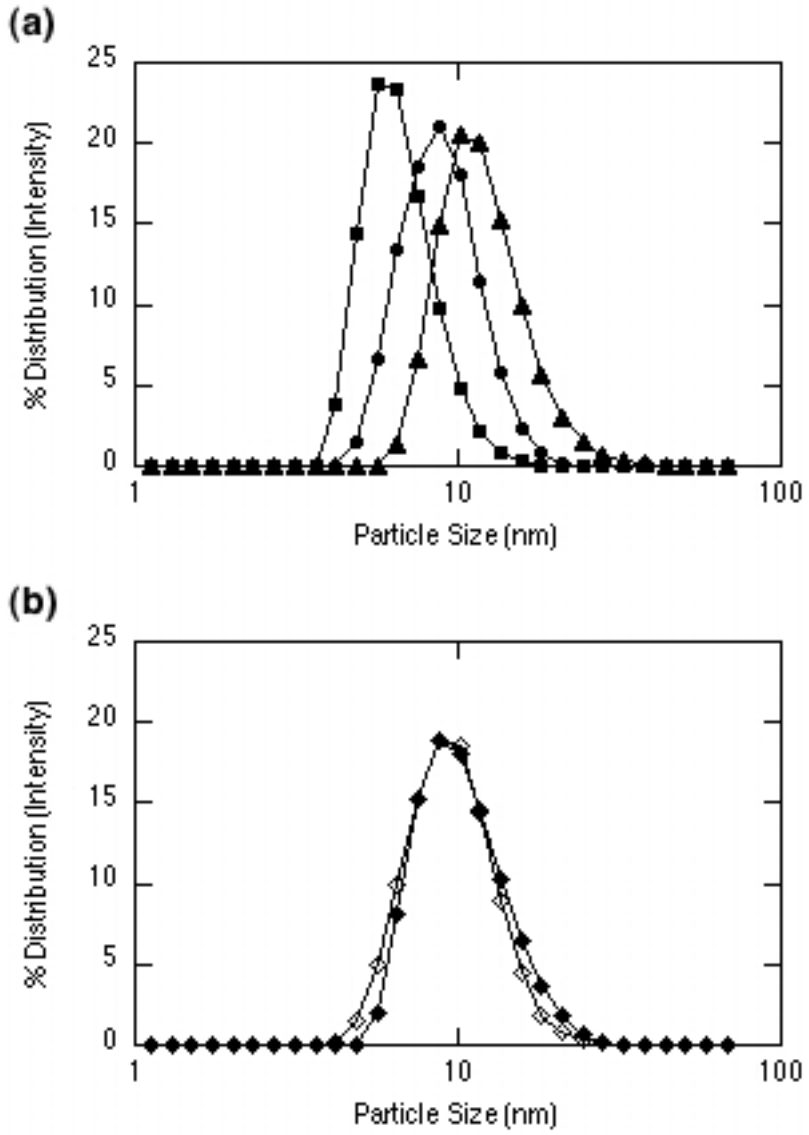

Figure 3.1: Particle size characterization of the QDs. (a) Particle size distributions as measured by dynamic light scattering of 520 nm (■), 580 nm (●), and 620 nm (▲) dispersed in toluene at the concentrations used in the bead preparation. (b) A 21.7:6.1:1 molar ratio mixture of these three QDs dispersed in toluene (⧫) and St/MAA/AIBN (◊). The distribution of the mixture appears to be skewed towards the larger particle sizes because the dynamic light scattering measurements inherently bias the intensity based size distributions of mixtures towards the particles of larger sizes.

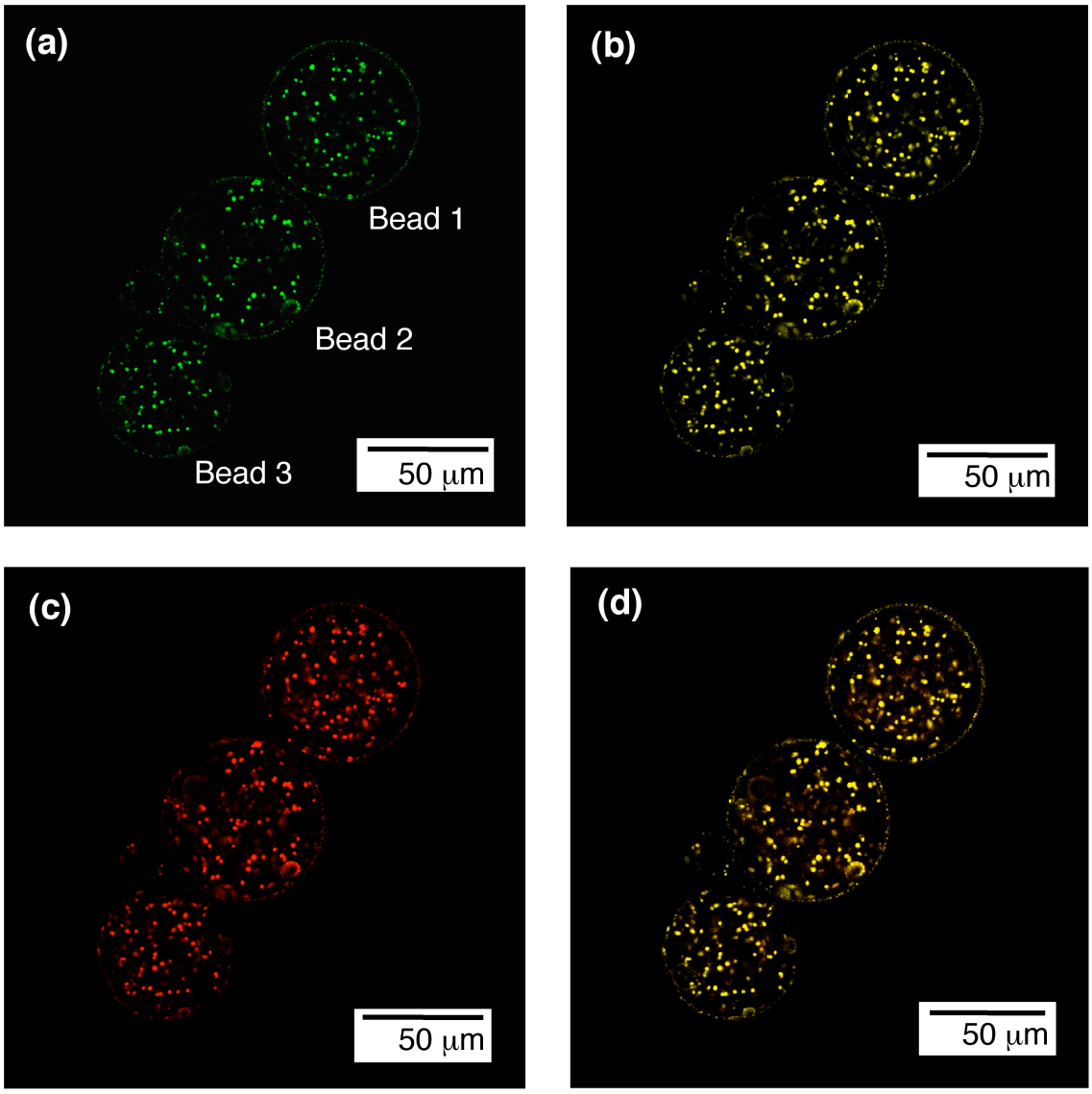

Figure 3.2: CLSM luminescence images of the PS beads embedded with 520 (a), 580 (b), and 620 nm (c) QDs in 21.7:6.1:1 molar ratio and total concentration of 5.29 x 10^{-6} M. The emission collection windows used were 480-545 (a), 545-590 (b), and 590-660 nm (c), respectively. (d) is a superimposition of (a–c).

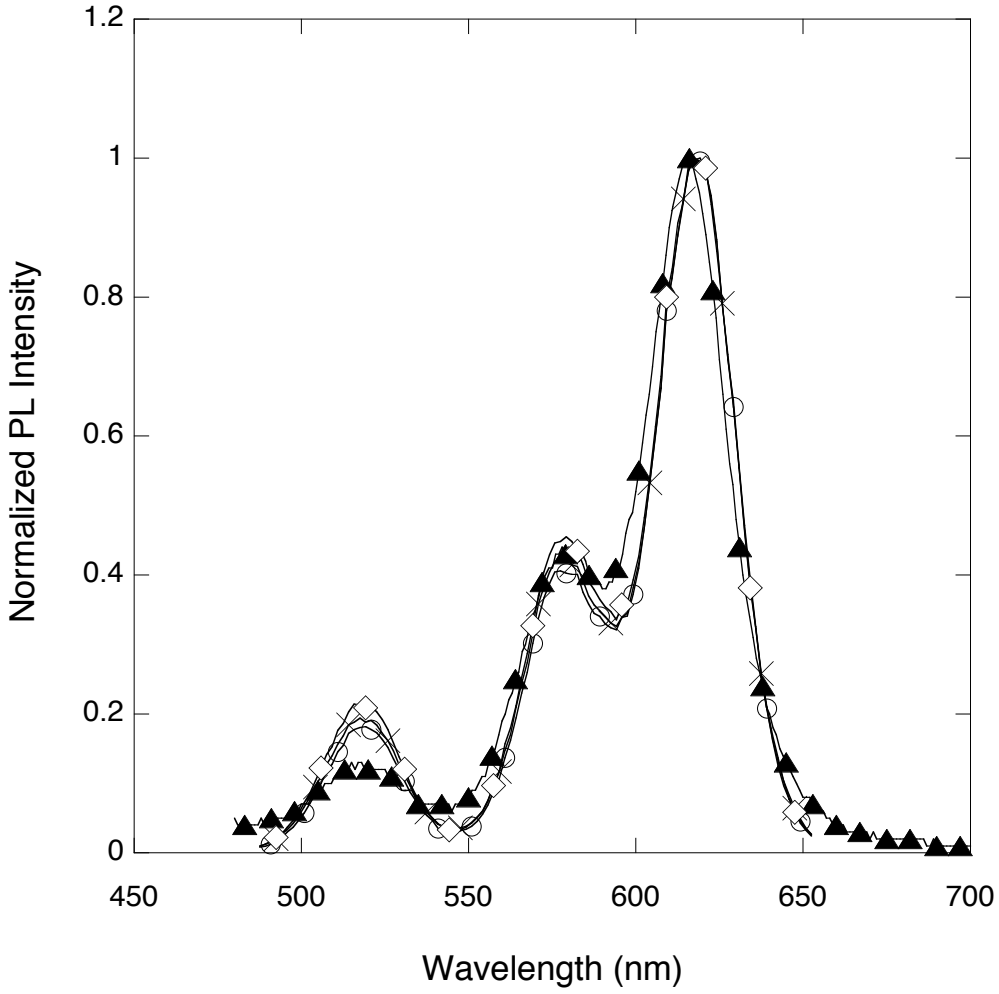

Figure 3.3: Comparison of the CLSM spectral scans of bead 1(×), bead 2 (◯), and bead 3 (◇) in Figure 3.2 with the emission spectrum (▲) of an ensemble of these beads obtained using the fluorimeter.

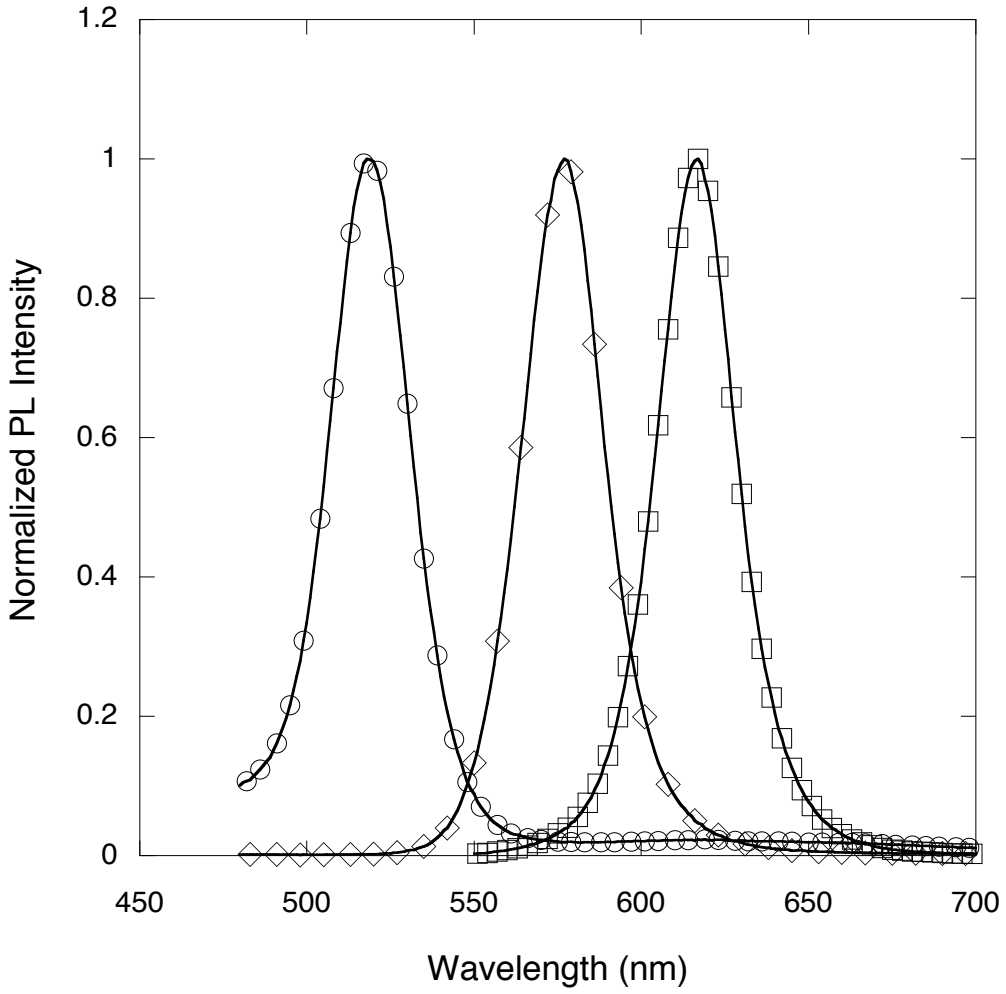

Figure 3.4: Fluorimeter emission spectra of 520 (◯), 580 ((◇), and 620 ((□) nm QDs dispersed individually in St/MAA/AIBN at the concentrations used in the preparation of three-colored encoded PS beads. All the QDs were excited at 458 nm.

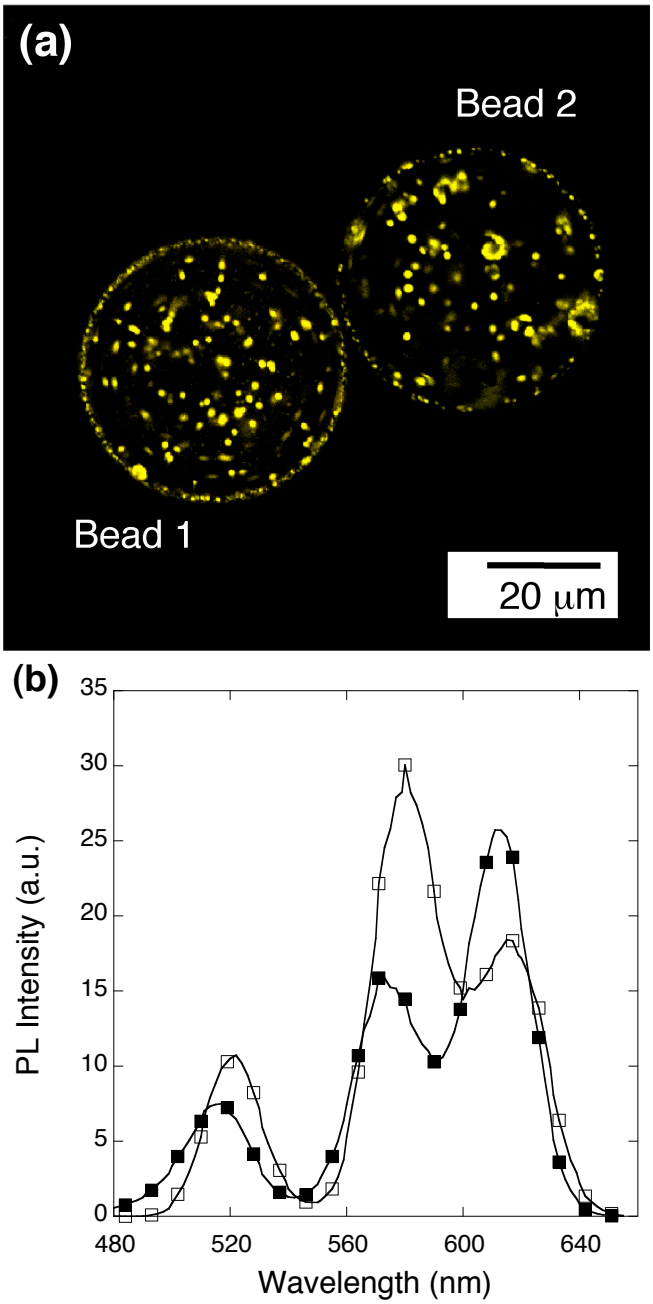

Figure 3.5: Comparison of the two PS beads embedded with 21.7:6.1:1 (bead 1) and 22.0:6.1:0.33 (bead 2) molar ratios of 520, 580, and 620 nm QDs in almost identical total concentrations. (a) Superimposition of the CLSM luminescence images of bead 1 and bead 2–dried together on a coverslip– in collection windows of 470–545, 545–600, and 600–660 nm. (b) Coaddition of CLSM spectral scans over volume of bead 1 (■) and bead 2 (□) clearly show the difference in the luminescence intensities obtained by change in the ratio of the incorporated QDs in the beads.

Chapter 4

Electronic Energy Transfer: Analysis and Reduction

4.1 Introduction

In Chapter 3, we discussed successful incorporation of multicolored quantum dots in polystyrene beads in two molar ratios to obtain distinct color and intensity based ratio-metric barcodes. A further comparison of the emission profiles of the multi-colored beads with that of the neat QDs dispersed in St/MAA/AIBN (see Figure 4.2) shows the mismatch in the emission intensities before and after incorporation of the QDs inside PS beads. We observed that a phenomenon called electronic energy transfer makes the lower wavelength QDs transfer their luminescence energy to the higher wavelength QDs, thus changing the relative emission intensities of the QDs after their incorporation in the beads. The energy transfer associated with the proximity of the multicolored QDs due to their observed aggregation (see Figure 3.2) in the polymerized beads limits our abilities to apriory define or script a ratio-metric barcode. In order to reduce the energy transfer, more uniform distribution of the QDs in the polymer matrix is needed. To this effect, we employed experimental procedures involving use of cross-linking agents such as divinyl benzene as one of the monomer units along with the styrene. In this chapter, we report the development of optically barcoded polymer beads by using styrene and/or di-vinyl benzene as monomers and study the effect of cross-linking on the energy transfer and subsequently on the development of ratio-metric barcode.

4.2 Experimental Section

4.2.1 Materials

Styrene, di-vinyl benzene (DVB; ACS reagent grade), toluene (ACS reagent grade), PVA (hydrolyzed, average molecular weight - 88,000), ethyl alcohol, acetone (ACS reagent grade), MAA, and methyl methacrylate (MMA; ACS reagent grade) were purchased from Spectrum Chemicals, CA. AIBN was obtained from Sigma Aldrich

Co. CdSe/-ZnS core/shell QDs, capped with trioctylphosphine oxide and hexadecylamine, dispersed in toluene were obtained from Evident Technologies, NY. Multicolored QDs with the emission maximums (as reported by the manufacturer) at 520 (denoted green), 560 (denoted yellow), 580 (denoted orange), and 620 nm (denoted red) were used. Deionized (DI) water with resistivity equal to 18 MΩ·cm was obtained using a Millipore system. All chemicals were used as is without further purification.

4.2.2 Experimental Procedure

Polystyrene beads encoded with three colored QDs (Bead 1 from Chapter 3) were dispersed in weight averaged mixture of glycerol and water for their characterization in spectrofluorimeter. Polymer beads embedded with multi colored QDs were obtained using the spraying suspension polymerization method. The aqueous phase was a 2 wt% aqueous PVA solution continuously stirred with a magnetic stirrer and maintained at 80 °C. PS beads embedded with two colored QDs (emitting at 520 and 580 nm and dispersed in St/MAA/AIBN at the relative molar ratio of 1:1 and a total concentration of 5.29 x 10^{-6} M (moles per liter of St)) were obtained. Polymethyl methacrylate (PMMA) beads embedded with 520, 580, and 620 nm QDs were obtained by dispersing the QDs – at the same composition and the total concentration as that used for Bead 1 in Chapter 3 – in a monomer mixture of MMA, MAA (5 wt% MMA), and AIBN (5 wt% MMA), abbreviated as MMA/MAA/AIBN.

In the next set of experiments, polymer beads embedded with two colored QDs were obtained using the spraying suspension polymerization method, wherein the aqueous phase was maintained at the conditions described above. 560 and 620 nm QDs were dispersed at room temperature into four different mixtures obtained by mixing the monomers as follows: i) 2 mL of styrene (St), MAA (5 wt% St), and AIBN (5 wt% St), abbreviated as St/MAA/AIBN-1, ii) 2 mL of styrene (St), MAA (5 wt%

St), and AIBN (10 wt% St), abbreviated as St/MAA/AIBN-2, iii) 2 mL of 50:50 volume mixture of St and DVB (St-DVB), MAA (5 wt% St-DVB), and AIBN (7.5 wt% St-DVB), abbreviated as St-DVB/MAA/AIBN, and iv) 2 mL of DVB, MAA (5 wt% DVB), and (5 wt% DVB), abbreviated as DVB/MAA/AIBN. Each mixture was sprayed using the Sono-Tek ultrasonic nozzle with the mixture being pumped to the nozzle using the Cavro syringe pump. After 3 hours of polymerization, the reaction mixture was cooled, and the beads were recovered using centrifugation and subsequently washed with a 40:60 mixture of ethanol and water. The beads were stored in DI water.

4.2.3 Characterization

Polymer beads were analyzed using CLSM, optical microscopy, and spectrofluorimetry (as described in Chapter 2). The distribution of the QDs in the bead matrix was studied using transmission electron microscopy (TEM) and high-resolution transmission electron microscopy (HRTEM). Differential scanning calorimetry (DSC) was used to characterize the effect cross-linking on distribution of QDs in the bead matrix. The principles of TEM and DSC are described below in brief.

Transmission Electron Microscopy, TEM

TEM is a microscopy technique in which high-energy electrons are passed through ultra-thin specimens to obtain nanometer level structural details. Electron microscopy techniques, TEM in particular, has magnification and resolution capabilities that are a thousand times (as low as 0.1 nm) beyond that offered by the light microscope (about 250 nm). The TEM instrument is a complex viewing system equipped with an electron gun, a set of electromagnetic lenses, specimen chamber, and a fluorescent screen or CCD camera. High-energy electrons are generated by a process known as thermionic emission from a filament, usually tungsten. These

electrons are then accelerated and focused by applying electric potential using the electromagnetic lenses. The focused beam passes through an ultra-thin specimen, where the differences in the density and chemistry (or refractive index) of the specimen materials cause the electrons to interact differently causing their scattering to obtain finer structural information about the specimen. This information from the transmitted beam is used to generate an image of the sample on the fluorescent screen or the CCD camera connected to a monitor. The scattered electrons appear dark in the image. Areas of the sample could be stained using compounds of heavy metals such as osmium, lead or uranium to enhance structural details.

TEM is used in the areas of materials science/metallurgy and biological sciences. In both these of areas, the specimens must be very thin - preferably less than 1 μm thick for biological samples, and able to handle the high vacuum present inside the instrument. For biological samples such as viruses or vesicles, specimens can be prepared by embedding the former in vitreous ice or fixating it using a negative staining material such as uranyl acetate or plastic embedding. In materials characterization, specimens are prepared either by plastic embedding of the sample followed by microtomy – a technique which uses diamond knives to obtain tens of nanometers thick sections or by deposition followed by rapid drying of diluted sample on the support grid in case of samples such as powders, nanoparticles, or nanotubes.

Recent advances in TEM have made it possible to obtain tomographical information of individual proteins/viruses in biological science and crystal lattice/defects information in materials science using diffraction contrast instruments. HRTEM instrument is the most powerful diffraction contrast TEM instruments. HRTEM is also known as phase contrast imaging as the images are formed due to differences in phase of electron waves scattered through a thin specimen.

TEM and HRTEM Specimen Preparation

PS beads embedded with the multicolored QDs were further analyzed using TEM (Zeiss EM-902, thermionic emission using tungsten filament, 80 kV accelerating voltage, point resolution of 0.5 nm) and HRTEM (FEI Tecnai G^2, field emission 200 kV accelerating voltage and point resolution of 0.1 nm). Specimens for TEM and HRTEM were prepared using the following protocol. The PS beads dispersed in DI water were first dehydrated by 5 minutes sequential cycles of rinsing and centrifugation using 30, 50, 70, 90, 95, 100%, and absolute (200 proof) ethyl alcohol. Hard epoxy resin mix was prepared using a one-step single mix formula of EMbed 812, wherein EMbed, DDSA, NMA, and DMP-30 (the initiator) were mixed in 20 ml, 9 ml, 12 ml, and 0.7 ml quantities, respectively. The dehydrated beads were further rinsed and centrifuged using a 50:50 volume mixture of the absolute ethyl alcohol and the epoxy resin. The beads were embedded in the epoxy resin by curing the separated beads and epoxy resin mixture at 60 °C for 72 hours. Electron transparent sections of thickness lower than 100 nm of the resin embedded beads were obtained by cutting the hard blocks using a diamond knife in a microtome.

Differential Scanning Calorimetry, DSC

DSC is a thermoanalytical technique that measures the enthalpies associated with transitions and reactions and the temperatures at which these processes occur. The method is used for the identification and characterization of materials. It yields valuable information relating to processing and application conditions, quality defects, identification, stability, reactivity, chemical safety, and the purity of materials.

In DSC, the difference between heat flows from the sample and reference sides as a function of temperature or time is measured. Both the sample and reference are maintained at nearly the same temperature throughout the process. Sample holder's temperature increases linearly with time and it's generally required that

the heat-capacities of reference sample should be known over the range of temperatures to be used. When the sample undergoes transition such as melting or crystallization, the temperature of the process stays constant with continuous absorption (for endothermic process such as melting) or release (for exothermic process such as crystallization) of heat and hence more or less heat required to raise sample temperature is recorded as shown in Figure 4.1 which shows a schematic DSC curve. Specific heat capacities and changes in heat capacity can also be determined from the difference in heat flow. DSC is designed to analyze and study polymers such as thermoplasts, thermosets, elastomers, and adhesives, foodstuffs, pharmaceuticals, chemicals and composite materials. In case of polymeric materials, thermal events and processes that could be studied using DSC are glass transitions, melting behaviors, effect of cross-linkers, reaction kinetics, etc.

We used DSC (Mettler Toledo) to analyze the effect of initiator concentration and cross-linker on the distribution of nanoparticles in the polymer matrix. The beads were first dried overnight under vacuum. A specific weight of the dried beads was then supplied the heat at constant heating and cooling rates of 10 °C/min and heat flow (mW) vs. temperature plots were obtained.

4.3 Results and Discussion

4.3.1 Electronic Energy Transfer

We characterized the multicolored beads obtained from the 21.7:6.1:1 molar ratio monomer mixture of the 520, 580, and 620 nm QDs by comparing the fluorimeter emission profile of the encoded PS beads and that of a reference sample prepared by dispersing these QDs, in the same molar ratio, in the St/MAA/AIBN prior to the polymerization (Figure 4.2). While the spectral scans and emission profiles indicate that the locations of the peak emissions of the three QDs in the beads are the same as those measured for the QDs dispersed in the monomer mixture, the ratio

of intensity levels do not agree. It is clear from Figure 4.2 that the luminescence intensity of the QDs with the longest emission wavelength has increased relative to the intensities of the QDs emitting at the shorter wavelengths. An identical behavior was also observed in beads loaded with two colored QDs (520 and 580 nm QDs, see Figure 4.3).

As mentioned in the Chapter 1, when QDs are brought in close proximity to one another, as is the case here in the domains inside the beads, electronic energy transfer can occur if the core nanocrystals are drawn to within ∼1–10 nm of each other. The visual evidence that the multicolored QDs as observed in Figure 3.2 are pushed together into inclusions, together with the existence of an electronic energy transfer pathway between proximal QDs, can be used to provide an explanation for the relative intensity changes observed in the spectra shown in Figure 4.2. Specifically, assuming the QDs are pushed to within 1–10 nm of each other, the 520 and 580 nm QDs transfer energy to the 620 nm QDs, since the 620 nm QDs absorption spectra overlaps with the emission spectra of the 520 and 580 nm QDs. This accounts for the observed changes in the ratio of the intensities in the emission spectra compared to the well-dispersed QDs in St/MAA/AIBN.

Reabsorption can also alter the relative intensity levels of the three colors both in the beads and in the reference in toluene or monomer solutions in which the QDs are non-interacting and dispersed individually. This change would be in the same direction as that caused by electronic transfer (*red* increased and *green* and *orange* decreased), with the 620 nm QDs absorbing the radiation from the 520 nm and 580 nm QDs because of the spectral overlap. The reference spectrum is measured in a fluorimeter with a 1-cm path length, while the bead spectrum is measured for a single bead (∼50 μm in diameter) with a confocal microscope. The overall concentration of QDs is the same in the reference solution and the bead. Thus, on a relative basis, we can in general expect reabsorption to be a more important energy

transfer process in determining the reference spectrum than the bead spectrum because of the larger path length. (This ignores the fact that the QDs are dispersed in concentrated pockets in the beads rather than uniformally as in the reference, which can affect the reabsorption process.) With regard to reabsorption in the reference solution, a comparison of the emission spectrum of a solution of dispersed QDs with the same relative composition as the reference but a total concentration 1/10th of the reference, measured by the fluorimeter, showed that the red intensity in the reference was slightly larger and the green and orange slightly lower than in the spectrum of the 1/10th solution (Figure 4.4). This indicates the presence of reabsorption in the reference solution, but the shifts were very small compared to the shift observed in the confocal measured bead spectrum relative to the reference. Thus the observed large change in relative intensities in the single bead spectrum relative to the reference - due to electronic transfer - is in excess of the small changes in relative intensity due to reabsorption radiative transfer in the reference.

We demonstrated this by dissolving the beads and re-dispersing the QDs in an acetone/toluene mixture and obtaining an emission spectrum in a fluorimeter. Following this procedure the non-confined QD emission spectrum, as can be seen in Figure 4.2, was recovered. Hence the aggregation of the QDs in the bead matrix is not an irreversible phenomenon and is responsible for the change in the relative emission intensities of the QDs.

In order to eliminate the possibility that the relative intensity change is due to the chemical nature of the polystyrene and some possible electronic interaction between QDs and the π-orbital rich environment in the bead, we used the exact same QD composition and total concentration to form poly-(methyl-methacrylate) (PMMA) beads using spraying suspension polymerization. The comparison of the emission profiles (Figure 4.5) of the QD embedded PMMA beads with PS beads as measured with the fluorimeter shows no effect of the surrounding polymer matrix

on the intensity enhancements of the higher wavelength QDs, and thus supports our hypothesis of the QD proximity effect on the intensity enhancement of the higher wavelength QDs.

As discussed above, electronic interactions between the QDs, aggregated as clusters in the polymerized bead, cause the transfer of the luminescence energy from the lower wavelength to the higher the wavelength QDs. In order to reduce or eliminate the observed electronic energy transfer, we need to reduce the electronic interactions between the QDs, and this could be achieved by separating the QDs at least by a distance of more than 10 nm from one another. We employed two approaches for achieving the spatial separation between the QDs in the polymer matrix. In the first approach, we obtained highly cross-linked polymer beads and studied the effect of cross-linking on distribution of the QDs, and subsequently on the energy transfer. Secondly, foreign particles, non-compatible with polystyrene, were incorporated along with the QDs into the PS beads. The first approach is discussed below in brief. Second approach is discussed in Chapter 5.

4.3.2 Cross-linking for Reducing Electronic Energy Transfer

The effect of cross-linking on the electronic energy transfer was examined by studying the distribution of QDs inside highly cross-linked, encoded polymer beads obtained using spraying suspension polymerization method. Four types of encoded polymer beads were synthesized by dispersing QDs emitting in the orange (560 nm) and red (620 nm) parts of the visible light spectrum in a relative molar ratio of 3:1 and a total loading concentration of 2.5 x 10^{-6} M (moles per liter of monomer) into the St/MAA/AIBN-1, St/MAA/AIBN-2, St-DVB/MAA/AIBN, and DVB/MAA/AIBN monomer mixtures. Henceforth, we represent the polymer beads synthesized using these monomer compositions as Beads A, B, C, and D,

respectively. The beads were characterized using CLSM, TEM, HRTEM, and DSC.

Reference Emission Spectrum of the QDs using CLSM

Reference emission spectra of the two QDs dispersed in styrene, at the same composition and the loading concentration as used in the bead synthesis, were obtained using the CLSM and the spectrofluorimeter. Panels (a) & (b) in Figure 4.6 show the CLSM luminescence images – obtained by simultaneous collection of the photoluminescence in the following two detection windows: 500-590 (for the yellow QDs), and 590-670 (for the red QDs) – of a non-aggregated dispersion of these QDs in styrene. A comparison of the CLSM spectral scan of the QD dispersion with an emission spectrum of the same dispersion obtained using the fluorimeter is shown in Figure 4.6(c). A considerable effect, on reabsorption, of the excitation and emission path-length, which is of the order of microns in CLSM and about 1 cm in the fluorimeter, is observed. As discussed in the previous section of this chapter, the reabsorption affects the energy transfer among the QDs and thus can change the ratio-metric barcodes. Hence, the CLSM spectral scan was used for consistency in comparisons with the CLSM emission profiles of the encoded polymer beads.

Characterization of Polymer Beads using CLSM

Panels a–d in Figure 4.7 are the superimpositions of the CLSM luminescence images – obtained by simultaneous collection of the photoluminescence in two detection windows: 500-590 (for the *yellow* QDs), and 590-670 (for the *red* QDs) – of equatorial z-sections of the A, B, C, and D beads, respectively. The comparison of these images provides visual evidence of the distribution of the QDs inside the polymer bead matrix. The QDs in A and B beads are present significantly in the form of aggregated domains inside the polymer matrix. These beads are similar to the multicolor QD encoded beads examined in Chapter 3. Whereas, the QDs in C and D beads are more dispersed (evident from the diffused luminescence from these beads),

with very few present as the aggregated domains. These luminescence images clearly provides a visual evidence of almost uniform distribution of the QDs inside polymer matrix when DVB is used as one of the monomer units for bead synthesis.

A comparison of CLSM spectral scans of these beads with a reference CLSM spectral scan of the two QDs is shown in Figure 4.8. The CLSM spectral scan for the specific bead was obtained by co-addition of the spectral scans taken at different z-positions in the bead, for multiple beads of the same batch, followed by normalization of the luminescence intensities by the area under the curve. Electronic energy transfer from yellow (lower wavelength) to the red (higher wavelength) QDs is observed in the beads A and B which are obtained from the St/MAA/AIBN-1 and St/MAA/AIBN-2 monomer mixtures, respectively. Also, a red shift of $\sim$5 nm in the peak positions of the emissions from the two QDs (originally at 561 & 621 nm in case of the QDs dispersed in styrene) is observed after their incorporation in A and B beads. These two phenomena can be explained as follows: i) the QDs are pushed into inclusions during polymerization, wherein the lower wavelength QDs in spatial proximity with the higher wavelength QDs, interact electronically to transfer luminescence energy from the lower to the higher wavelength QDs; ii) because of the Gaussian type size distribution of the QDs, the emissions from the QDs also have a gaussian distribution, where the back end of the curve corresponds to the emissions from smaller sized single colored QDs, and the front end of the curve corresponds to the emissions from the larger sized QDs of the same color. When these QDs are situated, via aggregation during polymerization, within 1–10 nm distance from one another, the inhomogeneity in their size distribution causes smaller sized QDs to electronically transfer energy to the larger sized QDs, thus red-shifting the emission peak positions towards that of the larger sized QDs. A similar type of shift in the peak positions of the CdSe QD emissions was reported by Kagan et al. [59, 60] when the characterized the close packed solid of these QDs for long-range resonance

electronic energy transfer calculations.

A significant reduction in the energy transfer from yellow to red QDs is observed when the spectral scans of the beads C and D are compared with that of the beads A and B. A comparison of the spectral scans of the beads C and D with the spectral scan of the neat QDs dispersed in styrene, shows a significant recovery in the energy lost through energy transfer by the yellow to the red QDs. Also, the peaks (561 & 621 nm for the yellow and the red QDs, respectively) of the emissions from the QDs for the beads C and D are repositioned closer to their original peak positions as observed in the reference spectrum. This reduction in the energy transfer and relocation of the emission peaks show that when the QDs are incorporated inside the beads with DVB as one of the monomer components, the electronic interactions between the QDs are reduced leading to the reduced energy transfer.

Characterization of the Polymer Beads using DSC and TEM/HRTEM

The higher degree of cross-linking, with the addition of DVB, was also observed in the differential scanning calorimetry (DSC) analysis (Figure 4.9) of the polymer beads. An increase in the glass transition temperature of the beads with the increasing amount of DVB was observed (see Figure 4.9(c)). DSC analysis also shows that, at the temperatures closer to 150 °C, a polymerization reaction is occuring. We believe that, at these temperatures, the end groups of the polymer chains react leading to the exothermic reaction. The entropic and enthalpic depletion-driven contributions towards the motion of the QDs are reduced by the presence of DVB radicals in the polymerizing droplets. This reduces the aggregation of the QDs, as has been observed in Figure 4.7. At the same time, large number of QDs are individually trapped in the polymerizing matrix because of faster kinetics of cross-linking in the presence of DVB. TEM images of bead A (Figure 4.10) show the aggregation of the QDs into big clusters. Individual QDs are observed at higher magnifications

(Figure 4.10 (b) & (d)). TEM and HRTEM images of bead C (Figure 4.11) show that this bead has lesser and smaller sized clusters of the QDs and a large number of individual QDs in the polymer matrix as compared to bead A.

Therefore, it can be safely claimed that the addition of DVB – either as the cross linker or one of the monomer units – provides higher cross linking and thus, helps in better distribution of the QDs in the polymer matrix. This phenomenon can be explained as follows. As has been discussed earlier (Chapter 2), the polymerization, at various uniformly distributed sites in the monomer droplet, is initiated as soon as the latter enters the aqueous phase, which is maintained at the polymerization conditions. In case of the encoded PS beads (Beads A and B), as the polymer chains grow linearly, the uniformly dispersed QDs in the monomer droplet begin experiencing a viscous drag force exerted by the polymerizing styrene molecules because of their (QDs) size dependent entropic and enthalpic interactions with the growing polymer chains. Hence, to avoid the energy penalty, the growing polymer chains push the QDs into the inclusions, which we observed in the CLSM luminescence images of these beads. However, in case of the Beads C and D, the presence of DVB, as one of the monomer components, during polymerization, increases the viscosity of the polymerizing matrix by cross-linking as soon as the polymerization begins. The QDs surrounding the cross-linking polymer molecules still experience the viscous drag force, but because of the increased viscosity and presence of the cross-linked polymer chains around them, their motion is restricted. Hence, the entropic depletion attraction force becomes energetically unfavorable, and a very few number of the QDs are pushed into the inclusions with a large number of them trapped between the cross-linked polymer chains. This trapping of the QDs during polymerization separates most of the QDs by more than 10 nm distance from one another. Owing to the separation, the electronic energy transfer between the QDs is reduced or eliminated. Thus, the higher degree of cross linking, obtained by using

DVB as one of the monomer units, reduces the electronic energy transfer among the multicolored QDs incorporated in polymer beads.

4.4 Conclusion

Comparison of the emission profiles of the polystyrene beads, encoded with three colored QDs, with a reference emission spectrum of the QDs dispersed individually in styrene, at the same loading concentrations as in the bead, showed the difference in the emission intensities of the QDs before and after their incorporation in the PS beads. An intensity cascade was identified in which the green and orange QD luminescence was diminished and the red luminescence enhanced. The observed intensity cascade was attributed to electronic energy transfer from the smaller QDs to the larger QDs segregated to form inclusions during droplet polymerization. This transfer has been observed in close-packed QD assemblies in which interdot distances are between 1 and 10 nm, and is possible in the QD incorporated beads due to the proximity of the QDs to each other in the microdomain inclusions.

The energy cascade was believed to reduce the obtainable number of ratio-metric barcodes from the QD incorporated PS beads. An approach was discussed for restricting the QDs from segregating into the inclusions during polymerization and, thus, minimizing the electronic interactions. Highly cross-linked beads, with DVB as one of the monomer units, were obtained using spraying suspension polymerization. CLSM luminescence images of the beads showed diffused QD luminescence. An observation, that the QDs were uniformly distributed in the polymer matrix, was supported by the TEM and HRTEM images, showing presence of the well separated individual QDs in the bead matrix. A comparison of the CLSM spectral scans of the polymer beads with a CLSM reference spectrum of the QDs, dispersed in styrene, showed the advantage of using higher-degree of cross-linking for reduction of the energy transfer.

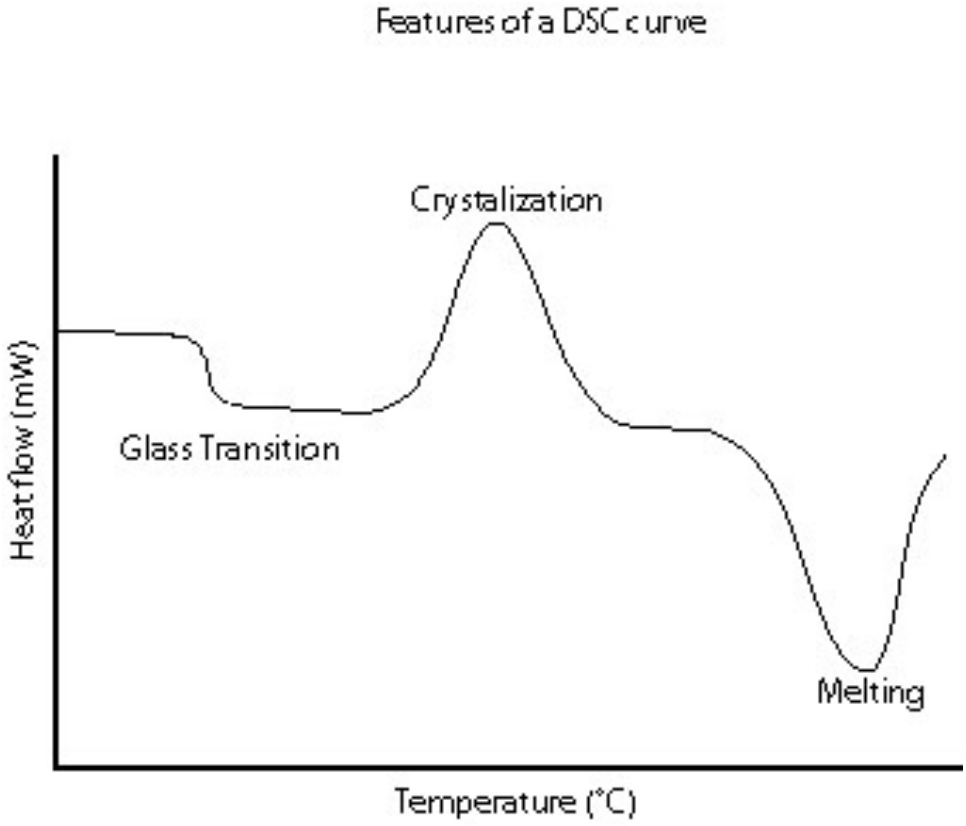

Figure 4.1: Schematic of a representative differential scanning calorimetry curve (heat flow vs temperature data) indicating physical processes involving generation or absorption of heat. For example, during glass transition the change in the curve is due to change in the specific heat of the material, while during crystallization the heat is released and during melting heat is absorbed by the process. *http://content.answers.com-/main/content/wp/en/4/4d/InterprettingDSCcurve.jpg*

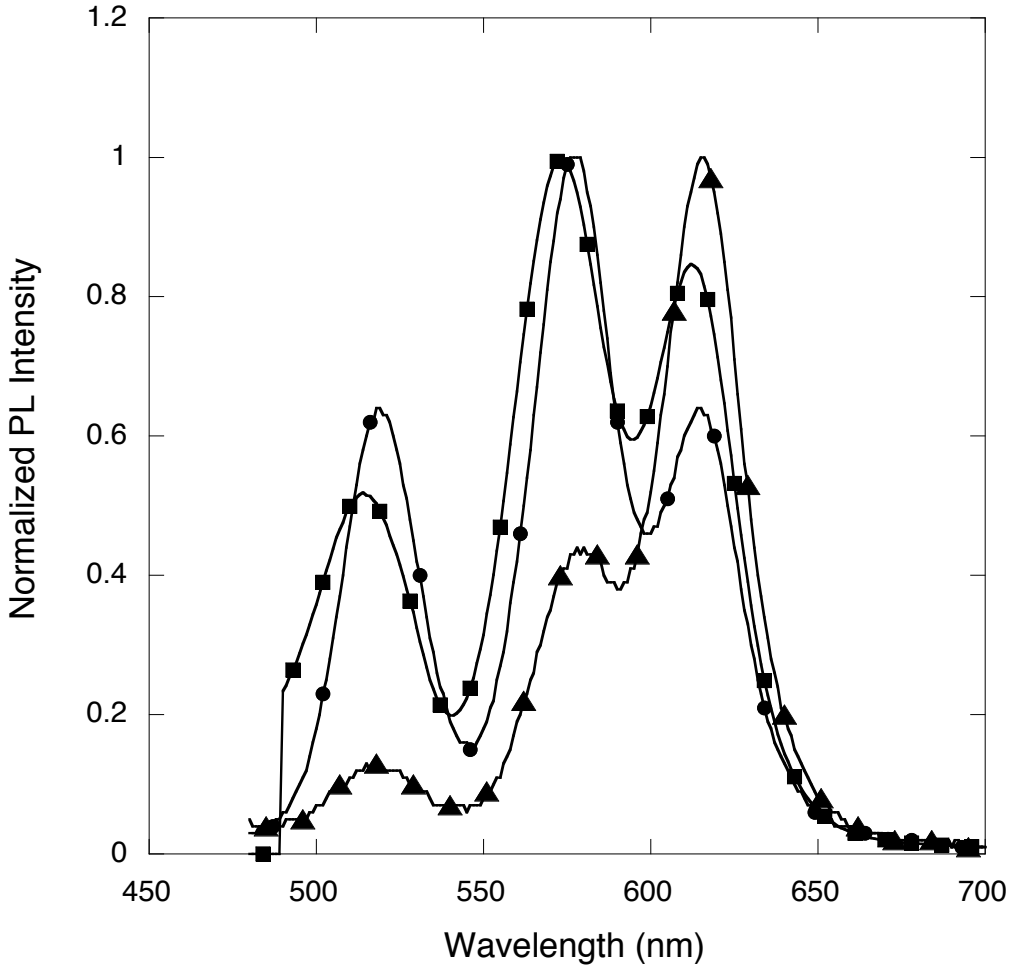

Figure 4.2: Fluorimeter emission profiles of the three colored QDs (molar ratio, 21.7:6.1:1) when embedded in PS beads (▲), dispersed in St/MAA/-AIBN (●), and after dissolution of these beads in acetone/toluene (50:50 v/v) mixture (■). PL intensity for each profile is normalized as $N_i/N_{i,max}$, where N_i is the PL intensity at any i wavelength of the profile.

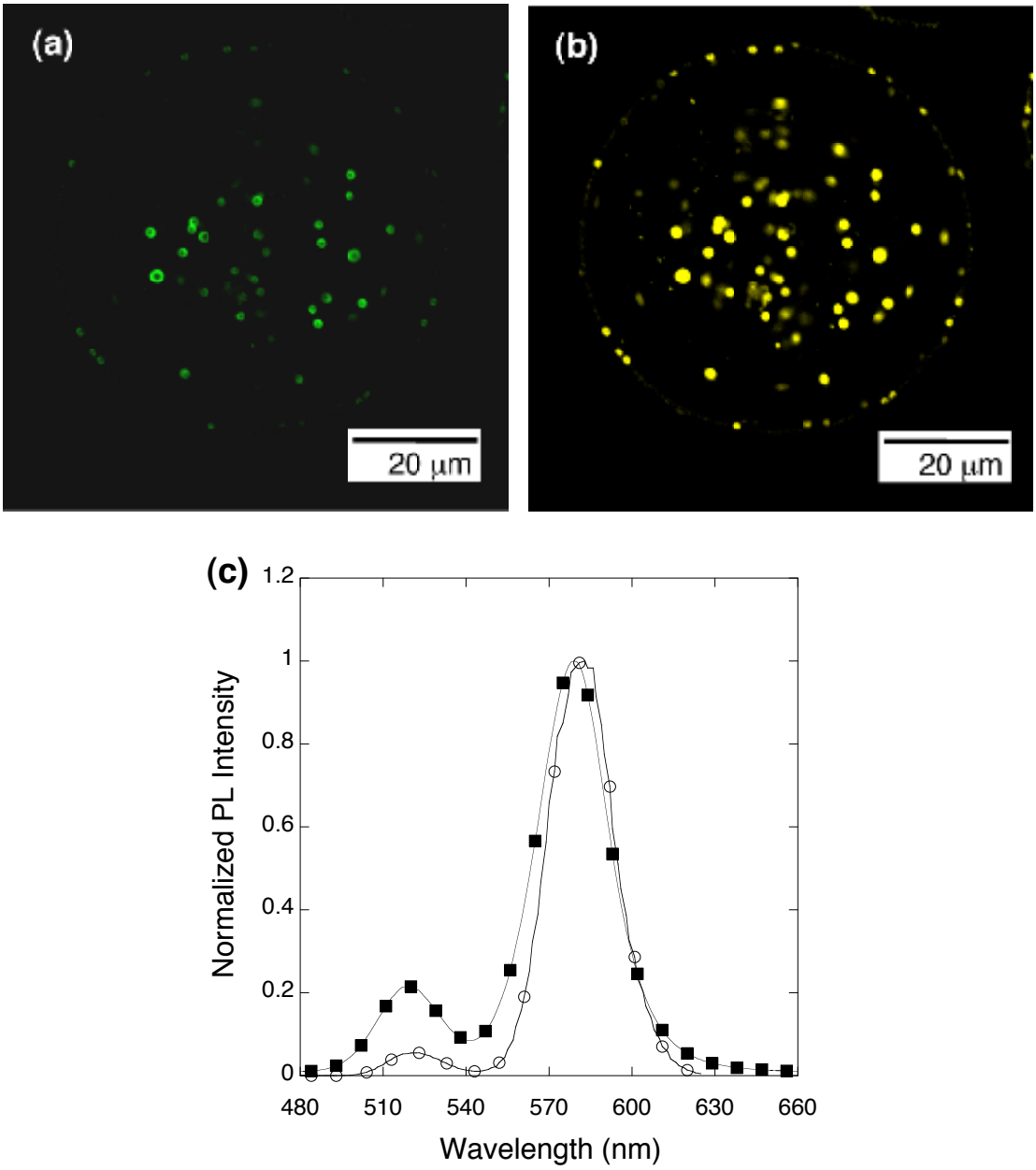

Figure 4.3: Characterization of the PS beads embedded with 1:1 molar ratio of 520 and 580 nm QDs. CLSM luminescence images collected in following collection windows: (a) 470–545 nm (b) 545–630 nm. (c) Comparison of the CLSM spectral scan (◯) of the bead in Figure 4.3(a–b) with the fluorimeter emission spectrum (■) of the 1:1 molar ratio of these QDs dispersed in St/MAA/AIBN.

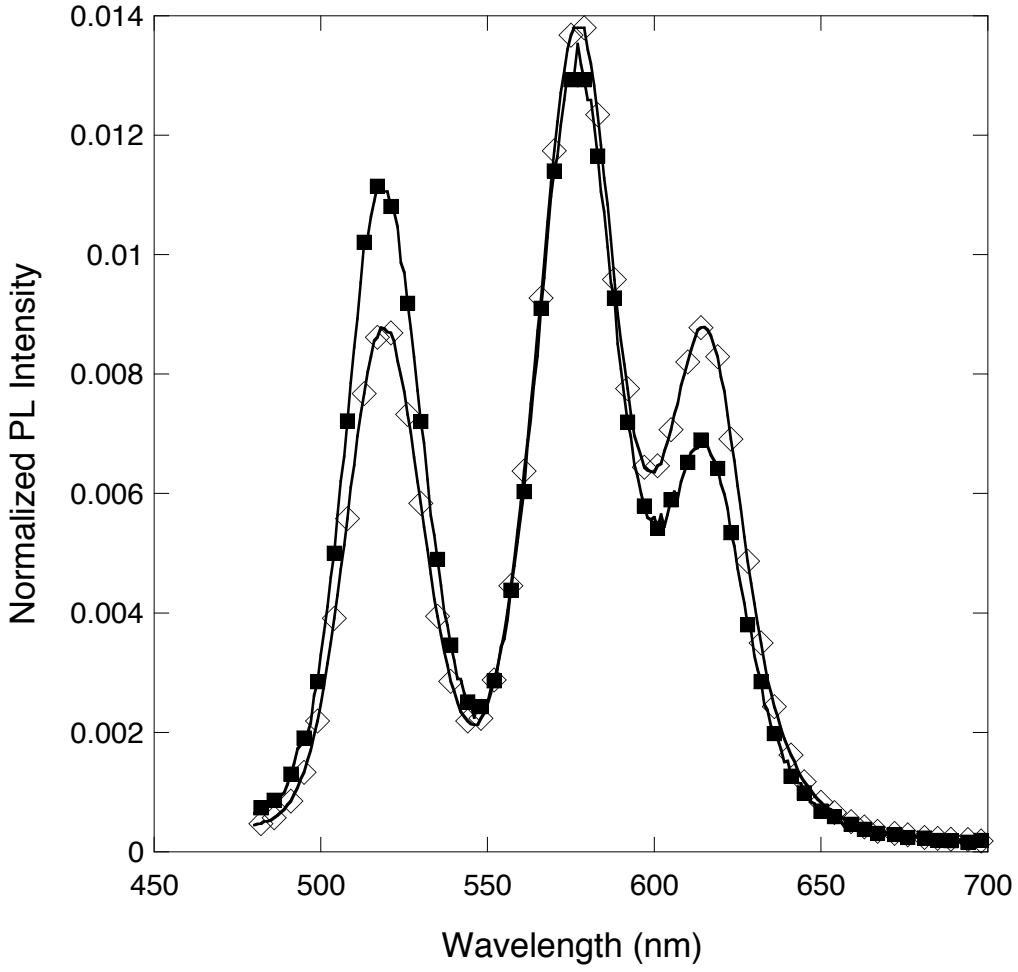

Figure 4.4: Comparison of fluorimeter emission profile of the 21.7:6.1:1 molar ratio mixture of 520, 580, and 620 nm QDs dispersed at 5.29 x 10^{-6} M (◇) and at 5.29 x 10^{-7} M (■) concentrations in St/MAA/AIBN. Normalized emission profiles are obtained by dividing the intensity values by total area of the profile.

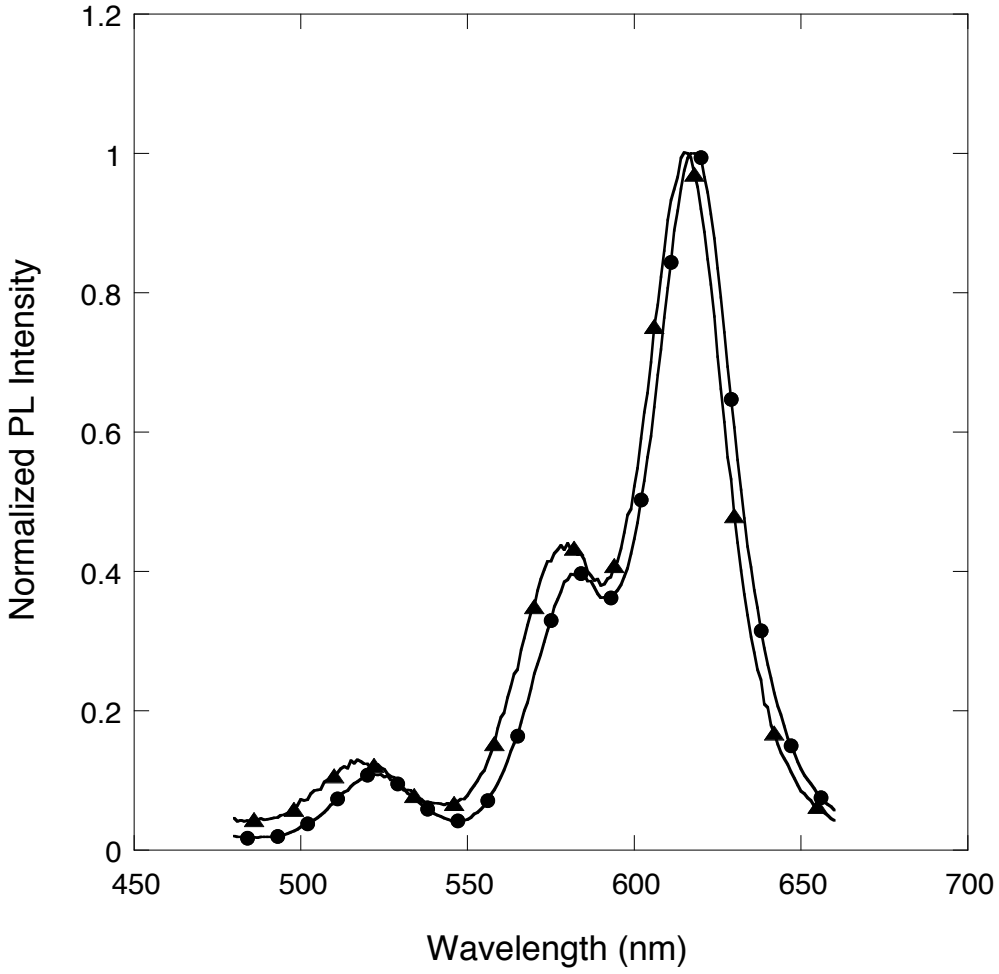

Figure 4.5: Comparison of fluorimeter emission profiles of the PS (▲) and PMMA (●) beads embedded with the identical molar ratios (21.7:6.1:1) of the 520, 580, and 620 nm QDs.

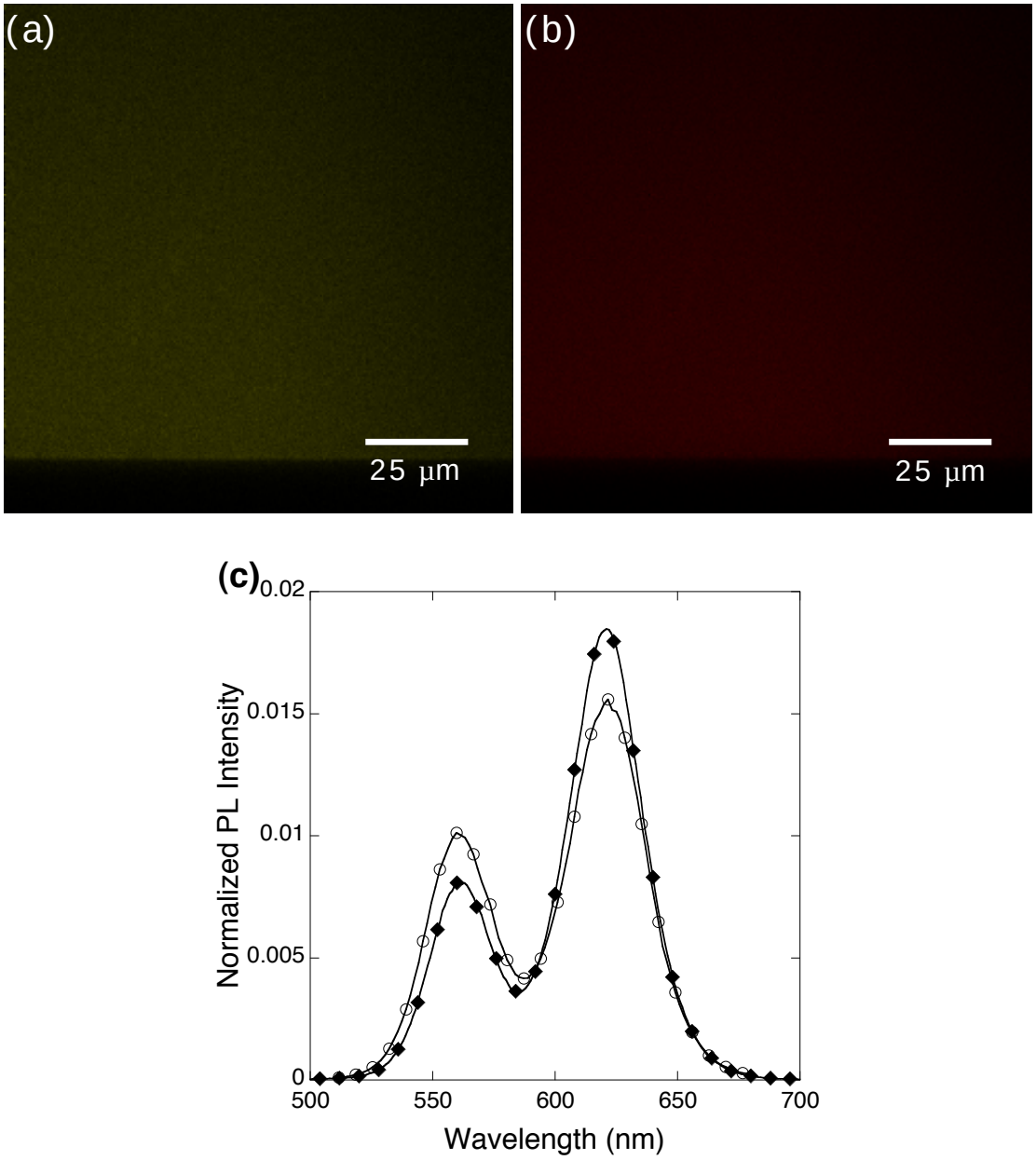

Figure 4.6: CLSM luminescence images of the QD dispersion with 560 (a) and 620 (b) nm QDs dispersed in styrene at the relative molar ratio of 3:1 and the total concentration of 2.5 x 10^{-6} M. The emission collection windows used were 500-590 (a) and 590-680 nm (b), respectively. (c) is a comparison of the CLSM spectral scan (♦) of the QD dispersion in (a-b) with its emission spectrum obtained using the fluorimeter (◯).

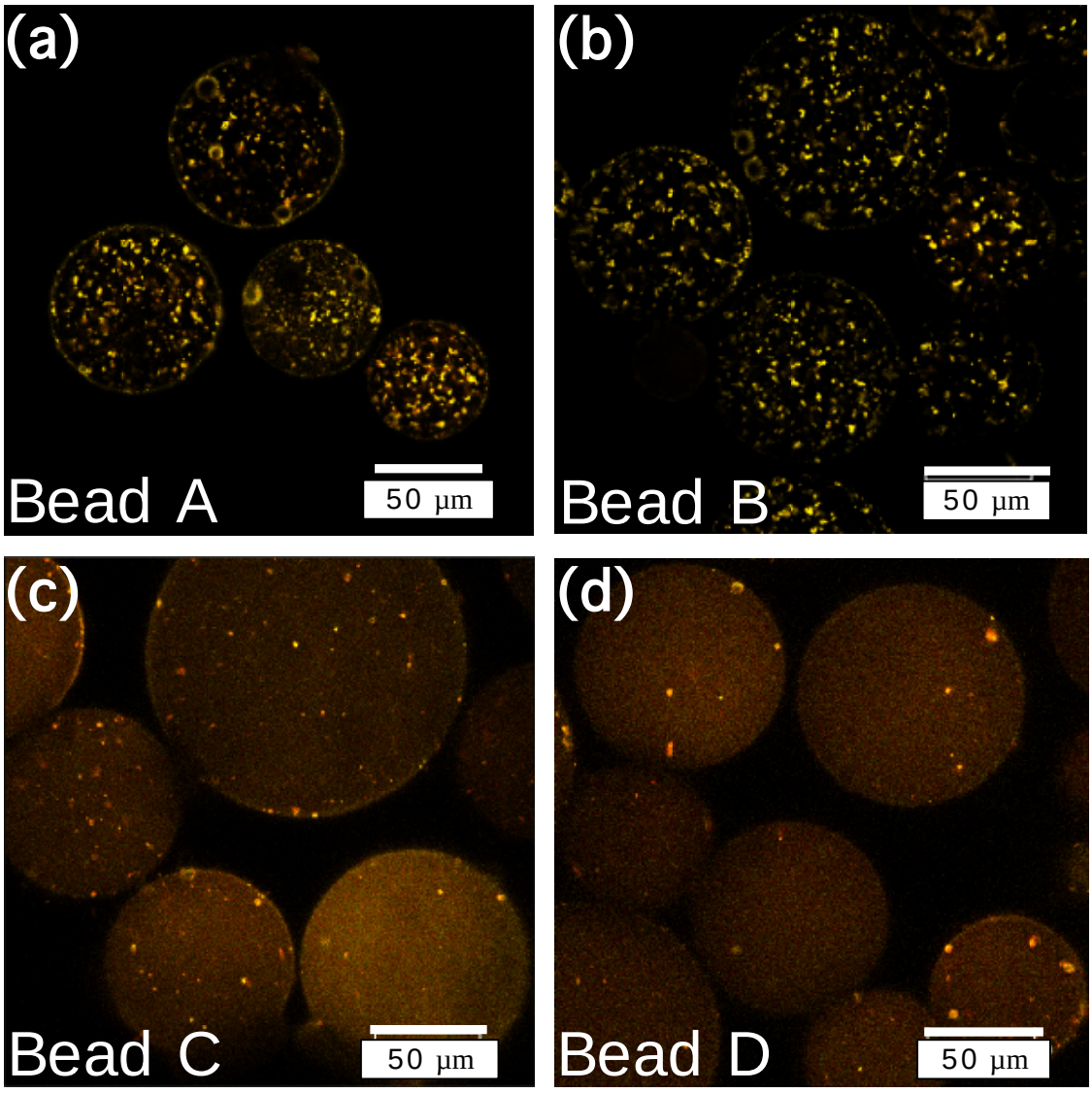

Figure 4.7: Superimposition of the CLSM luminescence images of the polymer beads embedded with 560 and 620 nm QDs in 3:1 molar ratio and a total concentration of 2.5 x 10^{-6} M. Beads were synthesized from the St/MAA/AIBN-1 (Bead *A*), St/MAA/AIBN-2 (Bead *B*), St-DVB/-MAA/AIBN (Bead *C*), and DVB-MAA/AIBN (Bead *D*) monomer mixtures. The beads were excited by 458 nm laser and the luminescence was collected in 500–590 nm and 590–670 nm collection windows.

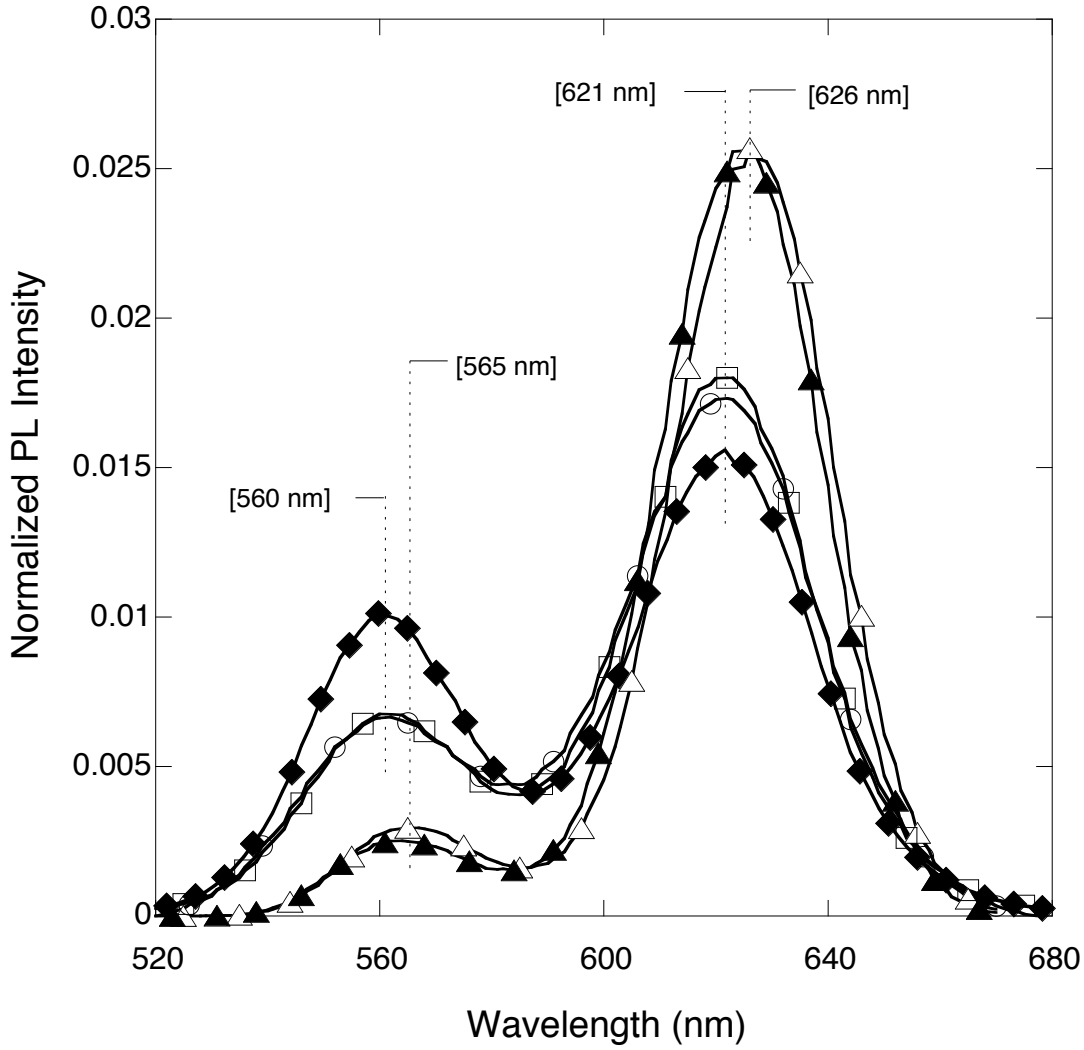

Figure 4.8: Comparison of CLSM spectral scans of Beads A (△), B (▲), C (□), and D (◯) with a CLSM emission profile (⧫)of the 560 and 620 nm QDs dispersed in styrene at the same composition and concentration as that used in the bead synthesis. A red-shift of 5 nm in peak positions for A and B beads is observed. Whereas, in case of the C and D beads, the peak positions coincide with that of the net QDs in styrene, thus depicting the almost uniform dispersion of the QDs in the cross-linked beads.

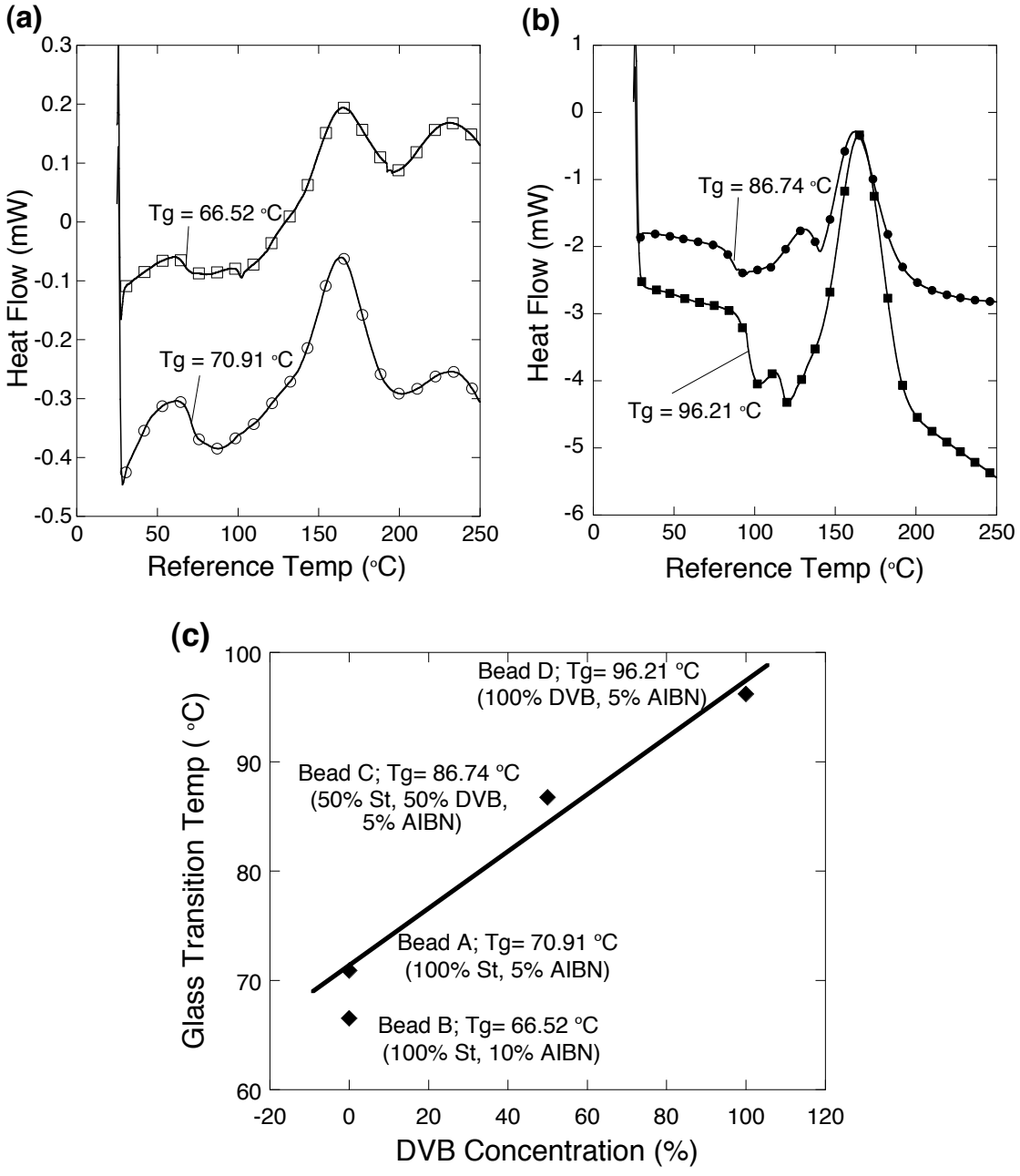

Figure 4.9: DSC analysis of the cross-linked polymer beads. (a) $ b) are the temperature (°C) vs. heat flow (mW) profiles for Beads A (◯), B (□), and C (•), D (■), respectively. (c) represents the glass transition temperature (T_g) as a function of the DVB concentration. Increased amount of AIBN lowers the T_g.

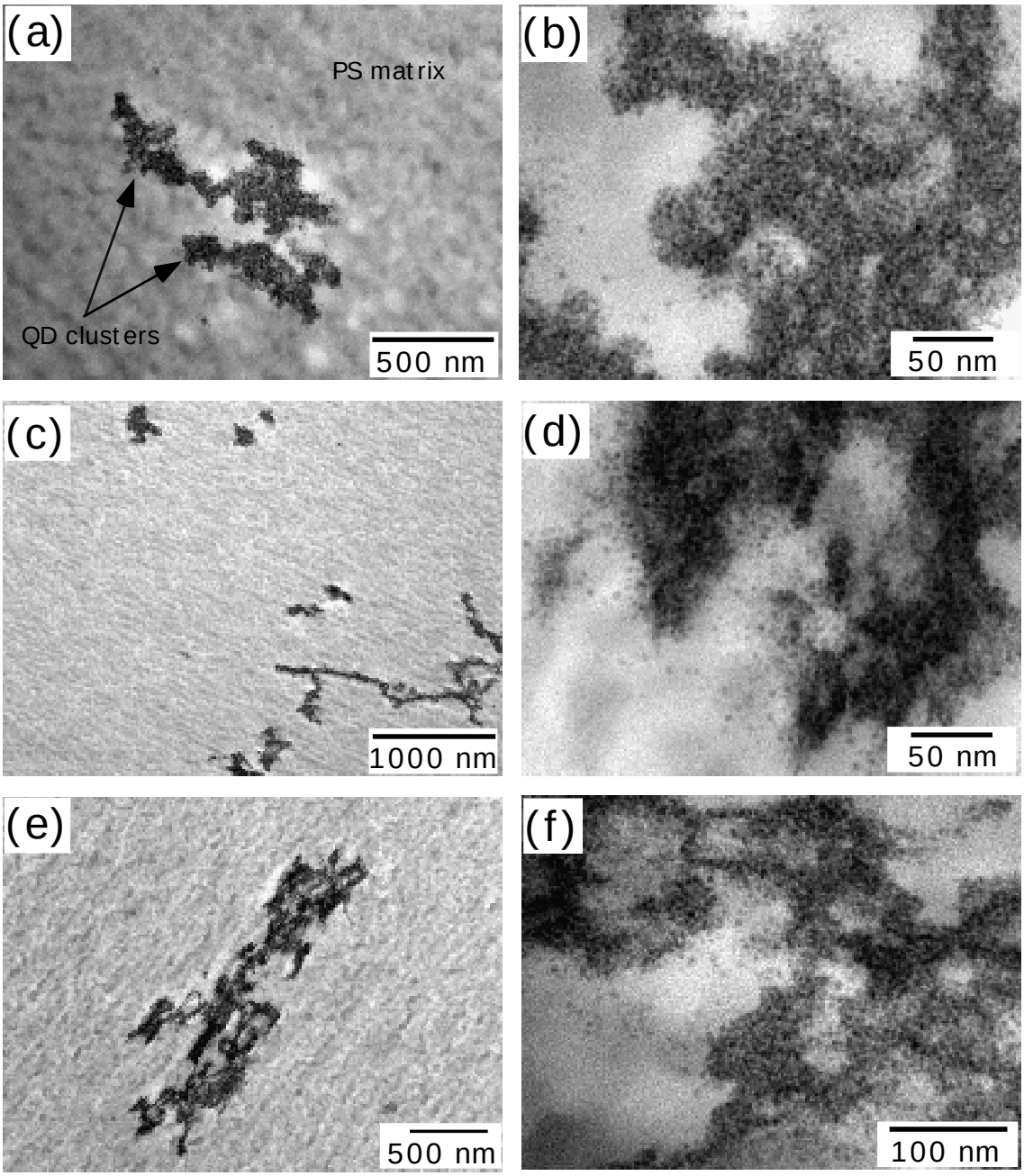

Figure 4.10: TEM analysis of Bead *A*. (a)–(f) are the TEM images showing the aggregated QDs inside the polymer matrix.

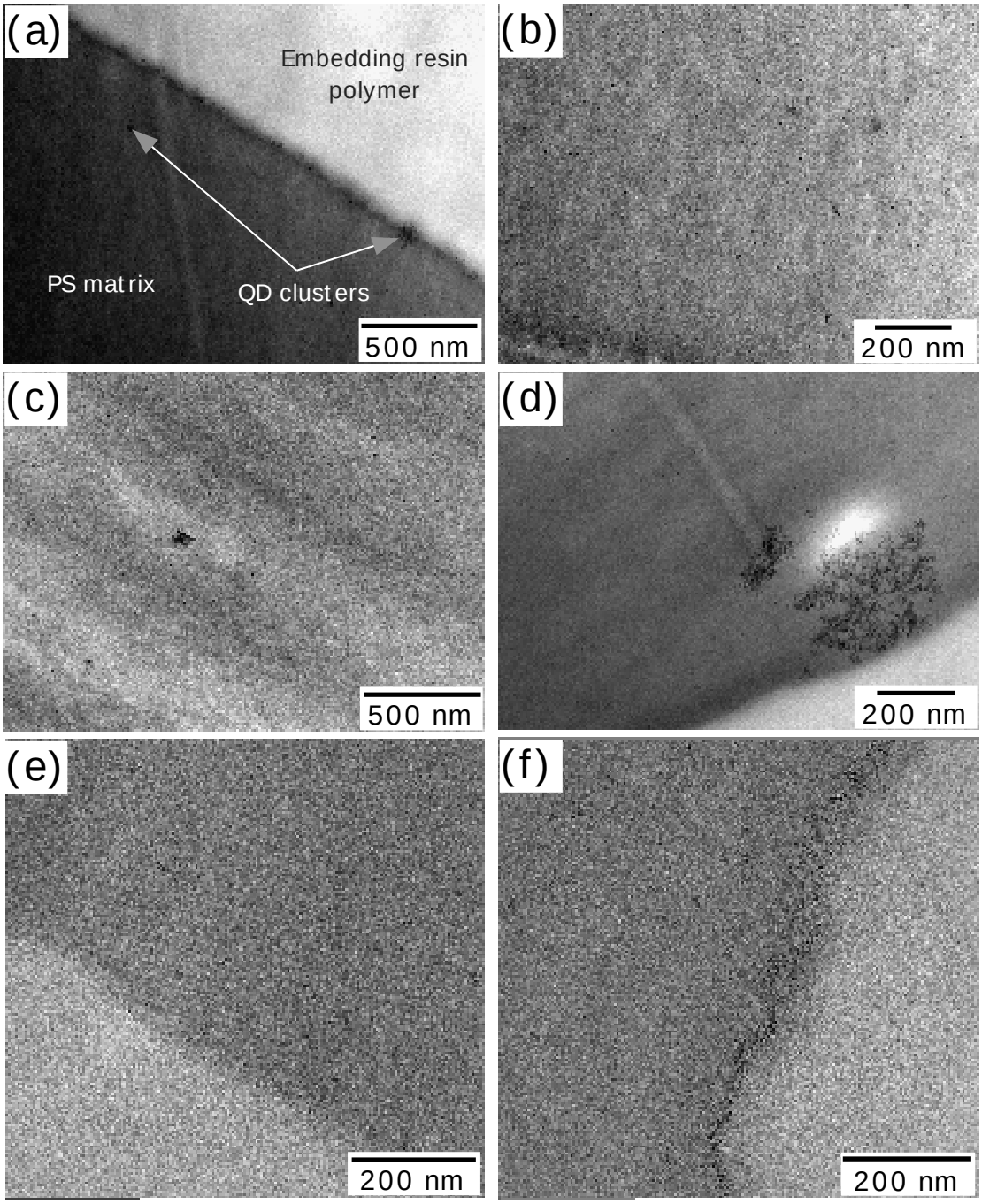

Figure 4.11: TEM and HRTEM analysis of Bead *C*. (a)–(d) are the TEM images showing the QDs, distributed uniformly inside the polymer matrix, with very few of them aggregating into small sized clusters, both near the edge and the interiors of the bead. (e) & (f) are the HRTEM images indicating the QD distribution close to the boundary of the microtomed specimen. The wave-natured collection of the QDs at the edge of the specimen is believed to be the after effect of microtoming and is not associated with the polymerization process.

Chapter 5

Future Work

5.1 Introduction

In Chapter 4, we demonstrated the use of higher degree of cross-linking for reduction of electronic energy transfer between quantum dots (QDs) when incorporated in polymer beads. One more approach, for reduction of the energy transfer, was also initiated, in which foreign particles, having size distribution similar to that of the QDs were incorporated along with the QDs in cross-linked polystyrene (PS) microspheres. Preliminary results obtained using this approach are briefly discussed below. Also, discussed further, is a methodology for synthesizing monodispersed, encoded polymer beads and arraying them on microarray platforms.

5.2 Incorporation of Foreign Particles in PS Beads along with QDs

We observed that the separation between the QDs, for the reduction of electronic interaction among them, could also be achieved by taking advantage of the segregation process occurring during the polymerization. To this effect, encoded polystyrene beads were obtained using spraying suspension polymerization method from the monomer mixture containing the QDs and added foreign particles, which have similar size distributions as that of the QDs, and, like the QDs, are incompatible with polystyrene. These particles will also be pushed, along with the QDs, into the inclusions being formed in the polystyrene matrix during the polymerization.

We used low-molecular weight polyethylene (PE) powder as the foreign particles. PE powder (low-density, average molecular weight - 35,000) was obtained from Spectrum Chemicals, CA. Other chemicals and the QDs used have been described in the Experimental Section of Chapters 3 and 4. A set of polystyrene beads was obtained using spraying suspension polymerization by incorporating 520 and 580 nm QDs at a relative molar ratio of of 3:1 and a total concentration of 4 x 10^{-6}

M (moles per liter of St). A prescribed amount of low-density polyethylene (PE) powder, forming a specific relative molar ratio with the QDs, was first dissolved in a solvent mixture containing styrene, DVB (10 wt% St), and MAA (5 wt% St) at 80 °C followed by addition of the QDs and AIBN (5 wt% St). This monomer mixture, abbreviated as St/DVB/MAA/AIBN/PE and with the PE concentration of 1.57 x 10^{-5} M, was then sprayed immediately, using the Sono-Tek nozzle, into the aqueous phase. These beads are represented as PS-PE Beads in the following descriptions. PS beads, encoded using the two QDs, incorporated in the same loading concentration, were also obtained from a St/DVB/MAA/AIBN monomer mixture containing no PE, and are, henceforth, represented as PS-noPE Beads. Polymerization was carried out for 2 hours, for both the beads, followed by separation using centrifugation and washing of the beads with a 40:60 mixture of ethanol and water.

CLSM, spectrofluorimeter, TEM, and HRTEM were used for characterization of the PS beads.

5.2.1 Low Molecular Weight Polyethylene Molecule as the Foreign Particle

Low molecular weight polyethylene (PE), based upon its solubility parameter of 7.9 cal/cm^3 at 25 °C, is not soluble in styrene (solubility parameter equal to ∼8.6 cal/cm^3) at room temperature. However, its solubility increases with the increasing temperature, and they are solubilized almost completely at higher temperatures. Figure 5.1 shows the particle size distribution of PE in styrene with temperature. A decrease in the particle size with the increasing temperature is observed. We believe that this decrease in the particle size is because of the unraveling followed by the separation of the entangled polymer chains. The size distributions at 60 °C and 80 °C are bimodal with most of the particle population in hundreds and tens of nanometers, respectively. The particle size analysis indicates that these solubilized

PE molecules, the foreign particles, have a particle size distribution closer to that of the QDs at the reaction temperature of 80 °C. At the same instance, PE is not compatible with PS; firstly, because of the solubility difference between the two – the solubility parameter of PS is equal to ∼8.5–9.7 cal/cm^3 at 25 °C– and secondly, because of the nature of the polymer chains. Therefore, both the QDs and the solubilized PE are excluded from the PS polymerizing loci, and pushed into the aggregated clusters. This hypothesis is represented using a schematic in Figure 5.2. The cluster formation is believed to be an intermediate stage, wherefrom the PE molecules consolidate to form large PE domains and in the process, push the QDs towards the interface between the consolidated domain and polystyrene matrix. The QDs help in minimizing the interfacial energy between the PE domains and the PS matrix. By creating large number of the consolidated PE domains, we assume that a large interfacial area could be generated between the PE domains and the PS matrix and this area would then be used by the segregated QDs during the polymerization, causing enough separation between the QDs to minimize the electronic interactions.

5.2.2 Luminescence Characterization of PS-PE and PS-noPE Beads

Panels (a–b) and (c–d) in Figure 5.3 represent CLSM luminescence images of the PS-PE and PS-noPE Beads, respectively. The luminescence from the two QDs was collected in 480–545 (for 520 nm QDs) and 545–640 nm (for 580 nm QDs) collection windows. Comparison of the luminescence images show that the luminescence from both the QDs is more diffused for the PS-PE Beads than the PS-noPE Beads. Panels (e) and (f) show the luminescence images, which were obtained by simultaneous imaging of both the PS-PE and PS-noPE Beads. A clear distinction in luminescence is observed, which indicates that the incorporation of PE along with the QDs into the polystyrene beads has changed the distribution of the QDs inside the polymer

matrix.

Figure 5.4(a) shows a comparison of the emissions from the PS-PE and PS-noPE Beads with a reference fluorimeter emission spectrum of a dispersion of the two QDs in the St/DVB/MAA/AIBN. The QDs were dispersed at the same composition and concentration as that used in the synthesis of the PS-PE and PS-noPE Beads. The emission curve for the PS-PE Beads lie between the emission curves for the PS-noPE Beads and the reference. This indicates that the electronic energy transfer, observed in case of the PS beads, was reduced to a significant amount in case of the PS-PE Beads. A comparison of the CLSM spectral scans (Figure 5.4(b)) of the two beads, also, show a significant reduction in the energy transfer. Unfortunately, we could not obtain a reference CLSM spectral scan for this set of the two QDs because of their contamination via excessive exposure to humid laboratory environment.

5.2.3 TEM Analysis of PS-PE Beads and PS Beads

We verified our hypothesis of PE molecules consolidating to form PE domains during the polymerization process by analysis the PS-PE Beads using transmission electron microscopy (TEM). TEM analysis (Figure 5.5) of the PS-noPE Beads, indicate the self-corraling of the QDs into the inclusions during the polymerization, as has been observed in CLSM luminescence images. TEM images of the PS-PE beads (Figure 5.6), indicates that the styrene solubilized PE molecules, because of the difference in their solubility parameters with PS, are also pushed into inclusions along with the QDs during the polymerization and consolidate together to form PE domains. As was described in the schematic representation of this process (Figure 5.2), the QDs are observed to be residing at the interface between the PE domains and the PS matrix in the TEM images. This could be explained using a thermodynamics principle of minimization of the interfacial energy as follows: The polymerizing chains of PS try to minimize the inter-chain energy by pushing the QDs and the

PE molecules into the accessible microscopic regions in the polymerizing droplet. Polymer chains of the PE molecules also try to minimize the inter-chain energy and align themselves to form large PE domains. Therefore, the QDs are left with only the interfacial place between the PS matrix and the PE domains, and reside at the interface contributing towards the minimization of the interfacial energy between PS and PE.

5.3 Development of Monodispersed, Encoded Polymer Beads and Arraying them on Microarray Platforms

Quantum dot encoded beads are required to have monodispersed size distribution for their consistent use in high-throughput screening applications. Next step in this research project is to obtain monodispersed, micron-sized encoded polymer beads, on the order of 10 μm in diameter by employing on-chip fabrication of the beads using a microfluidics platform and the on-chip attachment of biomolecular probes (capture molecules) to the surface of the beads. The beads displaying surface probes are to be used as tools in high-throughput, multiplexed assays of the binding interactions of proteins, and therefore the biomolecules of interest in this study will be proteins themselves (e.g. antibodies) or small, protein-binding molecules such as peptides.

In the proposed microfluidic design, a microfluidic "T" junction or flow focusing assembly (as depicted using a schematic in Figure 5.7) will be used to form a single file of droplets of monomer solution in a continuous immiscible aqueous phase in a microfluidic channel. The microfluidic channel is made by soft lithography, as an open channel, with a glass slide affixed over the channel to enclose the flow. The monomer solution is composed of styrene, divinyl benzene for cross-linking, methyl-acrylic acid for surface functionalization of the beads, and AIBN for pho-

toinitiation of polymerization. The monomer solution also contains a mixture of the QDs of different colors and, for each color, different concentrations to create the barcode, and magnetic nanoparticles to create a magnetic handle on the beads. The monomer droplets are photo-polymerized downstream using a UV light source, and then immobilized on the glass cover of the channel by a magnet. The biomolecule is then attached to the immobilized beads by flowing solutions of the biomolecule over the beads. Alternatively, small molecules are synthesized on the bead surface in the platform by flowing reactants over the beads. The magnet is removed, and the particles are collected downstream. The process is then repeated with a different encoding mixture of QDs and a different surface probe.

The beads are to be used in bead-based suspension assays in which encoded beads displaying probe molecules are incubated with a solution of target molecules. Beads with probes which bind the target are identified and the identity of the binding biomolecule is established from the encoding label. The proposed microfluidic platform designs solve many of the bottlenecks inherent in the current technologies of high-throughput proteomic screening, and the designs can lead to a new generation of technologies offering easier routes of preparation, and greater multiplexing at higher-throughput.

Over the past few years, we have demonstrated the ability of conjugating biomolecules, such as mobile lipid bilayers, on surface of silica beads [81] and arraying intact biomolecules, such as liposomes, and fluorescently labeled polystyrene microspheres in functionalized microwells [82].

5.4 Conclusion

PS beads, obtained by incorporating QDs along with foreign particles of the styrene solubilized PE, showed a significant reduction in the energy transfer. TEM analysis showed that the QDs and the solubilized PE molecules are excluded from the

polymerizing loci into the inclusions, where the PE molecules consolidate and the QDs arrange themselves at the interface between the consolidated PE domains and the PS matrix to minimize the interfacial energy penalty between PS and PE. This phenomenon of migration of the QDs towards the interface between the PS matrix and the PE domains could be studied and employed in other polymer–nanoparticle systems for effective distribution of nanoparticles in the polymer matrix. A methodology to obtain monodispersed, encoded polymer beads was described.

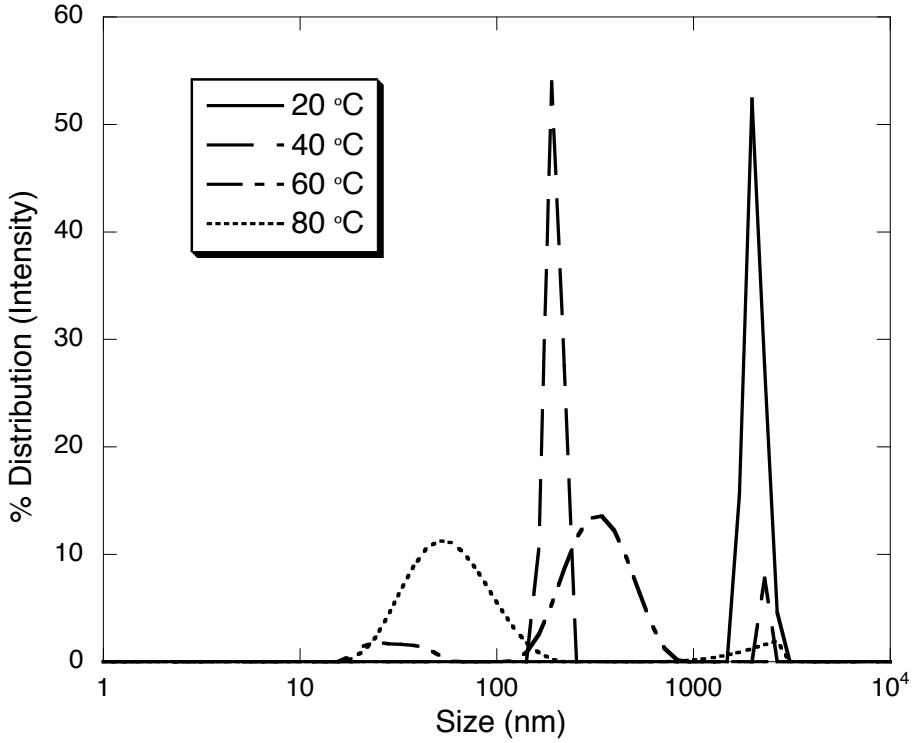

Figure 5.1: Particle size distribution analysis of the PE molecules solubilized in styrene with respect to temperature. The particle size decreased with the increasing temperature. Bimodal size distributions at 40, 60, and 80 °C show that, with the increasing temperature, percentage of the smaller sized solubilized PE molecules appear in the dispersion.

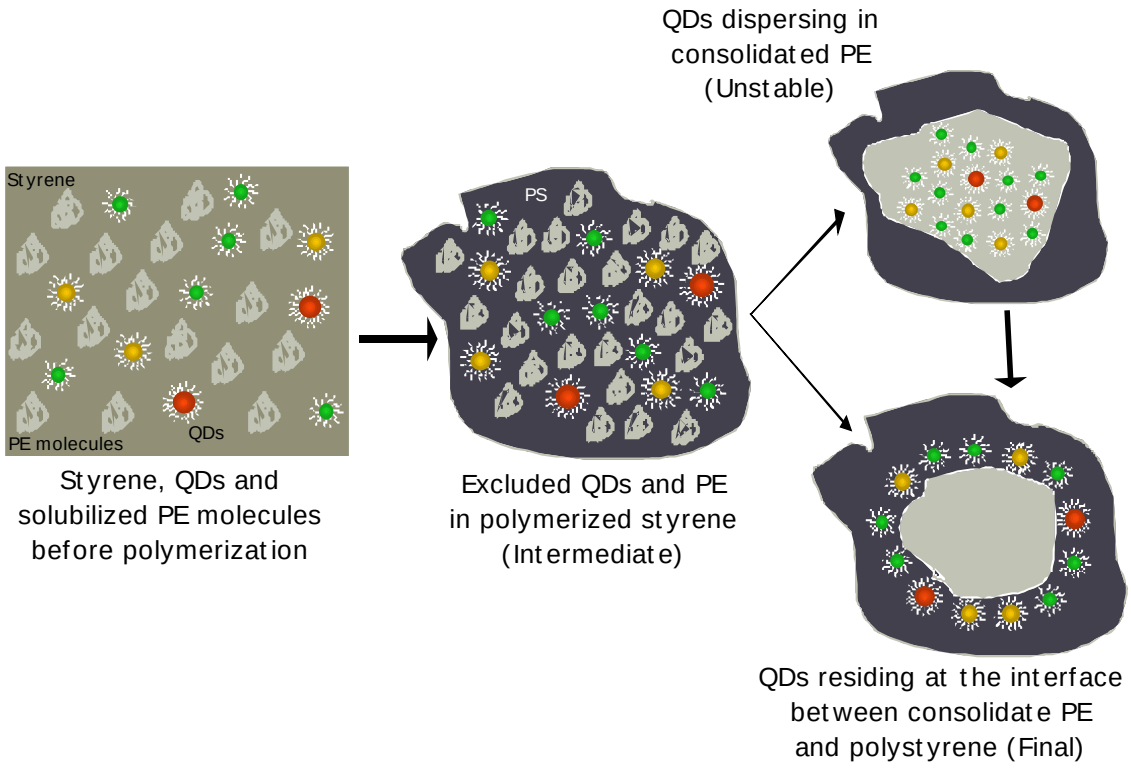

Figure 5.2: Schematic representation of the segregation of QDs and PE molecules during polymerization to form PS-PE Beads.

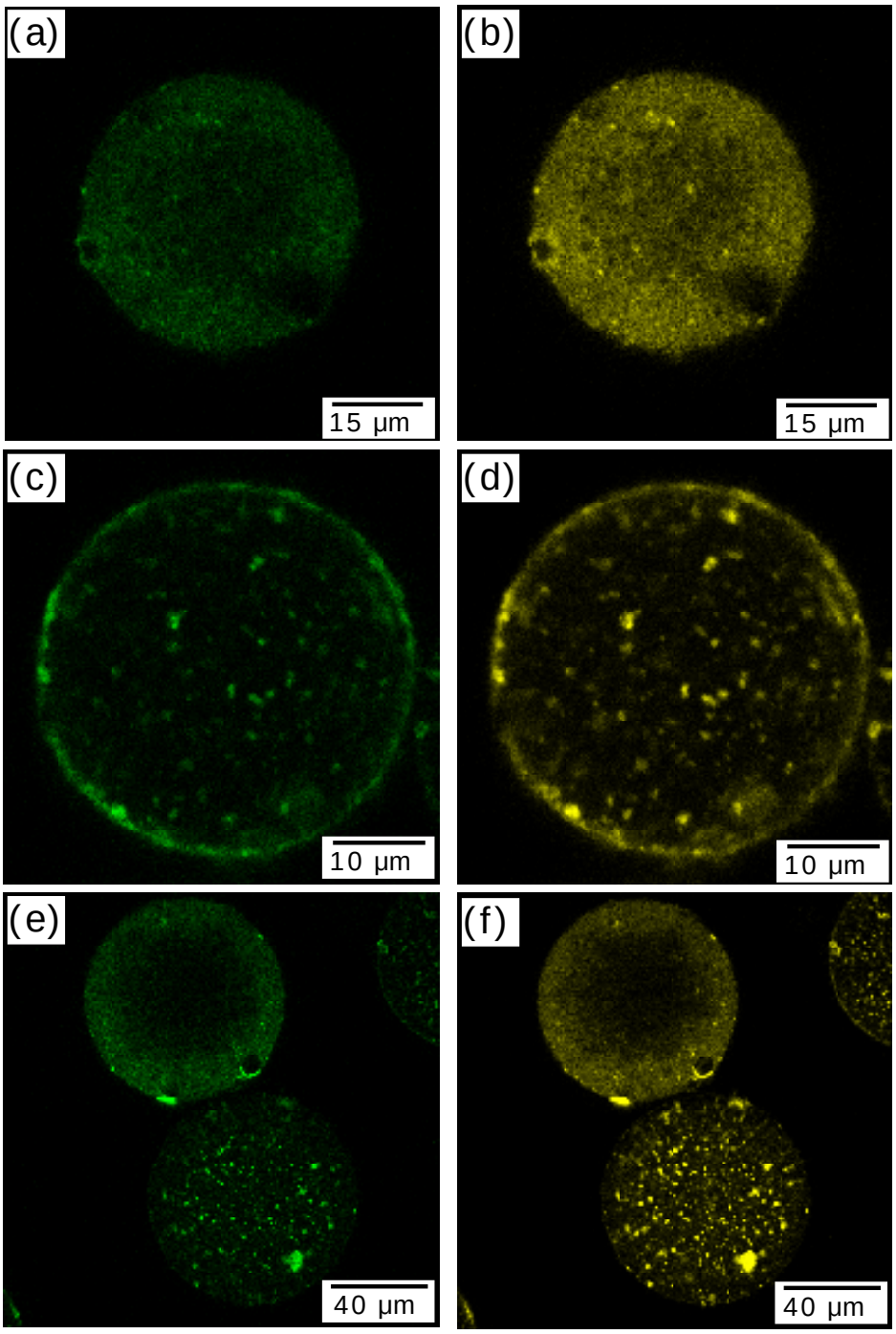

Figure 5.3: (a–b) and (c–d), respectively, are CLSM luminescence images of PS-PE Beads and PS-noPE Beads, embedded with 520 and 580 nm QDs at a 3:1 molar ratio and a total concentration of 4 x 10^{-6} M. (e–f) are the luminescence images of the PS-PE and PS-noPE Beads imaged simultaneously. The beads were excited by 458 nm laser and the luminescence was collected in 480–545 and 545–640 nm collection windows.

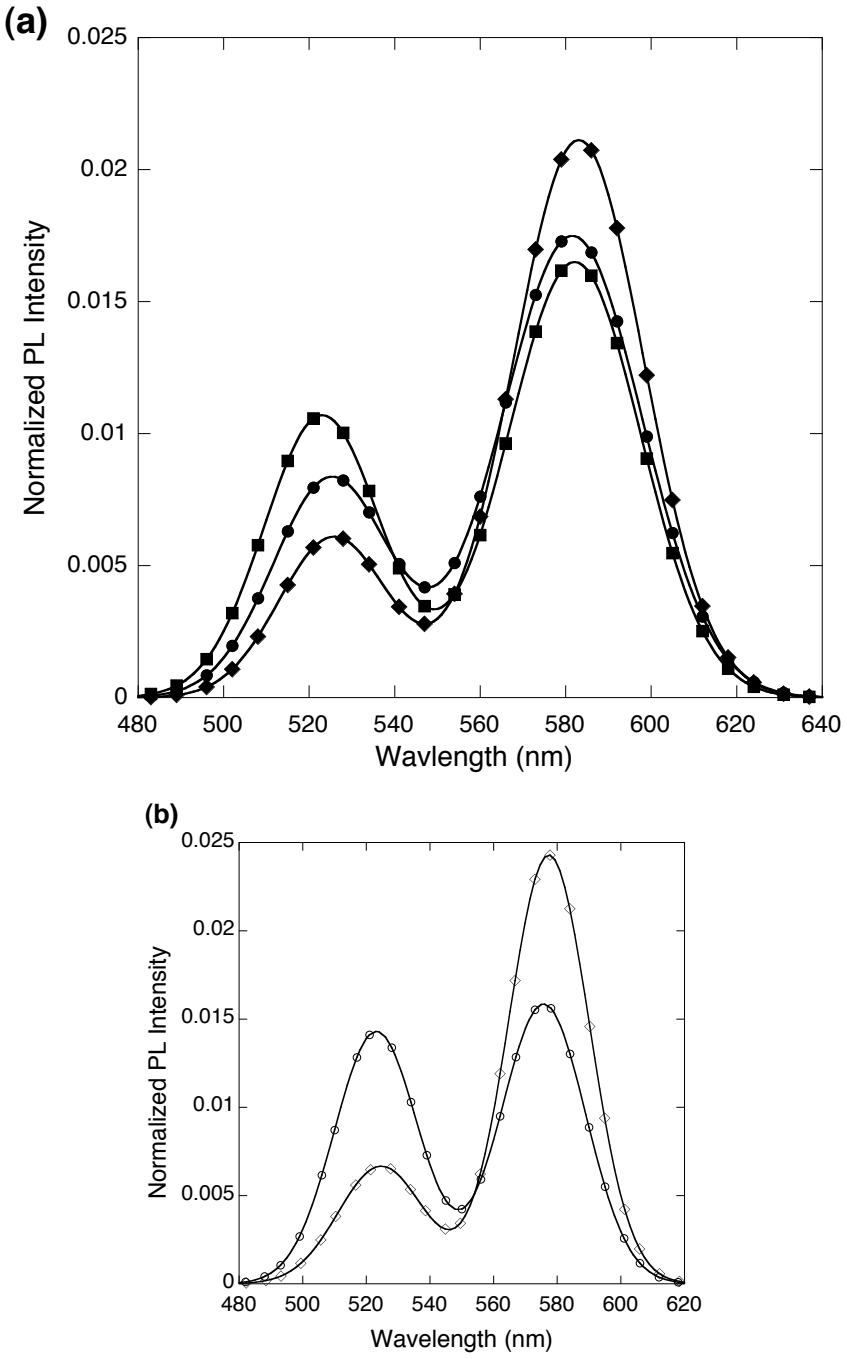

Figure 5.4: (a) A comparison of the fluorimeter emission spectrum of the PS-PE Beads (•) with the fluorimeter emission spectrum of PS-noPE Beads (⧫) and a reference QD dispersion (■) of 520 and 580 nm QDs, dispersed in St/DVB/MAA/AIBN at a relative molar ratio of 3:1 and a total concentration of 4 x 10^{-6} M (moles per liter of St). (b) A comparison of a CLSM spectral scan of PS-PE Beads (○) with CLSM spectral scan of PS-noPE Beads (◊) shows a significant recovery in the emission intensity of lower wavelength QDs.

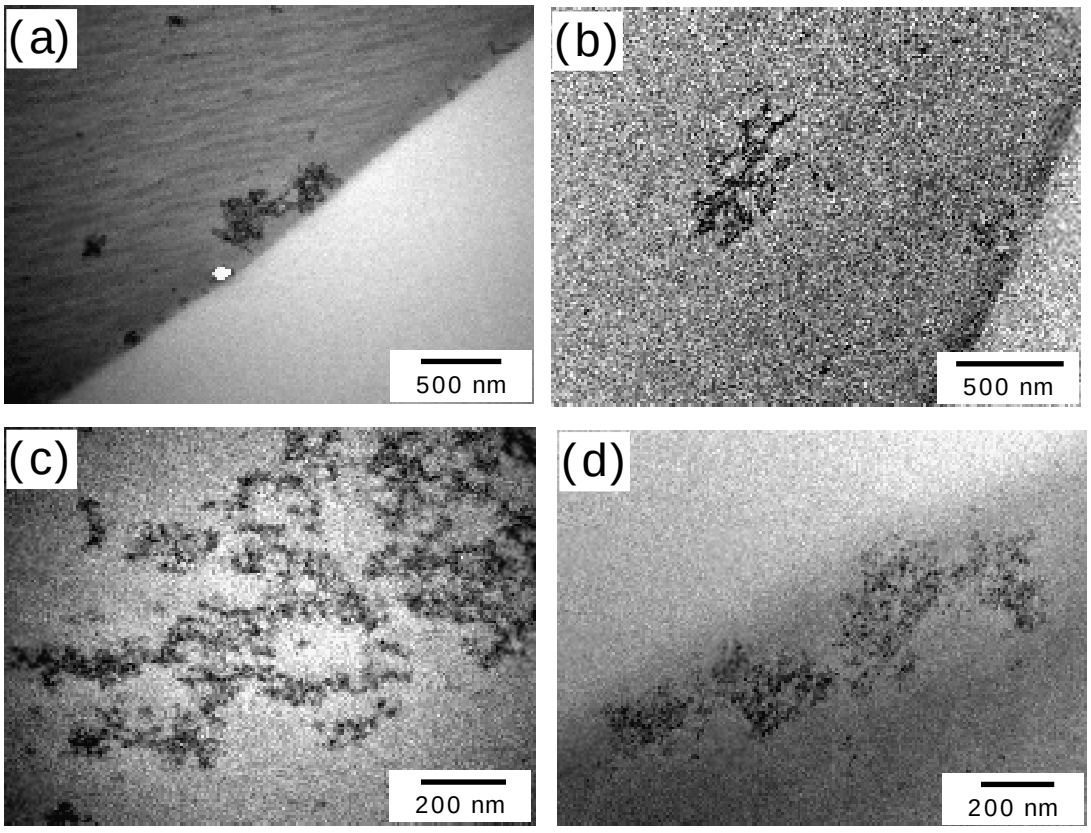

Figure 5.5: Transmission electron microscopy (TEM) analysis of the PS-noPE Beads. Self-corraling of the QDs, leading to the formation of clusters, as explained in Chapter 3 is observed. (a), (b) & (d) show the QDs aggregated into the clusters near the edges of the beads. Separation between the QDs is visible in (c), which is an image of a cluster in bead interior.

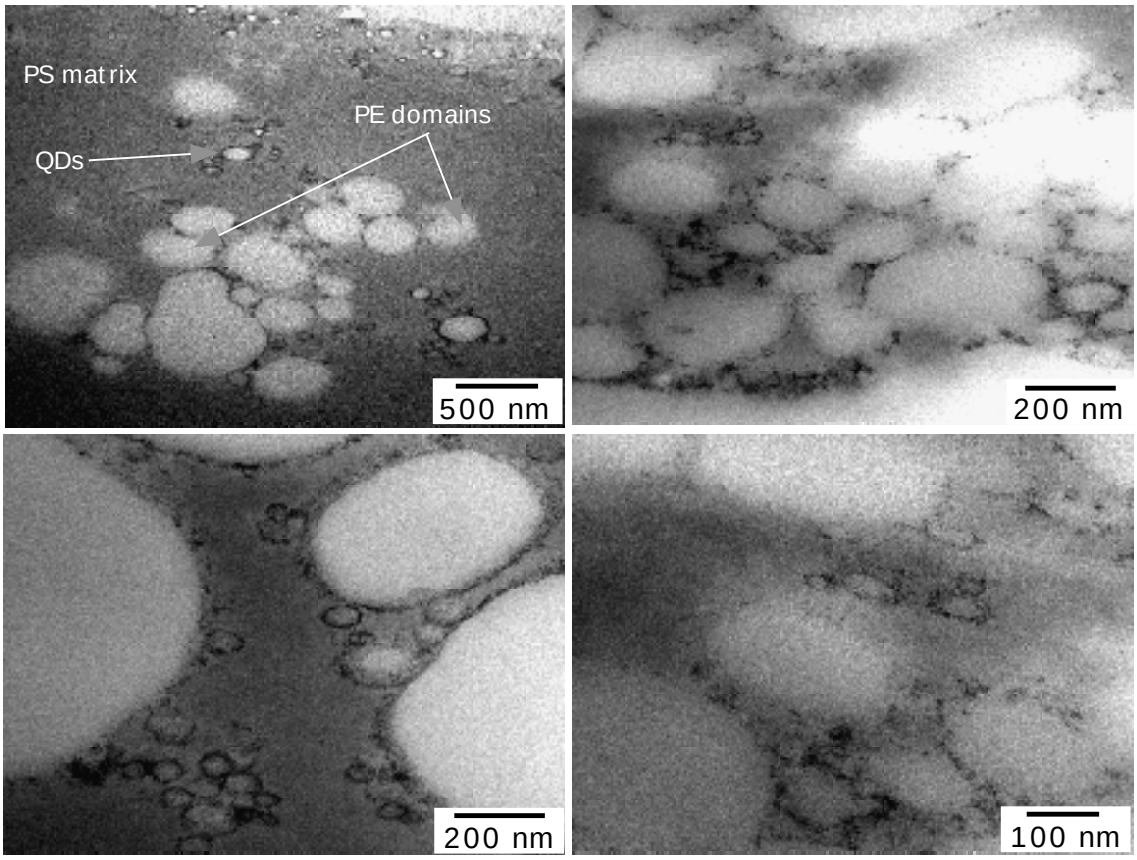

Figure 5.6: TEM images of the PS-PE beads. Styrene solubilized PE molecules are segregated into big domains during the polymerization. QDs minimize the interfacial energy between PS and PE by arranging themselves at the interface.

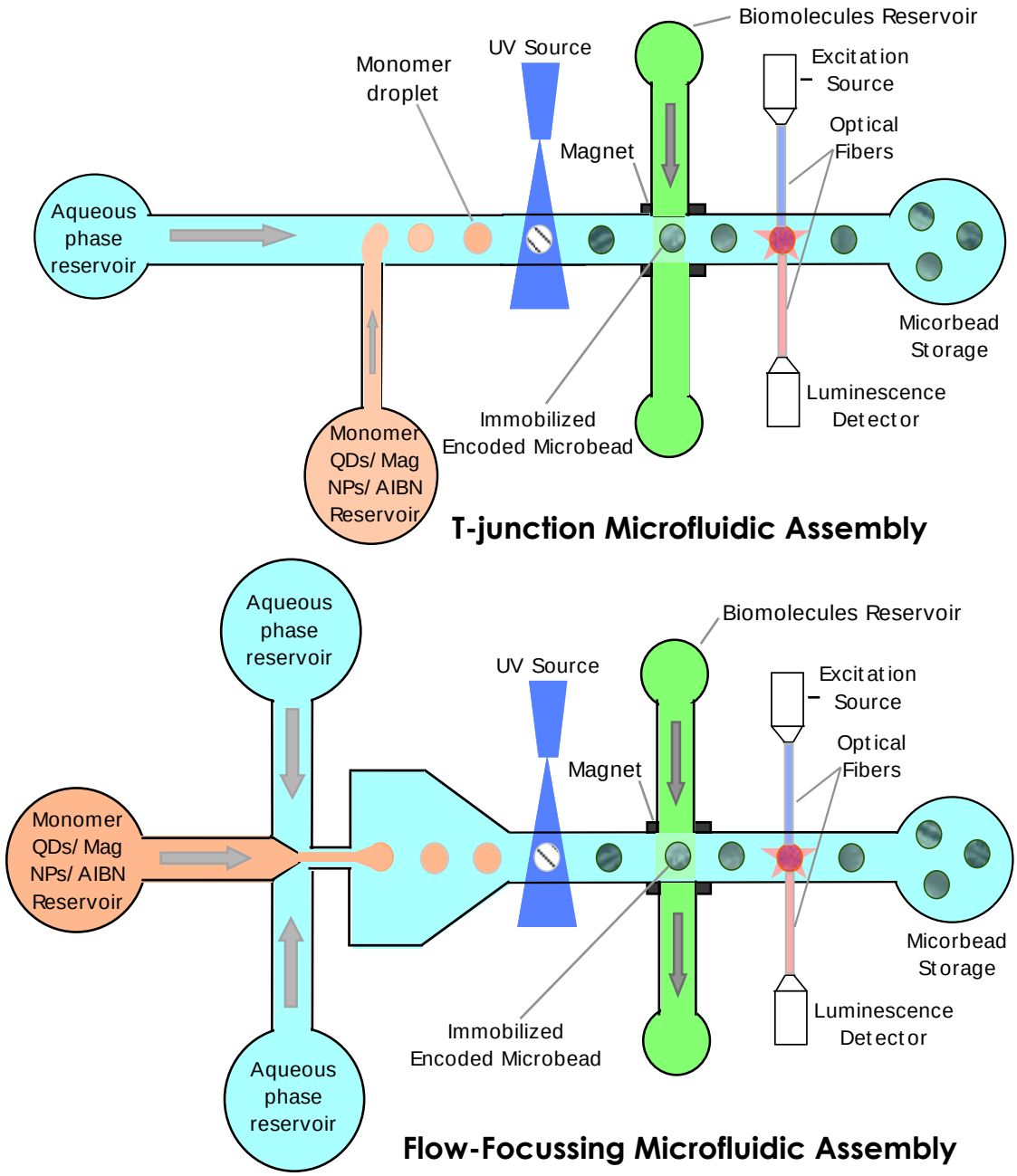

Figure 5.7: A schematic represention of "T"-junction and flow focussing microfluidics assemblies for generation of monodispersed, encoded polymer beads.

Bibliography

[1] N. Finkel, X. Lou, C. Wang, and L. He, "Barcoding the microworld", *Anal. Chem.* **76**, pp. 353A–359A (2004).

[2] R. Liu, J. Marik, and K. S. Lam, "A novel peptide-based encoding system for 'one-bead one-compound' peptidomimetic and small molecule combinatorial libraries", *J. Am. Chem. Soc.* **124**(26), pp. 7678–7680 (2002).

[3] S. Brenner and R. Lerner, "Encoded combinatorial chemistry", *Proc. Natl. Acad. Sci.* **89**(12), pp. 5381–5383 (1992).

[4] M. H. J. Ohlmeyer, R. N. Swanson, L. W. Dillard, J. C. Reader, G. Asouline, R. Kobayashi, M. Wigler, and W. C. Still, "Complex synthetic chemical libraries indexed with molecular tags", *Proc. Natl. Acad. Sci.* **90**(23), pp. 10922–10926 (1993).

[5] W. E. Doering and S. Nie, "Spectroscopic tags using dye-embedded nanoparticies and surface-enhanced raman scattering", *Anal. Chem.* **75**(22), pp. 6171–6176 (2003).

[6] H. Fenniri, L. Ding, A. E. Ribber, and Y. Zyrianov, "Barcoded resins: A new concept for polymer-supported combinatorial library self-deconvolution", *J. Am. Chem. Soc.* **123**(33), pp. 8151–8152 (2001).

[7] Z. I. Zhi, Y. Morita, Q. Hasan, and E. Tamiya, "Micromachining microcarrier-based biomolecular encoding for miniaturized and multiplexed immunoassay", *Anal. Chem.* **75**(16), pp. 4125–4131 (2003).

[8] M. Evans, C. Sewter, and E. Hill, "An encoded particle array tool for multiplex bioassays", *Assay Drug Dev. Technol.* **1**(199-207) (2003).

[9] A. R. Vaino and K. D. Janda, "Euclidean shape-encoded combinatorial chemical libraries", *Proc. Natl. Acad. Sci.* **97**(14), pp. 7692–7696 (2000).

[10] C. D. Keating and M. J. Natan, "Striped metal nanowires as building blocks and optical tags", *Adv. Mater.* **15**(5), pp. 451–454 (2003).

[11] S. Nicewarner-Pena, "Submicrometer metallic barcodes", *Science* **294**, pp. 137–141 (2001).

[12] B. D. Reiss, R. G. Freeman, I. D. Walton, S. M. Norton, P. C. Smith, W. G. Stonas, C. D. Keating, and M. J. Natan, "Electrochemical synthesis and optical readout of striped metal rods with submicron features", *J. Electroanal. Chem.* **522**(1), pp. 95–103 (2002).

[13] I. D. Walton, S. M. Norton, A. Balasingham, He. L., D. F. Oviso, D. Gupta, P. A. Raju, M. J. Natan, and R. G. Freeman, "Particles for multiplexed analysis in solution: Detection and identification of striped metallic particles using optical microscopy", *Anal. Chem.* **74**(10), pp. 2240–2247 (2002).

[14] F. Wang, W. B. Tan, Y. Zhang, X. Fan, and M. Wang, "Luminescent nanomaterials for biological labelling", *Nanotechnology* **17**, pp. R1–R13 (2006).

[15] V. M Pai, C. J. Chen, and Y. Haik, "Microscopic flow visualization system for fluids in magnetic fluids", *J. Magn. Magn. Mater.* **194**(1-3), pp. 262–266 (1999).

[16] D. Sinton, "Microscale flow visualization", *Microfluid. Nanofluid.* **V1**(1), pp. 2–21 (2004).

[17] R. K. Jain, "Delivery of molecular medicine to solid tumors: lessons from in vivo imaging of gene expression and function", *J. Control. Release* **74**(1-3), pp. 7–25 (2001).

[18] R. J. Fulton, R. L. McDade, P. L. Smith, L. J. Kienker, and Jr. Kettman, J. R., "Advanced multiplex analysis with flormetrixtm system", *Clin. Chem.* **43**, pp. 1749–1756 (1997).

[19] D. A. A. Vignali, "Multiplexed particle-based flow cytometric assays", *J. Immunol. Methods* **243**, pp. 243–255 (2000).

[20] B. J. Battersby, G. Lawrie, A. Johnston, and M. Trau, "Optical barcoding of colloidal suspensions: Applications in genomics, proteomics and drug discovery", *Chem. Commun.* **14**, pp. 1435–1441 (2002).

[21] S. J. Rosenthal, "Barcoding biomolecules with fluorescent nanocrystals", *Nat. Biotechnol.* **19**, pp. 621–622 (2001).

[22] J. P. Nolan and L. A. Sklar, "Suspension array technology: Evolution of the flat-array paradigm", *Trends Biotechnol.* **20**, pp. 9–12 (2002).

[23] M. Trau and B. J. Battersby, "Novel colloidal materials for high-throughput screening applications in drug discovery and genomics", *Adv. Mater.* **12**, pp. 975–979 (2001).

[24] J. A. Ferguson, T. C. Boles, C. P. Adams, and D. R. Walt, "A fiber-optic DNA biosensor microarray for the analysis of gene expression", *Nat. Biotechnol.* **14**, pp. 1681–1684 (1996).

[25] J. A. Ferguson, F. J. Steemers, and D. R. Walt, "High-density fiber-optic DNA random microsphere array", *Anal. Chem.* **72**, pp. 5618–5624 (2000).

[26] J. R. Epstein, A. P. K. Leung, K.-H. Lee, and D. R. Walt, "High-density, microsphere-based fiber-optic DNA microarrays", *Biosens. Bioelectron.* **18**, pp. 541–546 (2003).

[27] P. Wilkins Stevens and D. M. Kelso, "Imaging and analysis of immobilized particle arrays", *Anal. Chem.* **75**, pp. 1147–1154 (2003).

[28] A. P. Alivisatos, "The use of nanocrystals in biological detection", *Nat. Biotechnol.* **22**(1), pp. 47–52 (2004).

[29] M. Han, X. Gao, J. Z. Su, and S. Nie, "Quantum-dot-tagged microbeads for multiplexed optical coding of biomolecules", *Nat. Biotechnol.* **19**, pp. 631–635 (2001).

[30] W. C. W. Chan, D. J. Maxwell, X. Gao, R. E. Bailey, M. Han, and S. Nie, "Luminescent quantum dots for multiplexed biological detection and imaging", *Curr. Opin. Biotechnol.* **13**, pp. 40–46 (2002).

[31] X. Gao and S. Nie, "Quantum dot-encoded mesoporous beads with high brightness and uniformity: Rapid readout using flow cytometry", *Anal. Chem.* **76**, pp. 2406–2410 (2004).

[32] X. Gao and S. Nie, "Doping mesoporous materials with multicolor quantum dots", *J. Phys. Chem. B* **107**, pp. 11575–11578 (2003).

[33] M. Bradley, N. Bruno, and B. Vincent, "Distribution of CdSe quantum dots within swollen polystyrene microgel particles using confocal microscopy", *Langmuir* **21**, pp. 2750–2753 (2005).

[34] V. Stsiapura, A. Sukhanova, M. Artemyev, M. Pluot, J. H. M. Cohen, A. V. Baranov, V. Oleinikov, and I. Nabiev, "Functionalized nanocrystal-tagged fluorescent polymer beads: Synthesis, physicochemical characterization, and immunolabeling application", *Anal. Biochem.* **334**, pp. 257–265 (2004).

[35] J. Riegler, O. Ehlert, and T. Nann, "A facile method for coding and labeling assays on polystyrene beads with differently colored luminescent nanocrystals", *Anal. Bioanal. Chem.* **384**, pp. 645–650 (2006).

[36] M. Kuang, D. Wang, H. Bao, M. Gao, H. Mohwald, and M. Jiang, "Fabrication of multicolor-encoded microspheres by tagging semiconductor nanocrystals to hydrogel spheres", *Adv. Mater.* **17**, pp. 267–270 (2005).

[37] Y. Gong, M. Gao, D. Wang, and H. Mohwald, "Incorporating fluorescent CdTe nanocrystals into a hydrogel via hydrogen bonding: Toward fluorescent microspheres with temperature-responsive properties", *Chem. Mater.* **17**, pp. 2648–2653 (2005).

[38] H.-Q. Wang, Z.-L. Huang, T.-C. Liu, J.-H. Wang, Y.-C. Cao, X.-F. Hua, X.-Q. Li, and Y.-D. Zhao, "A feasible and quantitative encoding method for microbeads with multicolor quantum dots", *J. Fluoresc.* **17**, pp. 133–138 (2007).

[39] Y. Chan, J. P. Zimmer, M. Stroh, J. S. Steckel, R. K. Jain, and M. G. Bawendi, "Incoporation of luminescent nanocrystals into monodisperse core-shell silica microspheres", *Adv. Mater.* **16**(23-24), pp. 2092–2097 (2004).

[40] T. Hirai, N. Saito, and I. Komasawa, "Stabilization of CdS nanoparticles immobilized on thiol-modified polystyrene particles by encapsulation with polythiourethane", *J. Phys. Chem. B* **105**, pp. 9711–9714 (2001).

[41] C. Graf, S. Dembski, A. Hofmann, and E. Ruhl, "A general method for the controlled embedding of nanoparticles in silica colloids", *Langmuir* **22**, pp. 5604–5610 (2006).

[42] A. Rogach, A. Susha, F. Caruso, G. Sukhorukov, A. Kornowski, S. Kershaw, H. Mohwald, A. Eychmuller, and H. Weller, "Nano- and microengineering: 3-D colloidal photonic crystals prepared from sub-micron-sized polystyrene latex spheres pre-coated with luminescent polyelectrolyte/nanocrystal shells", *Adv. Mater.* **12**, pp. 333–337 (2000).

[43] D. Wang, A. Rogach, and F. Caruso, "Semiconductor quantum dot-labeled microsphere bioconjugates prepared by stepwise self-assembly", *Nano Lett.* **2**, pp. 857–861 (2002).

[44] N. Gaponik, I. L. Radtchenko, G. B. Sukhorukov, H. Weller, and A. Rogach, "Toward encoding combinatorial libraries: Charge-driven microencapsulation of semiconductor nanocrystals luminescing in the visible and near ir", *Adv. Mater.* **14**, pp. 879–882 (2002).

[45] Q. Ma, X. Wang, Y. Li, Y. Shi, and X. Su, "Multicolor quantum dot-encoded microspheres for the detection of biomolecules", *Talanta* **72**, pp. 1446–1452 (2007).

[46] W. Sheng, S. Kim, J. Lee, S. W. Kim, K. Jensen, and M. G. Bawendi, "In-situ encapsulation of quantum dots into polymer microspheres", *Langmuir* **22**(8), pp. 3782–3790 (2006).

[47] R. L. Sherman and W. T. Ford, "Semiconductor nanoparticle/polystyrene latex composite materials", *Langmuir* **21**, pp. 5218–5222 (2005).

[48] Y. Yang, X.; Zhang, "Encapsulation of quantum nanodots in polystyrene and silica micro-/nanoparticles", *Langmuir* **20**, pp. 6071–6073 (2004).

[49] A. L. Rogach, D. Nagesha, J. W. Ostrander, M. Giersig, and N. A. Kotov, ""Raisin bun"–type composite spheres of silica and semiconductor nanocrystals", *Chem. Mater.* **12**, pp. 2676–2685 (2000).

[50] P. J. Dowding and B. Vincen, "Suspension polymerisation to form polymer beads", *Colloid Surf. A* **161**, pp. 259–269 (2000).

[51] P. O'Brien, S. S. Cummins, D. Darcy, A. Dearden, O. Masala, N. L. Pickett, S. Ryley, and A. J. Sutherland, "Quantum dot-lebelled polymer beads by suspension polymerization", *Chem. Commun.* **20**, pp. 2532–2533 (2003).

[52] Y. Li, E. C. Y. Liu, N. Pickett, P. J. Skabara, S. S. Cummins, S. Ryley, A. J. Sutherland, and P. O'Brien, "Synthesis and characterization of CdS quantum dots in polystyrene microbeads", *J. Mater. Chem.* **15**, pp. 1238–1243 (2005).

[53] N. Joumaa, M. Lansalot, A. Theretz, A. Elaissari, A. Sukhanova, M. Artemyev, I. Nabiev, and J. H. M. Cohen, "Synthesis of quantum dot-tagged submicrometer polystyrene particles by miniemulsion polymerization", *Langmuir* **22**, pp. 1810–1816 (2006).

[54] K. Landfester, "Polyreactions in miniemulsions", *Macromolecular Rapid Communications* **22**, pp. 896–936 (2001).

[55] F. Fleischhaker and R. Zentel, "Photonic crystals from core-shell colloids with incorporated highly fluorescent quantum dots", *Chem. Mater.* **17**, pp. 1346–1351 (2005).

[56] Y. Yang, Z. Wen, Y. Dong, and M. Gao, "Incorporating CdTe nanocrystals into polystyrene microspheres: Towards robust fluorescent beads", *Small* **2**, pp. 898–901 (2006).

[57] C. Xu and E. Bakker, "Multicolor quantum dot encoding for polymeric particle-based optical ion sensors", *Anal. Chem.* **79**, pp. 3716–3723 (2007).

[58] W. Yin, H. Liu, M. Z. Yates, H. Du, F. Jiang, L. Guo, and T. D. Krauss, "Fluorescent quantum dot-polymer nanocomposite particles by emulsification/solvent evaporation", *Chem. Mater.* **19**, pp. 2930–2936 (2007).

[59] C. R. Kagan, C. B. Murray, and M. G. Bawendi, "Long-range resonance transfer of electronic excitations in close-packed CdSe quantum-dot solids", *Phys. Rev. B* **54**, pp. 8633–8643 (1996).

[60] C. R. Kagan, C. B. Murray, M. Nirmal, and M. G. Bawendi, "Electronic energy transfer in CdSe quantum dot solids", *Phys. Rev. Lett.* **76**, pp. 1517–1520 (1996).

[61] O. I. Micic, K. M. Jones, A. Cahill, and A. J. Nozik, "Optical, electronic, and structural properties of uncoupled and close-packed arrays of InP quantum dots", *J. Phys. Chem. B* **102**, pp. 9791–9796 (1998).

[62] M. V. Artemyev, A. I. Bibik, L. I. Gurinovich, S. V. Gaponenko, and U. Woggon, "Evolution from individual to collective electron states in a dense quantum dot ensemble", *Phys. Rev. B* **60**, pp. 1504 (1999).

[63] O. I. Micic, S. P. Ahrenkiel, and A. J. Nozik, "Synthesis of extremely small InP quantum dots and electronic coupling in their disordered solid films", *Appl. Phys. Lett.* **78**, pp. 4022 (2001).

[64] H. Dollefeld, H. Weller, and A. Eychmuller, "Semiconductor nanocrystal assemblies: Experimental pitfalls and a simple model of particle-particle interaction", *J. Phys. Chem. B* **106**, pp. 5604 (2002).

[65] S. A. Crooker, J. A. Hollingsworth, S. Tretiak, and V. I. Klimov, "Spectrally resolved dynamics of energy transfer in quantum-dot assemblies: Towards engineered energy flows in artificial materials", *Phys. Rev. Lett.* **89**, pp. 186802–06 (2002).

[66] S. F. Wuister, R. Koole, C. deMelloDonega, and A. Meijerink, "Temperature-dependent energy transfer in cadmium telluride quantum dot solids", *J. Phys. Chem. B* **109**, pp. 5504–5508 (2005).

[67] R. Koole, P. Liljeroth, C. deMelloDonega, D. Vanmaekelbergh, and A. Meijerink, "Electronic coupling and exciton energy transfer in cdte quantum-dot molecules", *J. Am. Chem. Soc.* **128**, pp. 10436–10441 (2006).

[68] M. Achermann, M. A. Petruska, S. A. Crooker, and V. I. Klimov, "Picosecond energy transfer in quantum dot langmuir-blodgett nanoassemblies", *J. Phys. Chem. B* **107**, pp. 13782–13787 (2003).

[69] T. Franzl, D. S. Koktysh, T. A. Klar, A. L. Rogach, J. Feldmann, and N. Gaponik, "Fast energy transfer in layer-by-layer assembled cdte nanocrystal bilayers", *Appl. Phys. Lett.* **84**, pp. 2904–2906 (2004).

[70] R. Osovsky, A. Shavel, N. Gaponik, L. Amirav, A. Eychmuller, H. Weller, and E. Lifshitz, "Electrostatic and covalent interactions in CdTe nanocrystalline assemblies", *J. Phys. Chem. B* **109**, pp. 20244–20250 (2005).

[71] D. Ramadurai, D. Geerpuram, D. Alexson, M. Dutta, N. Kotov, Z. Tang, and M. Stroscio, "Electrical and optical properties of colloidal semiconductor nanocrystals in aqueous environments", *Superlattices Microstruct.* **40**, pp. 38–44 (2006).

[72] T. Forster, *Modern Quantum Chemistry* volume 3, Academic Press: New York (1965).

[73] P. Wu and L. Brand, "Resonance energy transfer: Methods and applications", *Anal. Biochem.* **218**, pp. 1–13 (1994).

[74] K. Braeckmans, L. Peeters, N. N. Sanders, S. C. De Smedt, and J. Demeester, "Three-dimensional fluorescence recovery after photobleaching with the confocal scanning laser microscope", *Biophys. J.* **85**(4), pp. 2240–2252 (2003).

[75] A. Balazs, T. Emrick, and T. Russell, "Nanoparticle polymer composites: Where two small worlds meet", *Science* **314**, pp. 1107–1110 (2006).

[76] S. Gupta, Q. Zhang, T. Emrick, and T.P. Russell, ""Self-corralling" nanorods under an applied electric field", *Nano Lett.* **6**(9), pp. 2066–2069 (2006).

[77] L. Erskine, T. Emrick, A. Alivisatos, and J. Frechet, "Preparations of semiconductor nanocrystals-polystyrene hybrid materials", *Polym. Prepr.* **41**, pp. 593–594 (200).

[78] J.-Y. Lee, Q. Zhang, T. Emrick, and A.J. Crosby, "Nanoparticle alignment and repulsion during failure of glassy polymer nanocomposites", *Macromolecules* **39**(21), pp. 7392–7396 (2006).

[79] P. S. Eastman, W. Ruan, M. Doctolero, R. Nuttall, G. de Feo, J. S. Park, J. S. F. Chu, P. Cooke, J. W. Gray, S. Li, and F. F. Chen, "Qdot nanobarcodes for multiplexed gene expression analysis", *Nano Lett.* **6**(5), pp. 1059–1064 (2006).

[80] A. A. Deniz, T. A. Laurence, M. Dahan, D. S. Chemla, P. G. Schultz, and S. Weiss, "Ratiometric single-molecule studies of freely diffusing biomolecules", *Annu. Rev. Phys. Chem.* **52**, pp. 233–253 (2001).

[81] M.K. Sharma and M.L. Gilchrist, "Templated assembly of biomembranes on silica microspheres using bacteriorhodopsin conjugates as structural anchors", *Langmuir* **23**(13), pp. 7101–7112 (2007).

[82] N.D. Kalyankar, M.K. Sharma, S.V. Vaidya, D. Calhoun, C. Maldarelli, A. Couzis, and L. Gilchrist, "Arraying of intact liposomes into chemically functionalized microwells", *Langmuir* **22**(12), pp. 5403–5411 (2006).